ELASTIC AND STRUCTURES RESEARCH LABORATORY
MASSACHUSETTS INSTITUTE OF TECHNOLOGY

TECHNICAL REPORT 25-13

EXPERIMENTAL AND ANALYTICAL DETERMINATION OF THE TRANSIENT THERMAL STRESSES IN A ONE-CELL BOX BEAM

BY

J. W. MAR and S. J. ENGEL

FOR THE

OFFICE OF NAVAL RESEARCH

CONTRACT N5ori-07833

ONR PROJECT NR 064-259

MAY 1954

Pages 81-88

The correct labels for the column headings in Table A. 4 are as follows:

T_i, ΔT_i, $(\sigma_{x,1})_i$, N_i, A_i, F, $(\sigma_{x,2})_i$, Σ, Fz, $(\sigma_{x,3})_i$, $[\sigma_x(5)]_i$

The values for $(\sigma_{x,3})_i$ and $[\sigma_x(5)]_i$ should be rounded off to three significant figures as was done for $(\sigma_{x,1})_i$ and $(\sigma_{x,2})_i$.

Page 82

The F for Area No. 14 is 1390.

The ΔT_i for Area No. 19 should be 138 instead of 130.

Page 84

The T_i for Area No. 4 should be 118 instead of 111.

Page 86

The Fz for Area No. 14 should be 1480 instead of 1400.

The F for Area No. 21 should be 1650 instead of 16500.

AEROELASTIC AND STRUCTURES RESEARCH LABORATORY

MASSACHUSETTS INSTITUTE OF TECHNOLOGY

TECHNICAL REPORT 25-13

ERRATA-July 1954

The following corrections apply to ASRL TR 25-13, "Experimental and Analytical Determination of the Transient Thermal Stresses in a One-Cell Box Beam," dated May 1954:

Pages 3 and 4

The photographs in Figures 2.1 and 2.2 should be interchanged.

Page 21

The right-hand curve should be labeled "120 SECONDS HEATING TIME."

Page 30

Under Eq. (4.4) add: z is the distance from the centroidal axis to the centroid of the beam element.

Add the following to Eq. (4.7): Room Temperature = 75°F

Eq. (4.8) should read $(\sigma_{x,2})_i = \frac{1}{A}\sum_{i=1}^{n} 2 \cdot E\alpha\,\Delta T_i \cdot A_i \; ; A = 2.045\ in^2$

Eq. (4.9) should read $(\sigma_{x,3})_i = + \frac{z_i}{I_y}\sum_{i=1}^{n} 2 \cdot E\alpha\,\Delta T_i\, z_i \cdot A_i \; ; I_y = 1.365\ in^4$

Page 31

In the title of Figure 4.2 the a_i should be A_i.

Page 45

The "B" under Eq. (4.31) should be $\overline{B}$.

(over)

AEROELASTIC AND STRUCTURES RESEARCH LABORATORY

MASSACHUSETTS INSTITUTE OF TECHNOLOGY

TECHNICAL REPORT 25-13

EXPERIMENTAL AND ANALYTICAL DETERMINATION OF THE TRANSIENT THERMAL STRESSES IN A ONE-CELL BOX BEAM

FOR THE

OFFICE OF NAVAL RESEARCH

CONTRACT N5ori-07833

ONR PROJECT NR 064-259

MAY 1954

Reported by: J. W. Mar
J. W. Mar

S. J. Engel
S. J. Engel

Approved by: R. L. Bisplinghoff
R. L. Bisplinghoff

ACKNOWLEDGEMENTS

The authors wish to acknowledge the invaluable assistance of the shop personnel of the Aeroelastic and Structures Research Laboratory, under Mr. C. E. Wallin, who constructed and helped to test the box beam. They would also like to thank Mr. C. I. Wirpio of the Electronics Shop for guidance in operating the experimental equipment and the personnel of the Computing Section, under Mrs. E. W. Simmons, who reduced the data.

The manuscript of this report was edited by Mr. R. R. Staley who also arranged for the printing. Mr. C. Stalzer read a portion of Section IV critically. Thanks are also due to Messrs. G. Anitole and E. Zierhoffer for drawing the graphs and to Mr. Zierhoffer for writing in the equations. Miss M. Forsythe typed the reproduction copy of the manuscript.

TABLE OF CONTENTS

LIST OF ILLUSTRATIONS

ABSTRACT

The one-dimensional heat flow through a typical one-cell built-up box beam was investigated experimentally to determine the stresses and distortions which result from a transient, non-uniform temperature distribution. The model was exposed to a radiant heater which produced the desired maximum temperature of 400°F in the nearest surface within two minutes. Eleven temperature and nine strain gage readings were recorded continuously during the interval. A comparison of the time histories of the temperature distribution with the box beam interior empty and then with it filled with insulation show that conduction is the primary mode of heat transfer. Graphical and tabular comparisons between the experimentally determined stresses and the stresses calculated on the basis of the temperatures measured at eleven points are presented for heating times of 30, 60, 90 and 120 seconds. The agreement is fair for early heating times and poor for later times. Conditions at the lower flanges and thermal buckling may explain the discrepancies.

SECTION I

INTRODUCTION

The development of the atomic bomb and the advent of supersonic flight have raised the phenomenon of heat conduction to a very high position in the list of problems faced by aeronautical designers. Security measures have restricted the amount of information on the effects of thermal radiation from atomic bombs on aircraft that is generally available. But a sufficient amount can be gleaned from various sources (see Refs. 1 and 2) to realize that the calculation of temperature distributions and thermal stresses may be necessary. An excellent series of papers (Refs. 3, 4 and 5) have analyzed the time dependence of the temperature distribution in thin solid wings at high Mach numbers. The NACA has reported analytical and experimental investigations of the effects of non-uniform temperature distributions on semi-monocoque structures and their components (Refs. 6, 7, 8 and 9). Reference 10 presents a study of some aspect of thermal stresses in aircraft structures due to aerodynamic heating. The above ten references represent only a portion of the pertinent ones which are available in this field. Comparatively few published reports, however, contain experimental data on the temperature and stress distributions in any type of aircraft structure which is subjected to a rapid rate of heat input. It is the principal purpose of the report to describe and report the results from some experiments of this nature.

SECTION ii

DESCRIPTION OF EXPERIMENTAL METHOD

The purpose of this investigation is to study experimentially the manner in which heat is conducted through a one-cell box beam and to determine the stresses and distortions which accompany the resulting transient, non-uniform temperature. By designing the box beam with a fairly large span-to-depth ratio, the local effects of the free end and of the root were made negligible. As a result, the heat flow was essentially a one-dimensional phenomenon, and the measured stresses could then be compared with the values obtained from a simple analysis.

2.1 The Model

The experimental model in this test program consisted of a one-cell box beam, which was 3 inches deep, 6 inches wide and 25 3/4 inches long. The box was bolted together with 24 S-T Phillips flat head machine screws and 24 S-T hexagonal nuts. An inch and three quarters of the length at one end of the model was used to mount heavy steel angle irons that fastened the model to the bed plates of an erector set in a cantilevered position (see Figure 2.1). Although the cross section of this box beam is simple, several problems had to be solved before the design assumed the form shown in Figures 2.2, 2.3, 2.4 and 2.5. The design had two basic aims: (1) to duplicate a typical one-cell built-up box beam consisting of spar caps, shear webs and skin and (2) to minimize the number of contact surfaces without undue fabrication effort in order to gain better heat transfer between the web and the spar cap. The shear webs and the spar caps were simulated by an 0.065 inch thick 24 S-T aluminum alloy sheet and a 3 inch 61 S-T structural aluminum channel, respectively. Aluminum sheet of 0.065 inch thickness was used because of its availability and also because the desired duration of the heat input could not be obtained without seriously damaging the thinner skin. A structural aluminum channel was used because it was easily obtained from current stock and because the mechanical properties of 61 S-T are not very different from those of 24 S-T aluminum sheet (see Table A.1 in Appendix A). The cross section of the channel is shown in Figure 2.5. The shaded portions indicate the material which was removed in order to simulate a perfect joint between the shear web and spar cap.

The one-inch spacing of the bolts which connected the skin panels to the channel was chosen so as to preclude the possibility of inter-bolt thermal buckling. The stresses in the skin panels were calculated on the basis of an assumed cubic temperature variation across the depth of the beam with an assumed maximum temperature for the bottom skin of 400° F. These calculated stresses were then used to compute the spacing necessary to prevent buckling between the bolts.

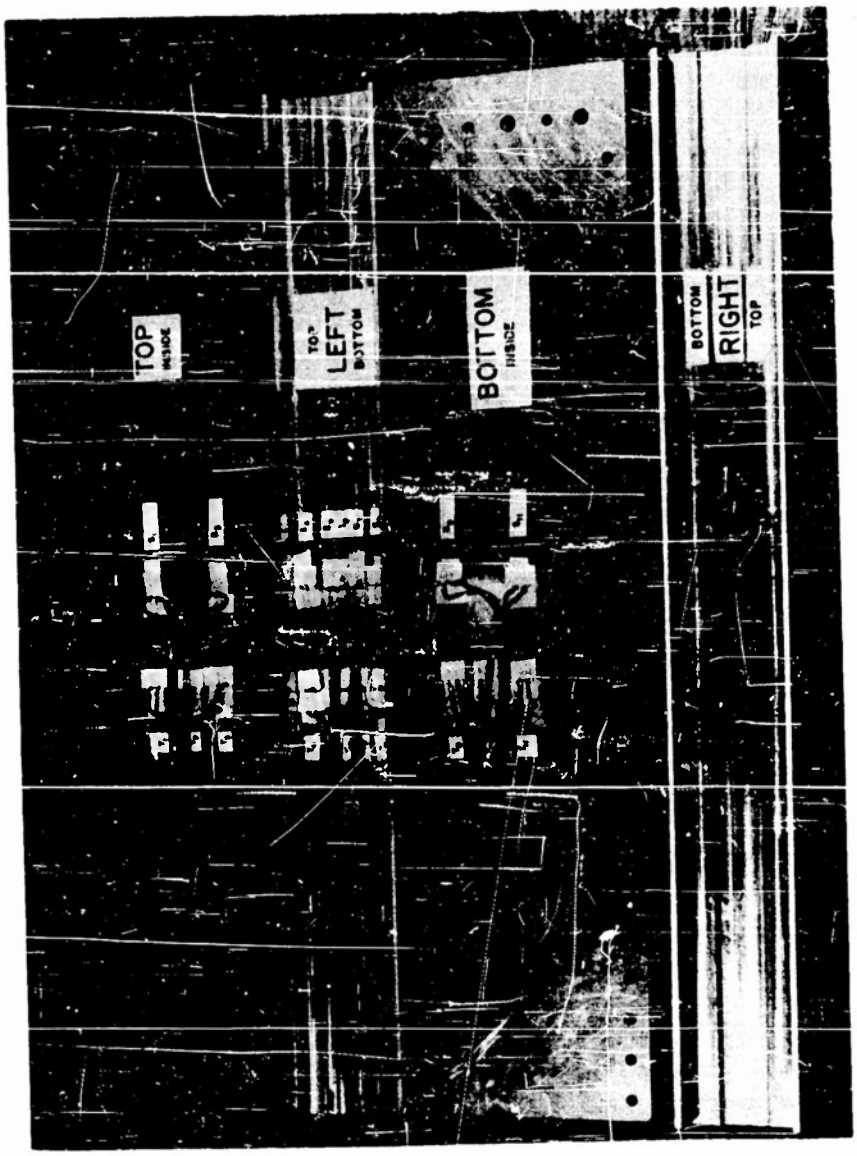

FIGURE 2.1 EXPERIMENTAL SETUP

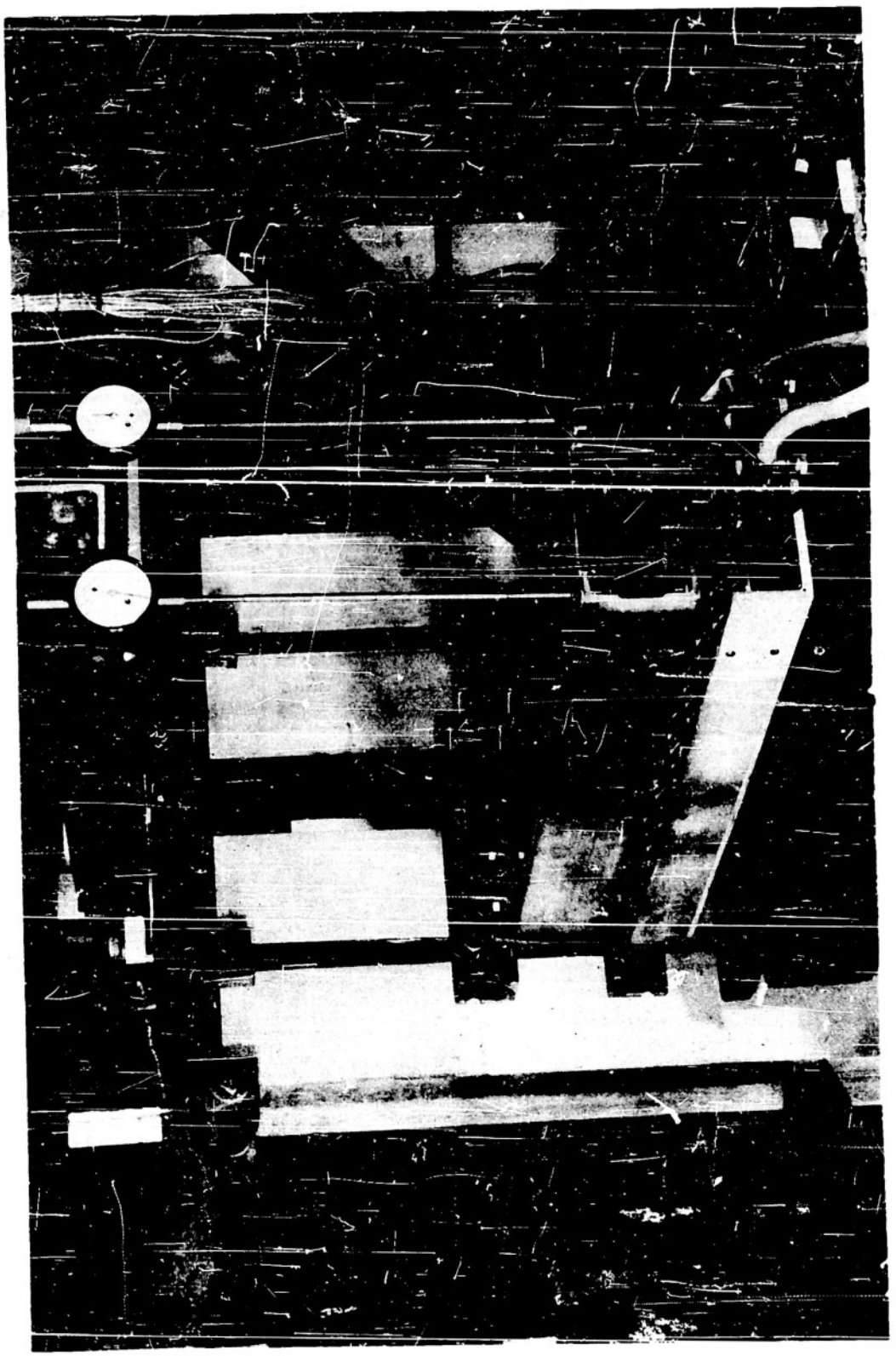

FIGURE 2.2 EXPLODED VIEW OF MODEL

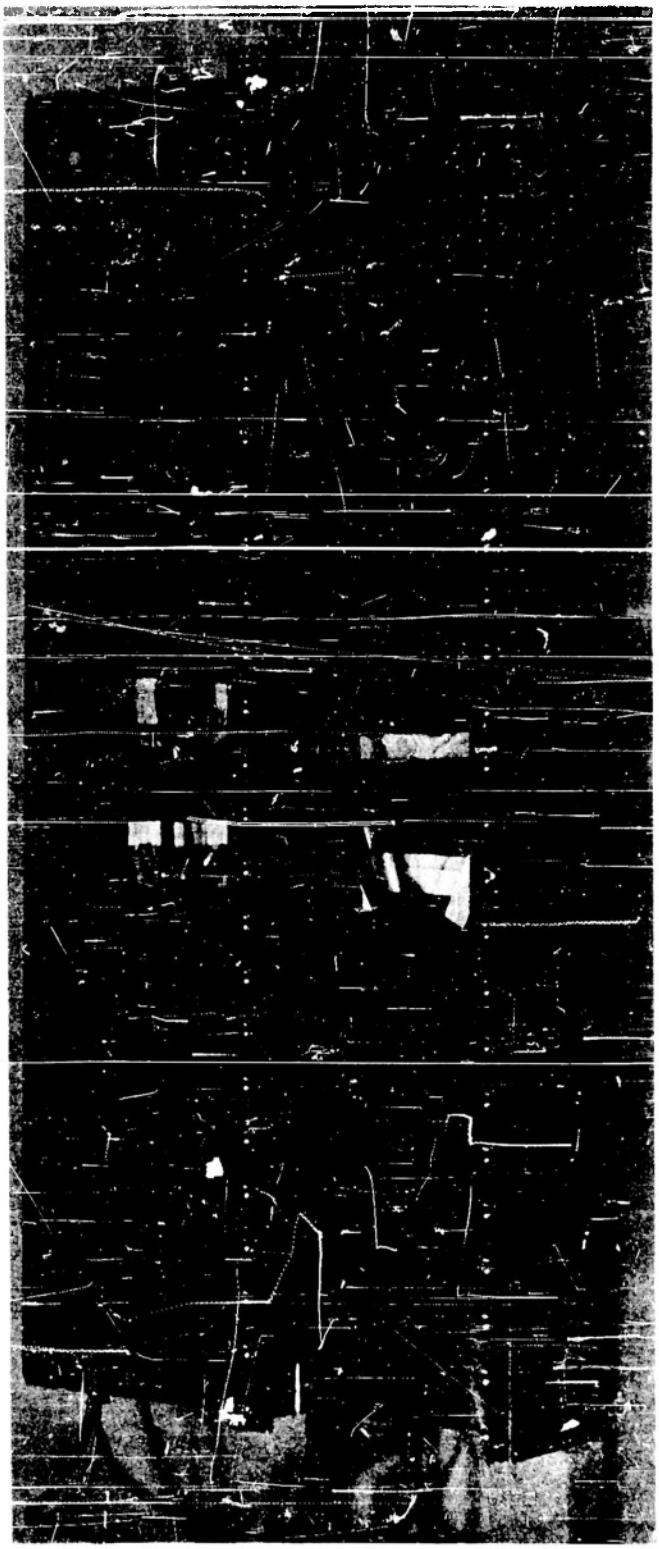

FIGURE 2.3 PARTIALLY ASSEMBLED MODEL

MATERIAL LIST

2 - 3X0.170X25$\frac{3}{4}$ 61 ST AL. ALLOY CHANNEL SECTIONS.
2 - 0.065X6X25$\frac{3}{4}$ 24 ST AL. ALLOY SHEET.
96 #10 HEXAGONAL NUTS. (24 ST)
96 #10 PHILLIPS FLAT HEAD MACHINE SCREWS (24 ST).

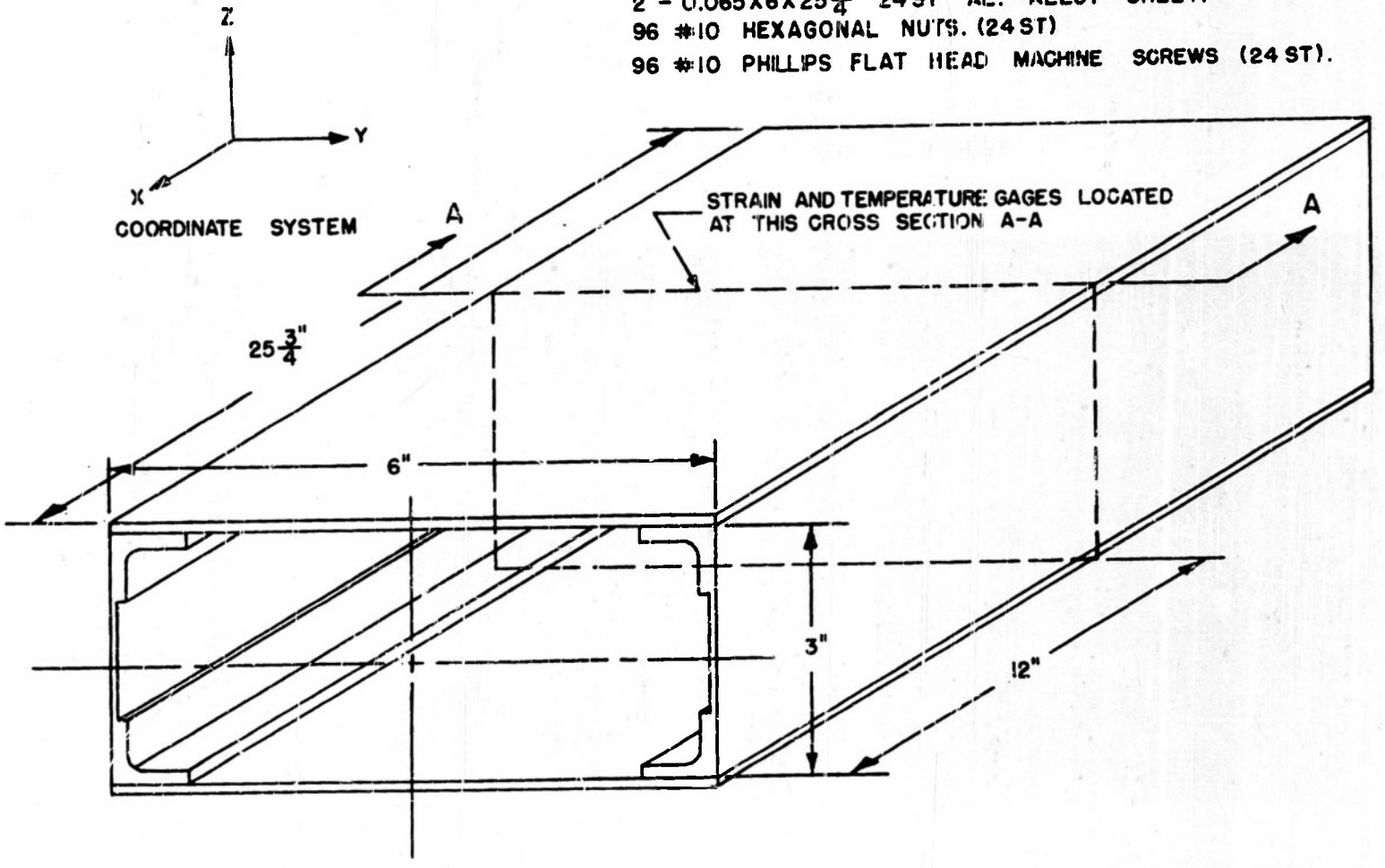

FIGURE 2.4 EXPERIMENTAL MODEL

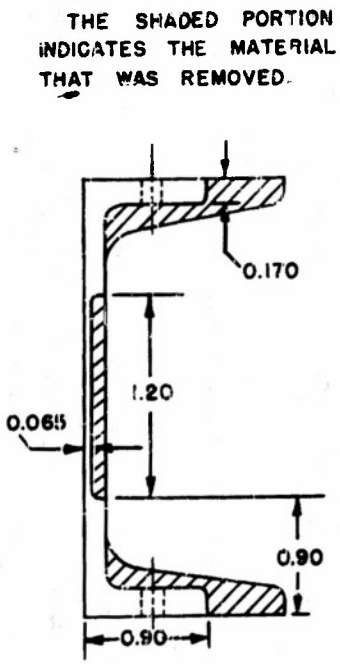

FIGURE 2.5 THREE INCH 61 S-T STRUCTURAL ALUMINUM ALLOY CHANNEL

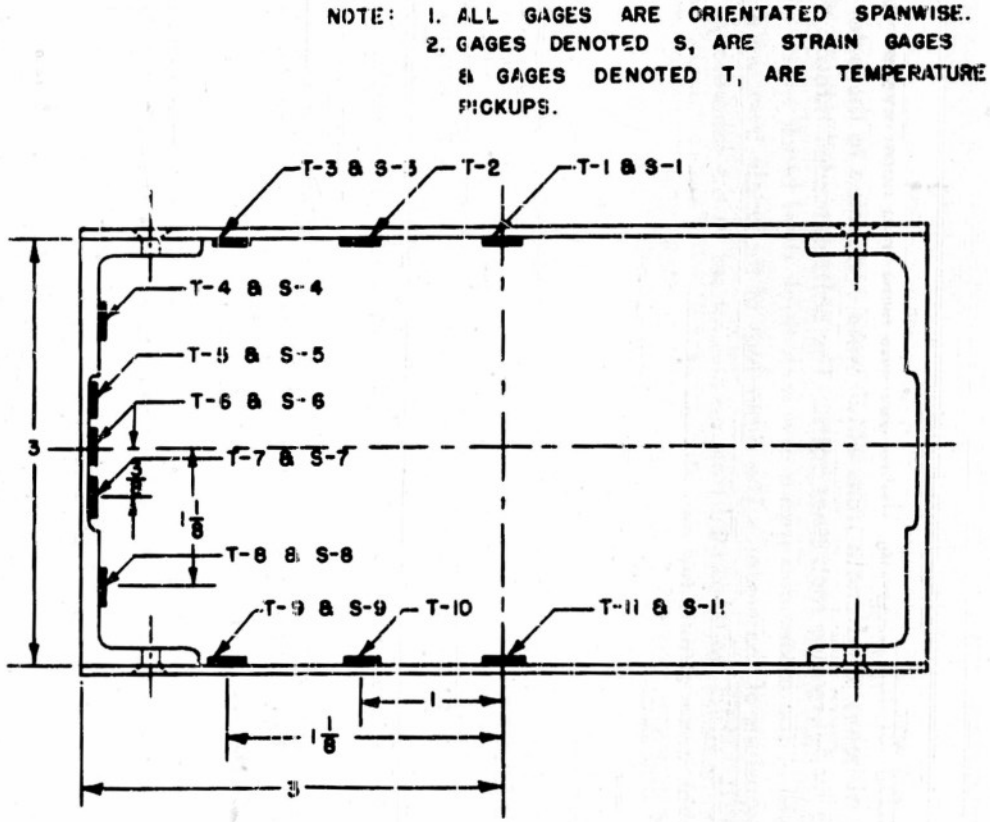

FIGURE 2.6 LOCATION OF STRAIN GAGES AND THERMOMETER RESISTANCE ELEMENTS ON CROSS SECTION A-A

During the test program, the model was held in a cantilevered position by means of a pair of heavy steel angle irons which were connected to the outer skin on each side of the model by 3/8 inch steel bolts. The bolts extended through the angle irons and the skin of the model and into a one inch thick steel block which was fitted to the inner dimensions of the model. The other legs of the angle irons were fastened to heavy bed plates which were formed from an erector set in the laboratory. This rigid support for the box beam eliminated any chance of unwanted displacements of the model (see Figures 2.1 and 2.3).

2.2 Instrumentation

The temperature distribution in the box beam was found by using eleven Ruge-DeForest RDF Stikons, Type BN-3 resistance thermometer elements, mounted at the midspan station as shown in Figure 2.6 and designated by the symbols, $\bar{T}$-i to $\bar{T}$-ii. These gages were found to be well suited to transient measurements because of their low thermal inertia. Their sensitivity to strain is negligible, and their operating range extends up to 400°F, although at higher temperatures the gages could be used only for short periods of time.

The strain pickups used on the lower skin and shear web were Baldwin SR-4 temperature compensated (from + 50° to + 250°F) strain gages, type EBDF-7D designed specifically for the use on aluminum alloy. It should be noted that the type EBDF-7D gages give outputs which are proportional to the quantity,

$$\epsilon - \bar{\alpha} \cdot \Delta T$$

where

ϵ is the total strain

$\bar{\alpha}$ is the coefficient of thermal expansion

ΔT is the change in temperature from its equilibrium value.

The above quantity represents only the strain due to stress and, hence, the gages do not read strain in the conventional sense of the word. The coefficient of thermal expansion must, of course, be the same as that for the material under test. The upper skin had only Baldwin SR-4 bakelite base strain gages, Type AB-7, because of the small temperature changes expected. It was found, however, that even though the temperature changes in the AB-7 gages were small, a temperature correction had to be applied to their strain readings because the dummy gages used in the bridge circuit were wire-wound resistors which operated at room temperature. No correction for gage factor due to temperature changes was necessary for either type of strain gage. The EBDF-7D gages

are temperature compensated, while the gage factor of the AB-7 is constant for temperatures up to 300°F (Ref. 20). All of the above gages were installed according to the manufacturer's recommended procedures and baking cycles. The strain gages are designated by the symbols, S-1 to S-11, and their locations are shown in Figure 2.6.

A twelve-channel Consolidated Engineering Company recording oscillograph was used to record the temperature changes at the slowest possible film speed of 1/8 of an inch per second so as to minimize the amount of film that had to be developed. A special set of dummy resistors, used in conjunction with the bridge circuits of the oscillograph, reduced the amplitude of the signal received from the Stikon gages. Baldwin Portable Strain Indicators, Type L, measured the strain gage reading directly in micro-inches per inch. Figures 2.7 and 2.8 present block diagram sketches of the elements of each circuit. Figure 2.10 shows the test equipment which was used. In addition, two dial gages, shown in Figure 2.1, were mounted at the free end of the model for the purpose of measuring deflections. These gages were used to mark the beginning of the heating cycle and also indicated total deflection at the end of the heating period.

2.3 The Radiant Furnace

An investigation of both commercial and special purpose heaters disclosed that the heater of Reference 2 would be adequate. This radiant furnace originally consisted of twelve heating elements of open coiled windings of nichrome wire which were mounted in an insulated aluminum reflecting box, 6 inches wide and 24 inches long. Each element is composed of 0.064 inch diameter wire and has a resistance of 36 ohms. The heating coils were connected in parallel and mounted on heavy buss bars located at the ends of the reflecting box. Additional supports, consisting of transite separators spaced approximately 3 1/2 inches apart, proved necessary to minimize the sag of the coils.

An 87 KW D.C. generator, which normally drives the M.I.T. Flutter Tunnel also usually supplies the power required by the heater (see Figure 2.9). But since the tunnel was in operation during most of this investigation, the heater had to be modified so as to operate on the electric power provided by the Cambridge Electric Power Company. The alternate power available in the Structures Laboratory was supplied by a 220 volt, 100 ampere, three phase, Y-connected transormer. Modification of the heater consisted of separating the twelve heating coils into three equal groups to form a Y-type three-phase circuit. This alteration was accomplished very easily by dividing the buss bar at one end into three sections with four coils per section (see Figure 2.9). In the original construction of the heater, the resistance of each coil was considered equal within 0.01 ohm. Thus, it was assumed that there would be no unbalance of power in the circuit. Since the current varied only 0.1 of an ampere between branches, the assumption was justified. In addition, the current in each branch remained essentially constant (13.5 amperes) during the heating period.

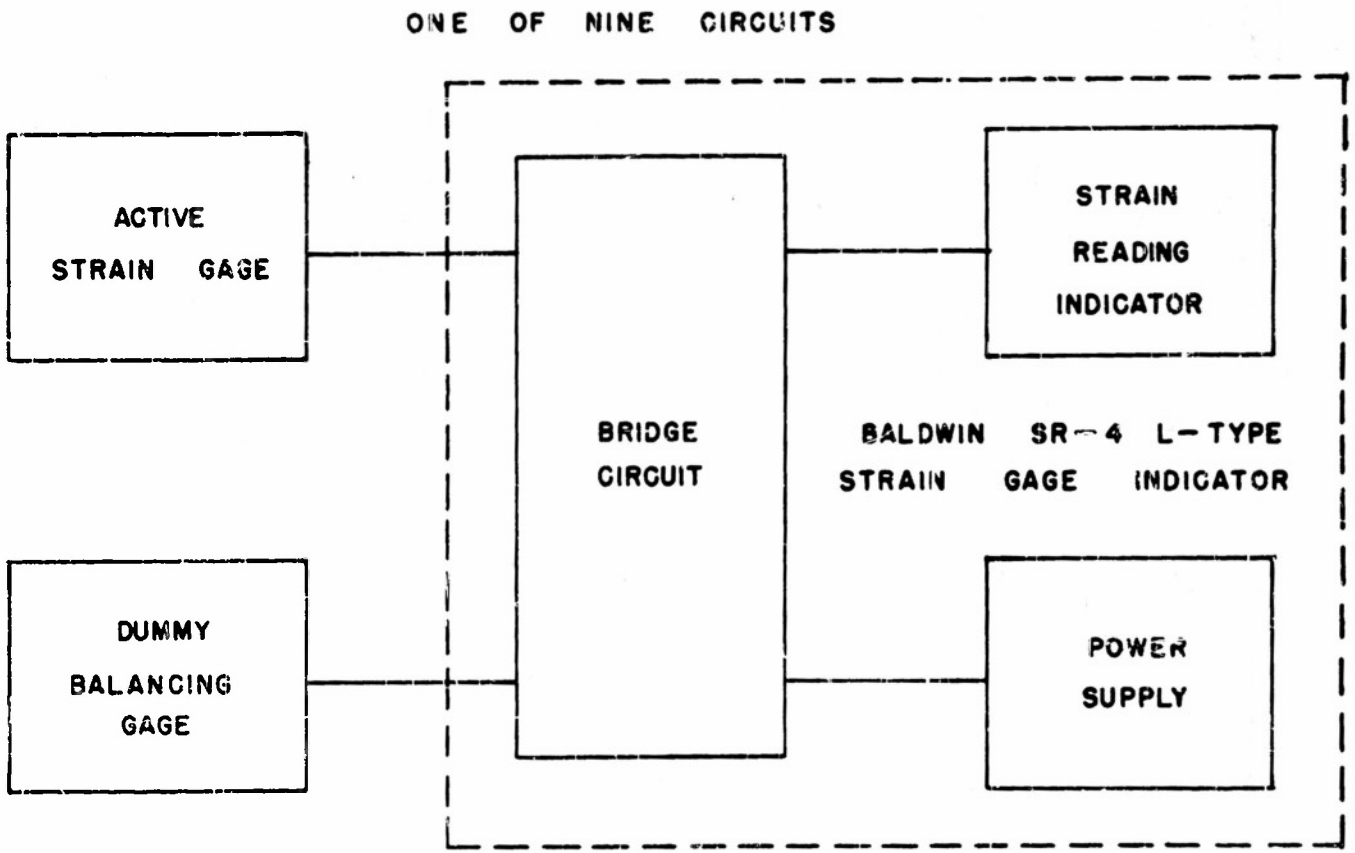

FIGURE 2.7 BLOCK DIAGRAM OF TYPICAL STRAIN GAGE MEASURING CIRCUIT

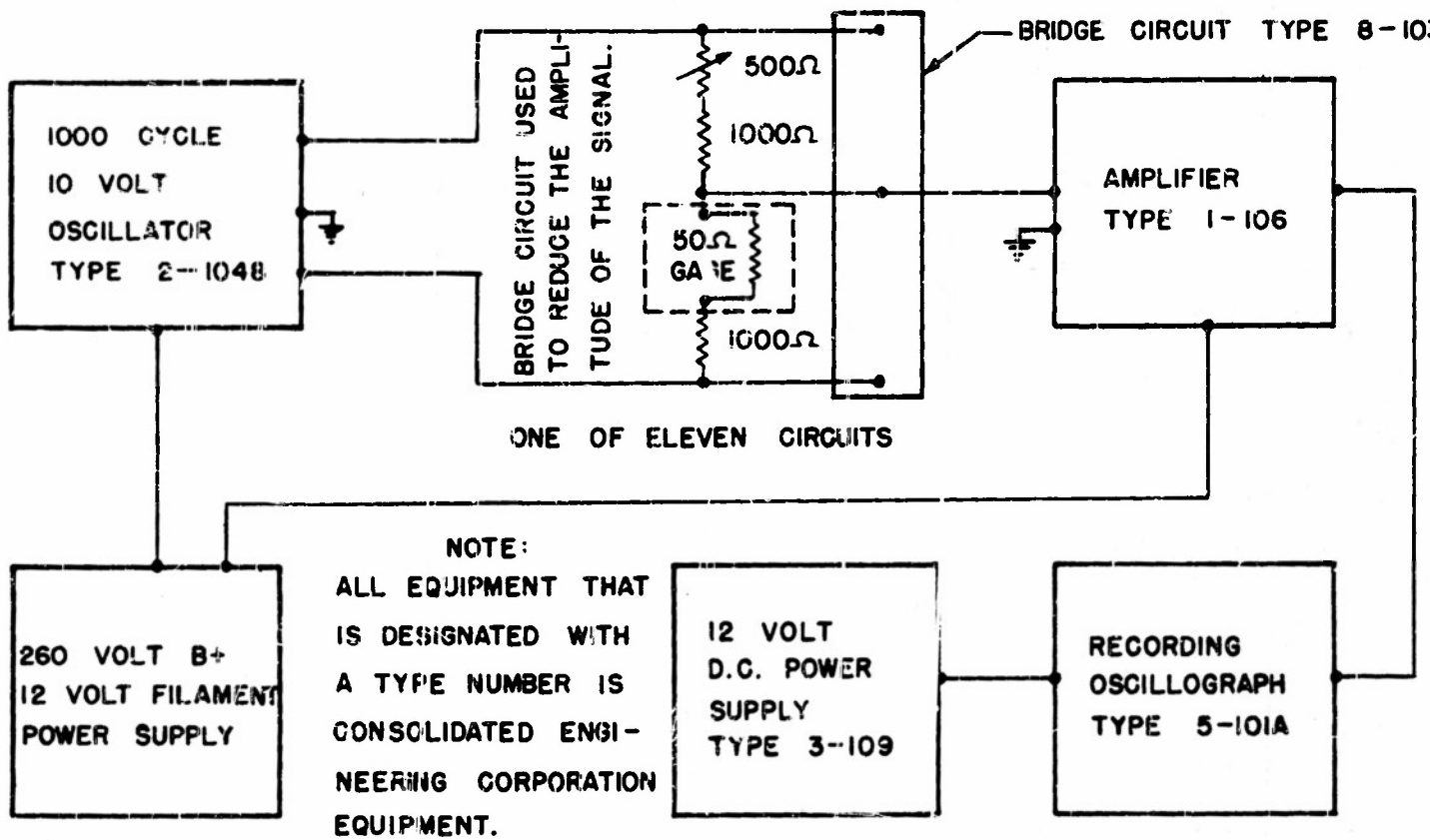

THE INJECTED CARRIER FROM THE OSCILLATOR WAS NOT USED. INSTEAD, THE BRIDGE CIRCUIT WAS SLIGHTLY UNBALANCED IN THE SAME DIRECTION THAT A TEMPERATURE RISE WOULD UNBALANCE THE BRIDGE CIRCUIT. THIS PERMITTED A LARGER DEFLECTION OF THE GALVANOMETER WITHOUT OVERLOADING THE AMPLIFIER.

FIGURE 2.8 BLOCK DIAGRAM OF TEMPERATURE RECORDING CIRCUIT

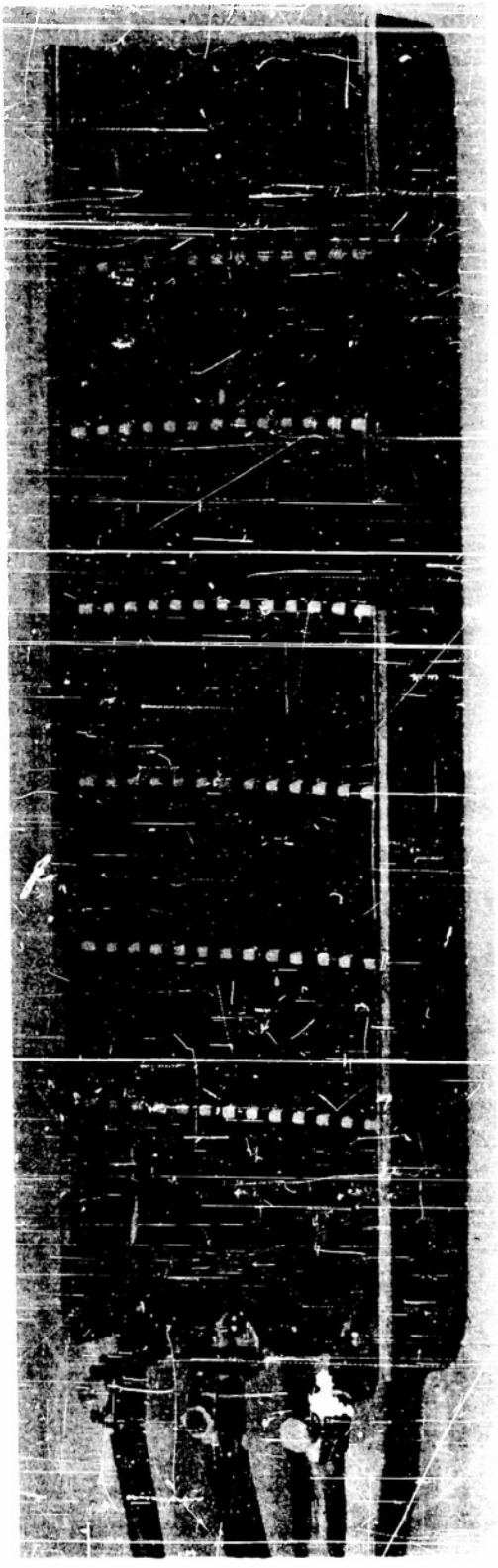

FIGURE 2.9 THE RADIANT HEATER

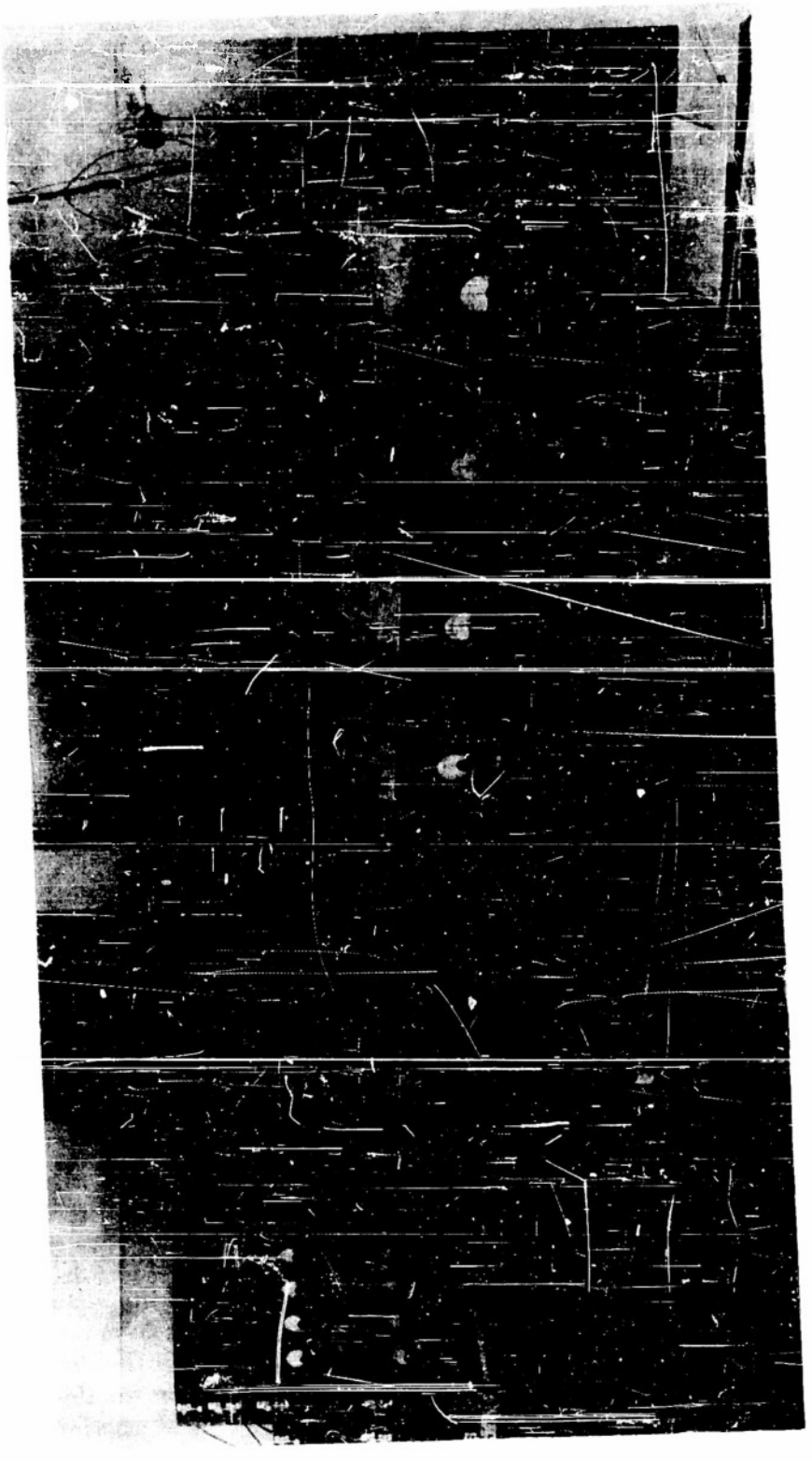

FIGURE 2.10 RECORDING EQUIPMENT

Previous tests showed the heater capable of suppiying up to 20,000 watts (Ref. 2). With above configuration, however, the heater supplied only 5,200 watts. The heater rested on a small table and was directly under the box beam with an average distance of 7/8 of an inch between the box beam and the heating coils (see Figure 2.1). The power output could have been increased either by connecting more nichrome heating coils in parallel in each branch of the three phase circuit, or by connecting the heater as a delta, three phase circuit. This increase proved unnecessary, however, since the desired maximum temperature of 400°F in the bottom skin of the model was obtained within two minutes of heating time for the heater in its present configuration. The power of 5.2 KW, supplied to the coils, is equivalent to approximately 5.0 BTU/sec of radiant heat energy on the assumption that there are no losses. The absorption by the model depends upon a number of factors such as absorptivity of the aluminum, the distance from coils to skin and convective losses. There is reason to believe that less than 50% of the electrical power input was absorbed by the model, but a more detailed analysis and experimental study of such losses was deemed beyond the scope of this investigation.

2.4 The Test Procedure

The peak temperature for any portion of the box beam was limited to 400°F because at higher temperatures the material properties begin to decrease very rapidly (see Figure 2.11). This limitation required the selection of a heating time which would not overheat any point of the model but which would still be of sufficient duration to induce appreciable thermoelastic effects. Calculations indicated that the bottom skin would reach 350°F in approximately one minute if all the electrical energy of the radiant furnace at its rated output of 5.2 kilowatts were absorbed by the bottom skin alone. A more realistic duration of two minutes was determined by the following simple experiment. A flat sheet of 24 S-T aluminum alloy was placed over the furnace and subjected to various heating durations. From measurements with copper constantin thermocouples mounted on the sheet, it was found that a period of approximately two minutes was required to raise the temperature of this test sheet to 350°F.

To define further the capabilities of the furnace, the aluminum test sheet was heated continuously until a steady-state condition was attained. This steady-state condition was reached after 8 minutes of heating time with the sheet at a final temperature of 650°F. In this experiment free convection took place, and the opposite side of the sheet radiated to the rest of the laboratory. Similar conditions do not prevail in a box beam since the interior surfaces are radiating to a relatively small volume and free convection in the interior is also restricted. The importance of heat transfer by radiation and convection in the interior of the box was investigated by comparing measured temperatures and strains for two different configurations, namely, an empty interior and an interior filled with batts of insulation.

An actual test run proceeded in the following manner: The power supplies

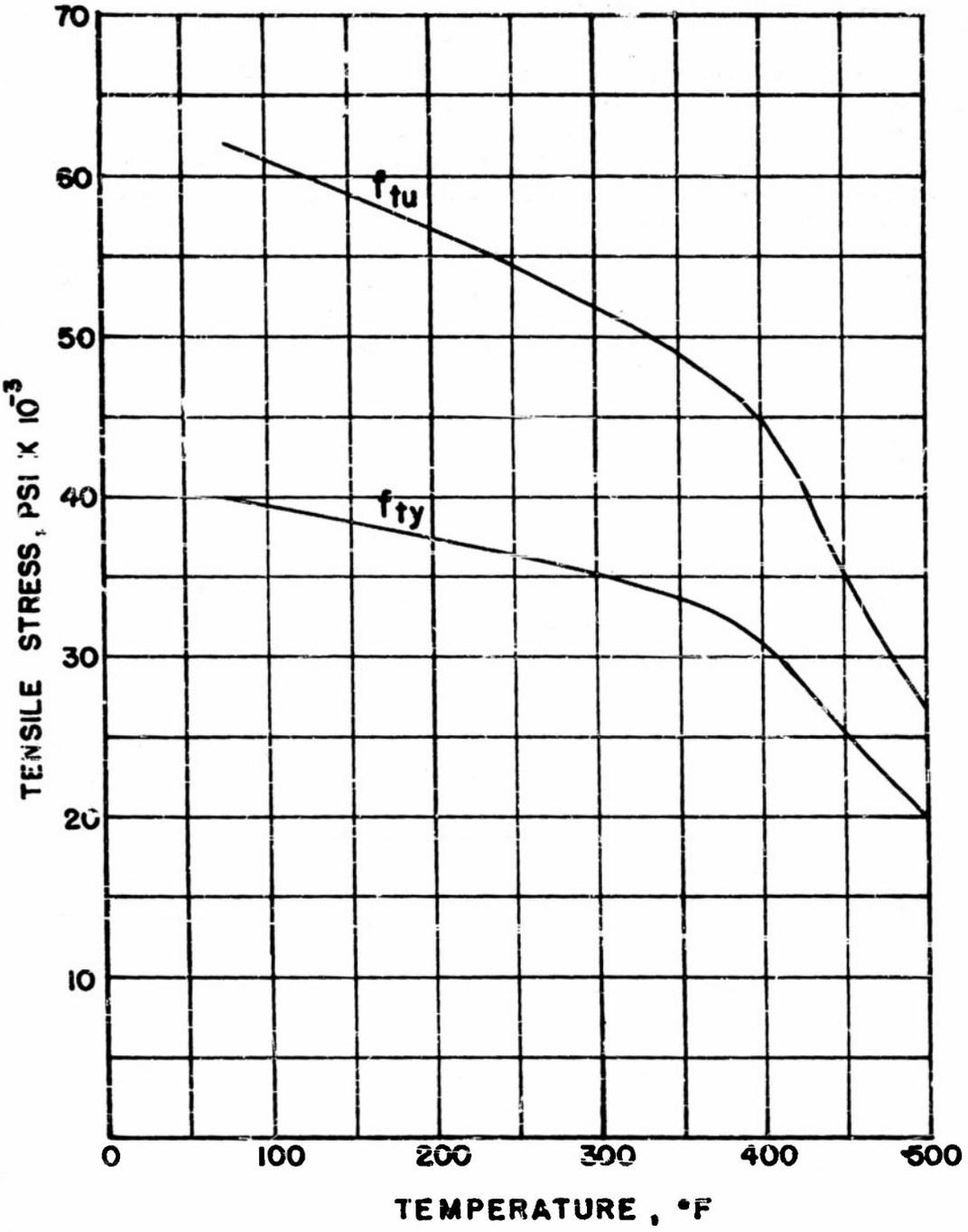

FIGURE 2.11 VARIATION OF ULTIMATE TENSILE STRESS AND YIELD STRESS WITH TEMPERATURE FOR 24 S-T ALUMINUM ALLOY FOR HALF AN HOUR HEATING TIME

to the test equipment were turned on to allow the equipment to warm up. The eleven channels of the temperature recording equipment were balanced at identical signal levels, and the room temperature displacements were recorded for each channel. The portable strain indicators were balanced, and their initial readings were recorded since these instruments are null devices. Only four of the nine strain gages on the model could be read during each test run because of limitations in the equipment available. It was found that the temperature and strain distributions were similar for each test run, and the strain readings used in the calculations are average strains for at least five test runs for each configuration. An asbestos insulating blanket was placed over the model and heater to minimize the effects of convection currents. Before each test run, the room temperature was read from a bulb thermometer and recorded. It was necessary to know the room temperature because it was the initial temperature of model which, in turn, was also the reference temperature for the temperature gages. As it happened, the room temperature remained almost constant during the test program. The model was insulated from the heater by a transite sheet placed between them until the heater reached the desired temperature. Then the transite was removed.

When all was in readiness, the power for the electric heater was turned on, and the dial gages attached to the model were watched for the initial deflection. As soon as they began to deflect, the transite insulating sheet between the model and the heater was withdrawn, and the timing period started. A stop watch was used to indicate ten second intervals during the two minute heating period; at these times the strain gages were read directly. An internal timing pulse was used to insert 10 second reference marks directly on the oscillograph film using the twelfth channel, while the other eleven channels were continuously recording the readings of the eleven temperature gages. At the end of the two minute heating cycle, the tip deflections of both dial gages were recorded. The power to the heater was shut off and an electric fan near the model was turned on to aid in cooling the model to room temperature. This process required a half an hour.

After the completion of tests on the model with and without the insulation, the temperature recording equipment was calibrated. Each of the eleven temperature gages on the model were replaced in the oscillograph channel circuits by a decade box. Then, known changes in resistance were applied through the amplifier circuits, and the corresponding deflections were recorded by the oscillograph for the same attenuations of the amplifiers that were used during the test runs. This procedure produced a relation between the change in galvanometer deflection and change in resistance for a particular attenuation. The deflections of all of the temperature gages during the test runs were converted to resistance changes, and since the initial temperature of the model was known, the total resistance could be determined. These total resistances were converted to temperatures by using the temperature gage calibration charts supplied by the manufacturer.

SECTION III

THE EXPERIMENTAL RESULTS

The experimental results consist of the readings obtained from eleven temperature gages and nine strain gages which were located at the mid-span station as shown in Figure 2.6. The strain readings were recorded directly in microinches whereas the temperatures, recorded in analogue form on oscillograph paper, had to be converted into temperatures by calibration charts.

3.1 The Temperature Distribution

Figures 3.1 and 3.2 present the transient temperature curves for the eleven temperature gages with uninsulated and insulated box-beam interiors, respectively. The same data is tabulated in Table A.2. A comparison of the two figures shows that the temperatures for the uninsulated Configuration 1 are approximately seven to twelve degrees higher than those at corresponding points on the insulated Configuration 2 at the end of heating period. The smallest differences both in absolute and percentage terms occurred along the bottom skin. On the other hand, the top skin with the smallest temperature increases had the largest differences both in absolute terms and in terms of the percentage of the temperature rise. Thus, the rock wool insulation appears to have two effects: (1) the prevention of heat transfer across the interior whether by radiation or convection and (2) the retention of a portion of the thermal energy which it receives from the interior surfaces of the box through conduction and radiation, i.e., a heat sink. The first effect would account for the fact that the temperature differences produced by the insulation are larger in the top skin than in the bottom skin. In the uninsulated case, heat reaches the top skin by conduction, convection and radiation, and the addition of the insulation suppresses the latter two modes of heat transfer.

Figures 3.3 and 3.4 show the time variation of the temperature distribution in the web of the box beam for Configurations 1 and 2, respectively. Figures 4.16 and 4.17 present composite curves of the temperature distribution in the model for the insulated case at four different times. These curves are plotted in a peripheral coordinate system which originates at the mid-point of the bottom skin. The increments of temperature increase, ΔT , are plotted instead of the absolute values of the temperature, and an assumed mode of temperature is also plotted for purposes of comparison (see Section IV).

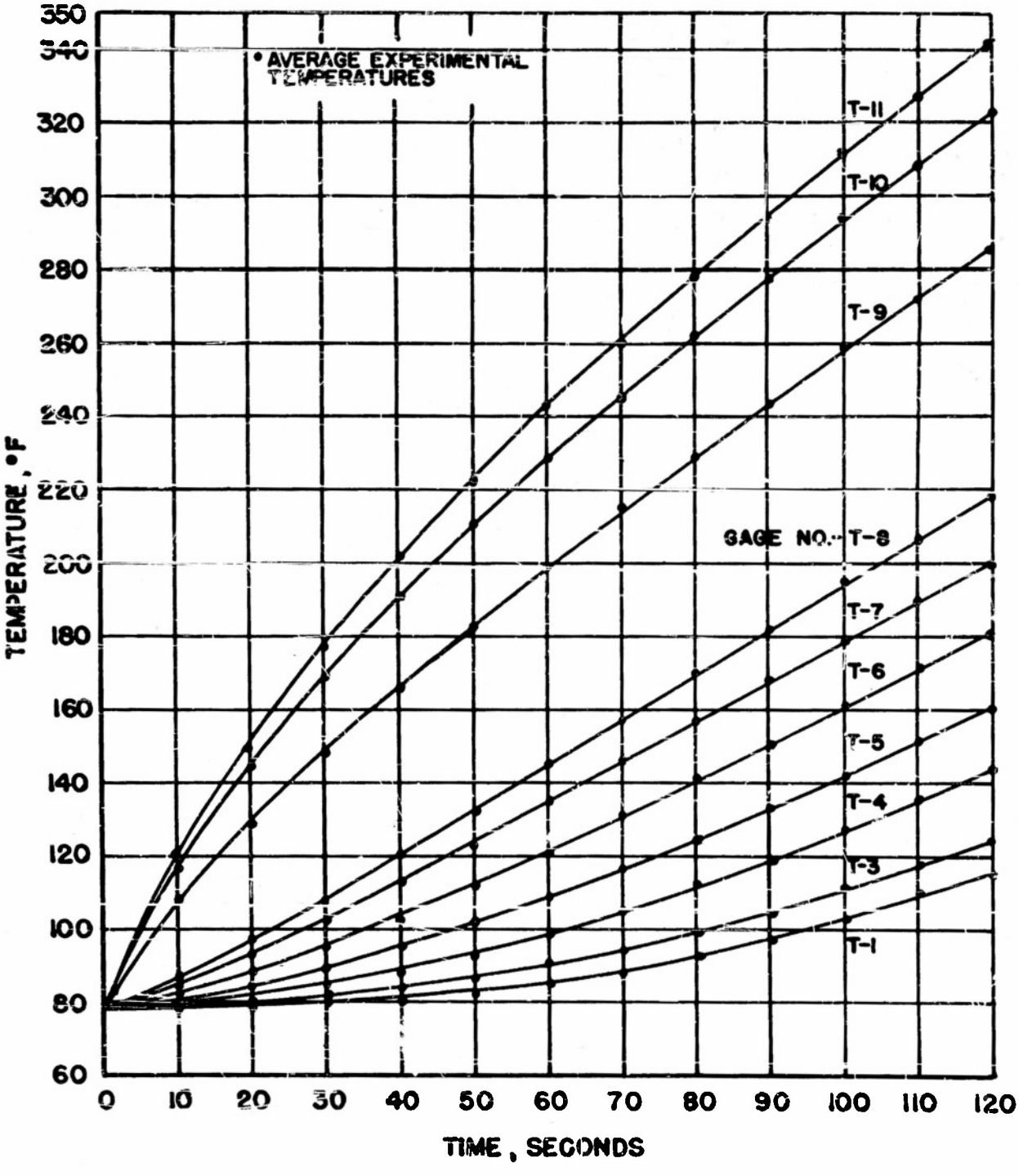

FIGURE 3.1 VARIATION OF TEMPERATURE VS TIME FOR CONFIGURATION 1, (NO INSULATION)

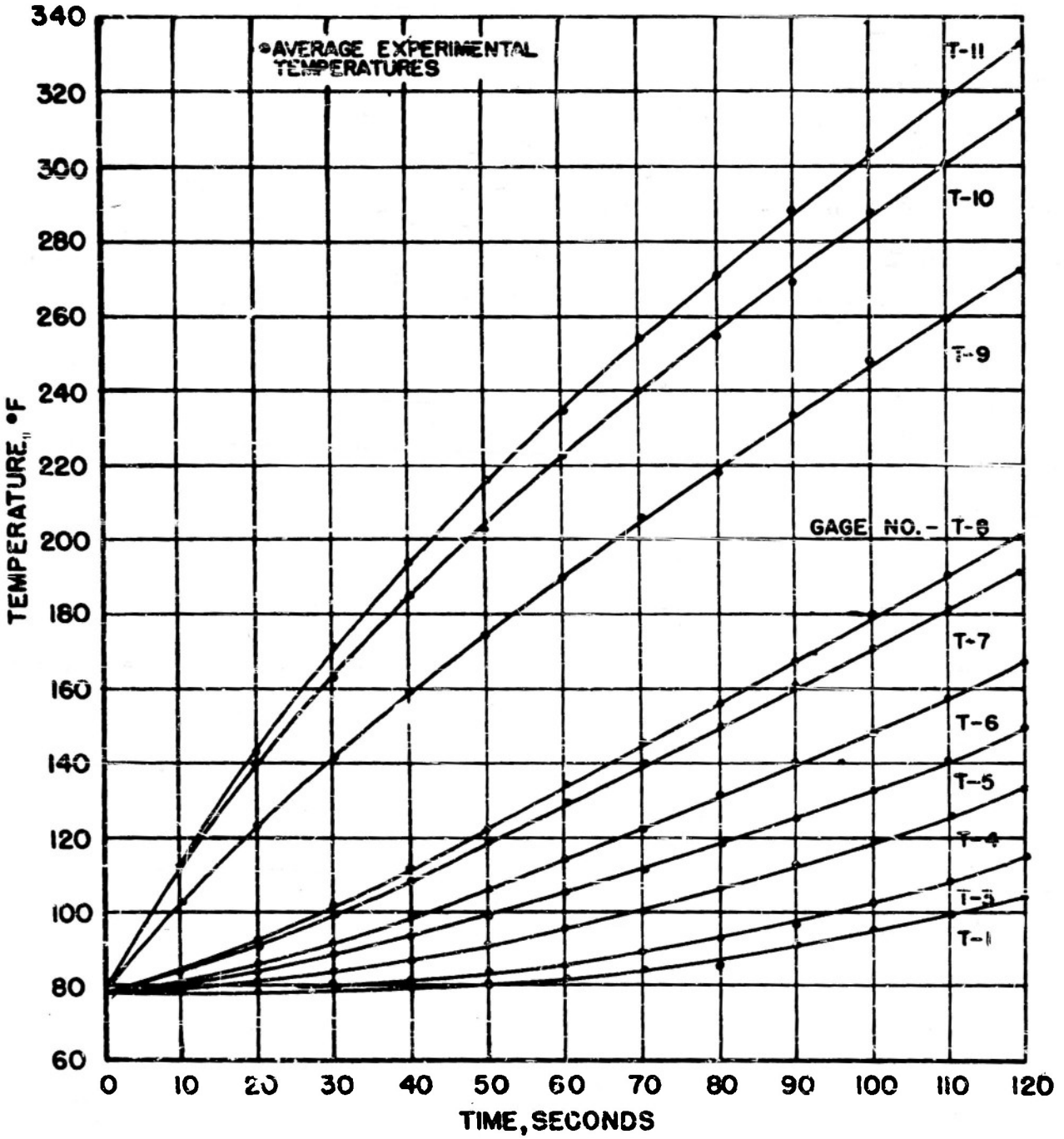

FIGURE 3.2 VARIATION OF TEMPERATURE VS TIME FOR CONFIGURATION 2, (ROCK WOOL INSULATION)

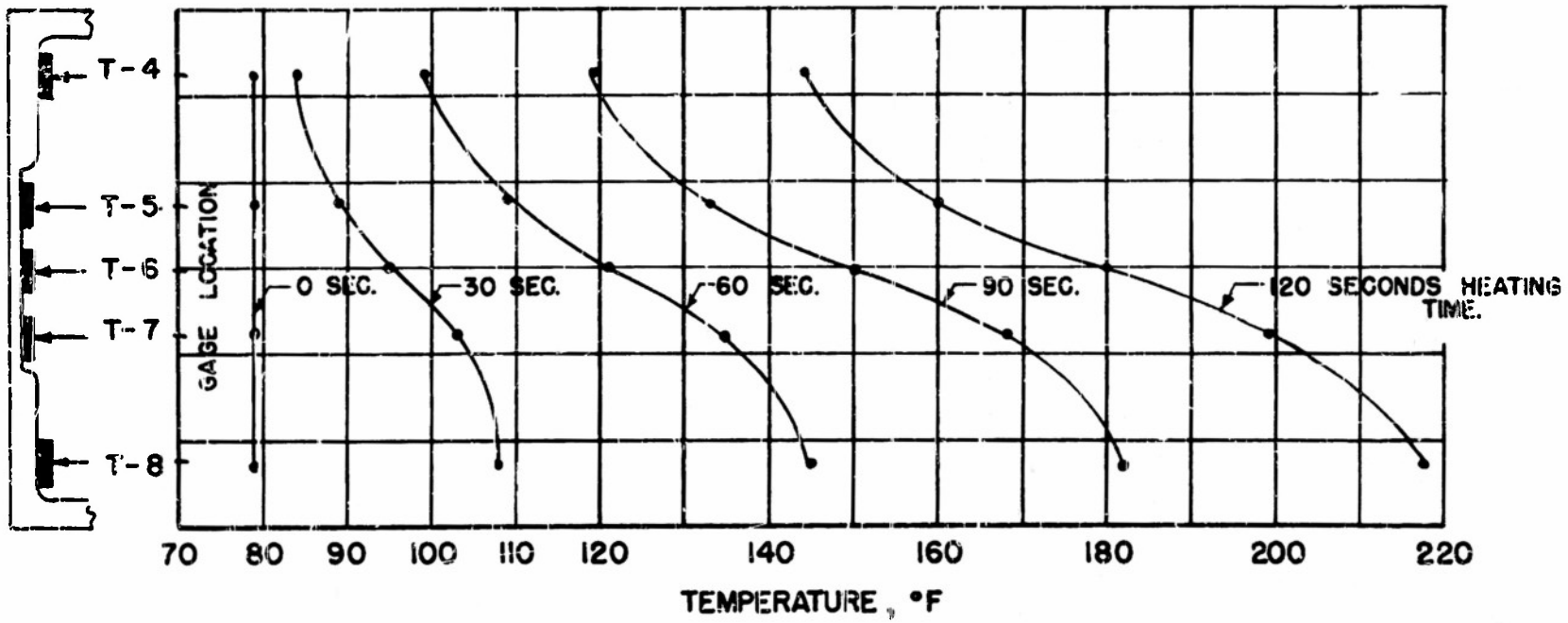

FIGURE 3.3 TEMPERATURE DISTRIBUTION IN WEB AT VARIOUS HEATING TIMES FOR CONFIGURATION 1 (NO INSULATION)

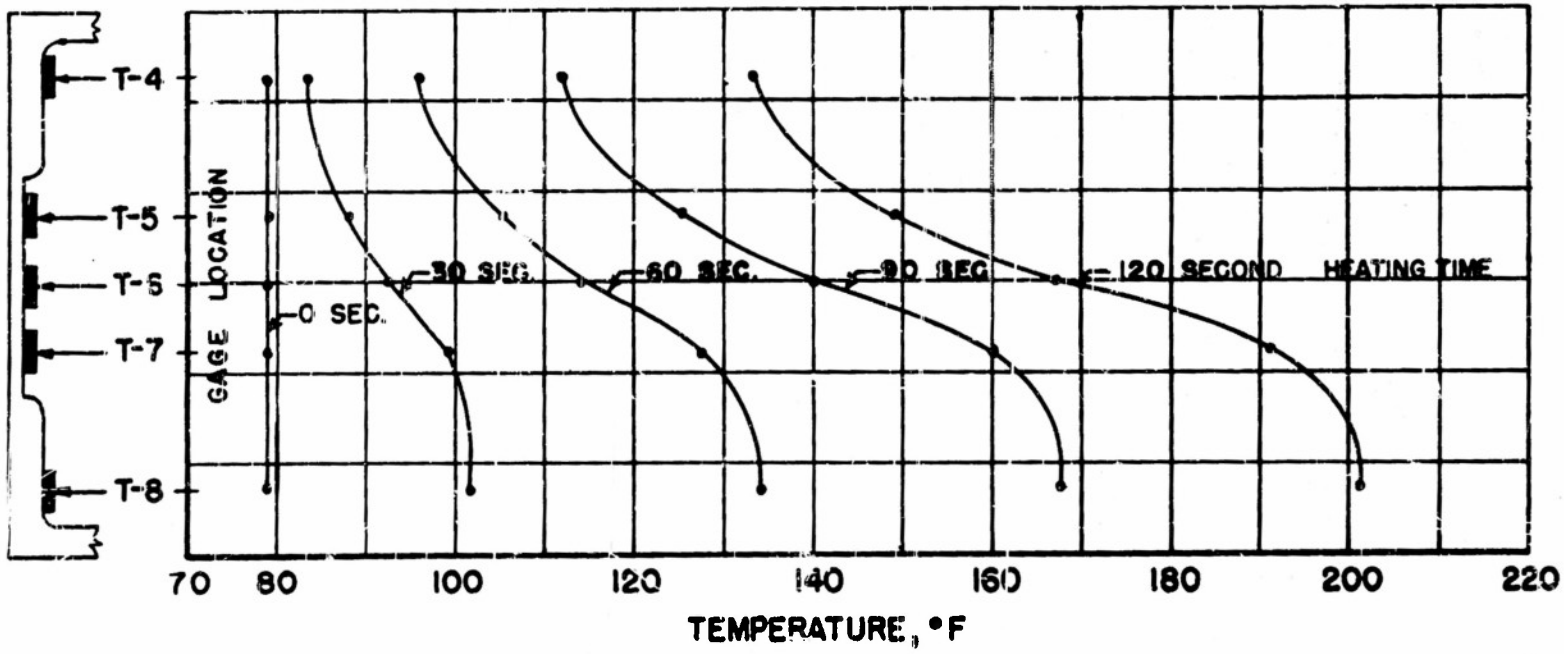

FIGURE 3.4 TEMPERATURE DISTRIBUTION IN WEB AT VARIOUS HEATING TIMES FOR CONFIGURATION 2 (ROCK WOOL INSULATION)

3.2 The Distribution of the Strain due to Stress

Figures 3.5 and 3.6 give the experimental time variation of the stress at the nine strain gage locations for the two configurations. The same data is tabulated in Table A.3. The largest strains are compressive and occur in the bottom or heated skin. The largest tensile strains occur in the web.

The time variation of the strain distribution in the web is shown in Figure 3.7. For the first 50 seconds, the strain distribution is essentially linear, but after that time interval, the distribution in the web becomes increasingly complex. If, however, only a narrow portion at the center of the web is considered, i.e., the middle 1.20 inches, the strain distribution is observed to progress from a linear distribution to a gradually curved distribution. The character of the strains changes rather drastically in the distance between this central portion and the flanges. Zero strain, however, occurs at about the same point for all times. Figure 3.8 presents the time variation of the strain distribution in the bottom skin. If a linear distribution is assumed, the strains at various times intersect at approximately the same location.

3.3 The Deflection at the Free End

The fact that the readings of the two dial gages never differed more than 0.002 inches affords evidence that only negligible twisting of the model occurred during the test runs. This agreement between the gages gives a fairly good indication that the temperature distribution in the beam was symmetrical about the vertical center line, although the evidence is not conclusive. Also, the maximum displacement at the end of each run was within 0.005 inches of the average for all runs. The average displacement for Configuration 1 was 0.168 inches and for Configuration 2, 0.161 inches. This evidence, together with the close agreement of the measured temperatures, offers a fairly good indication that the test conditions were duplicated in the series of runs required by the limited number of strain reading devices (see Section 2.4).

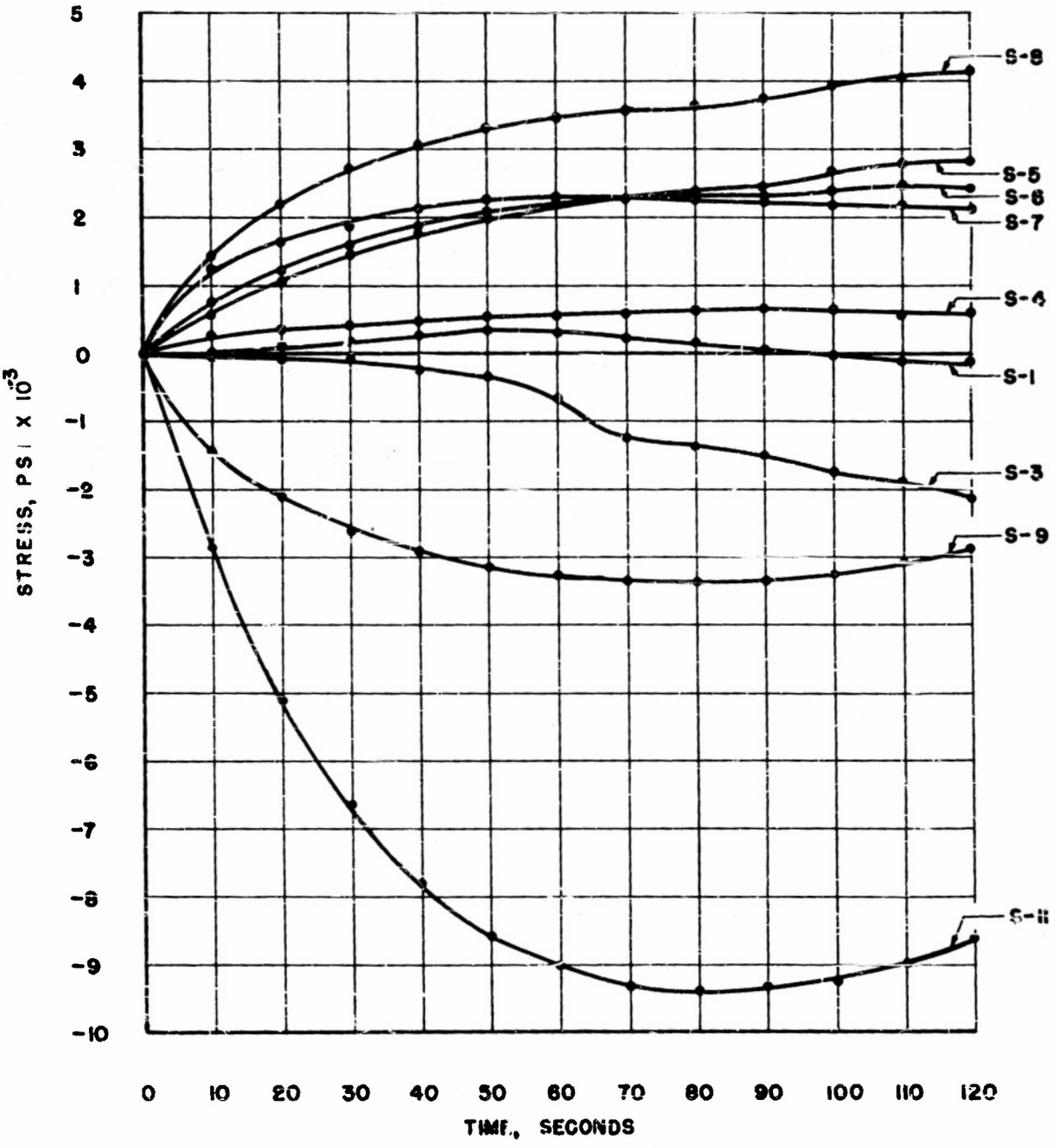

FIGURE 3.5 EXPERIMENTAL TIME HISTORY OF STRESS AT STRAIN GAGE LOCATIONS, CONFIGURATION 1

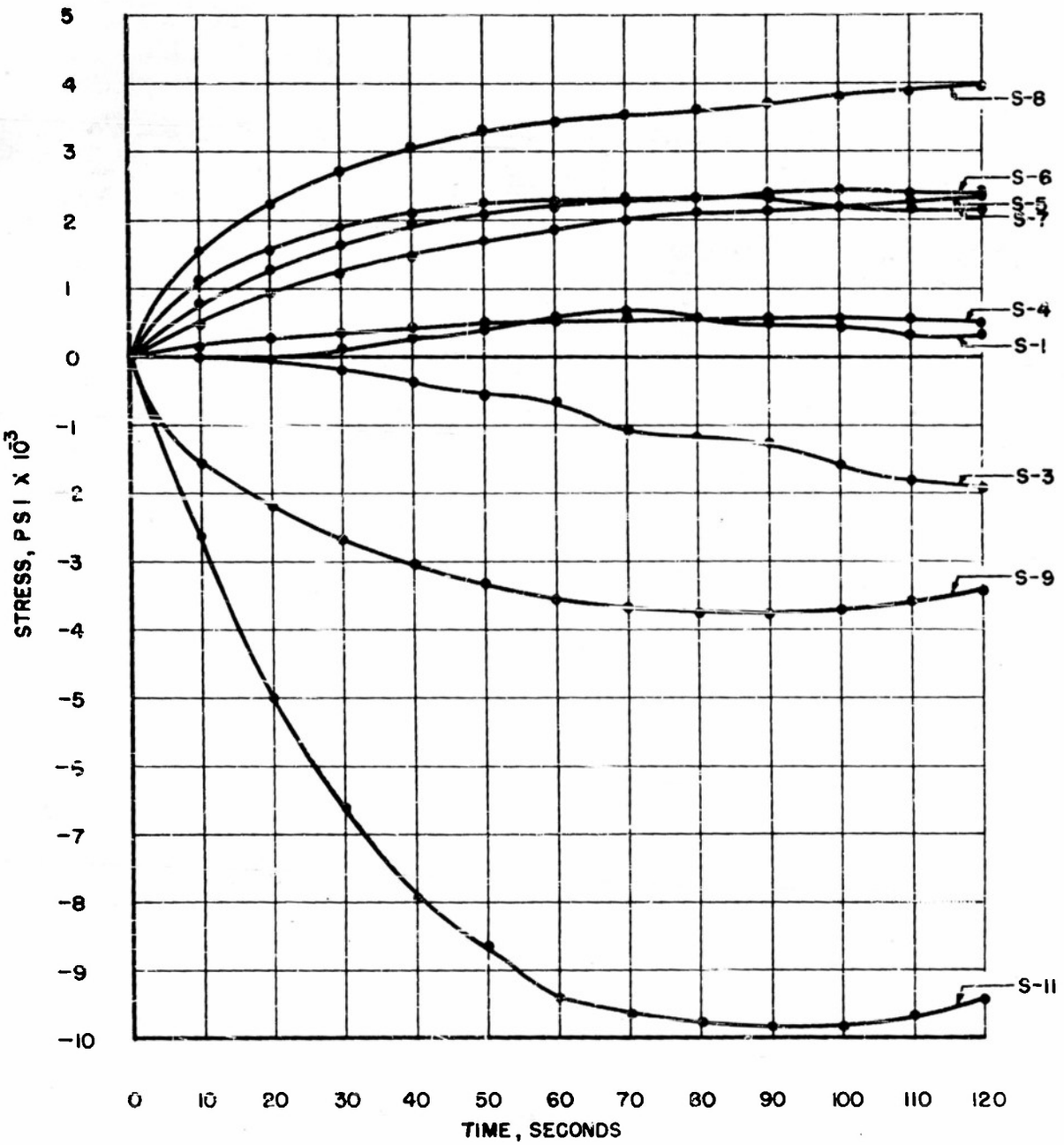

FIGURE 3.6 EXPERIMENTAL TIME HISTORY OF STRESS AT STRAIN GAGE LOCATIONS, CONFIGURATION 2

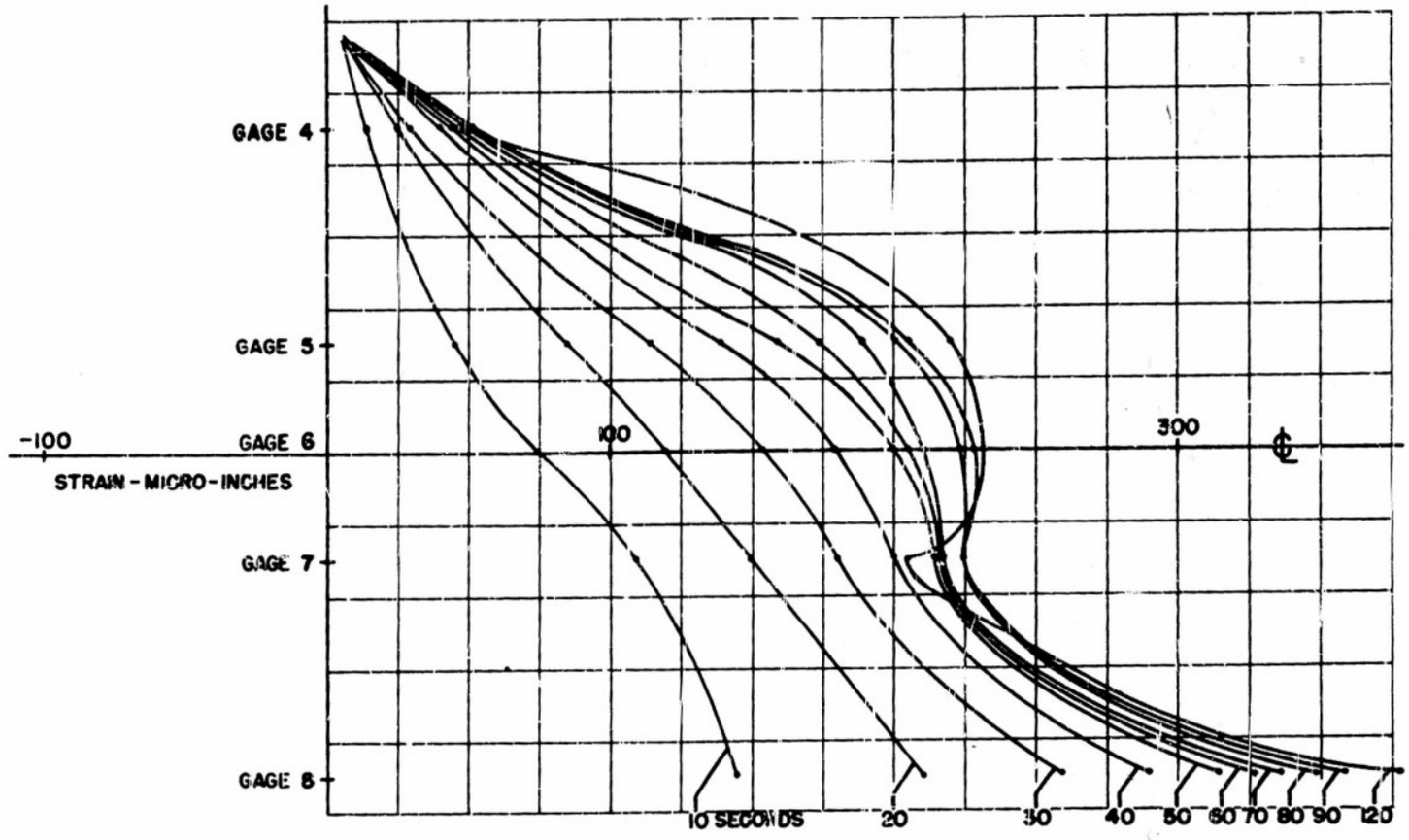

FIGURE 3.7 DISTRIBUTION OF STRAIN DUE TO STRESS IN WEB AT VARIOUS TIMES

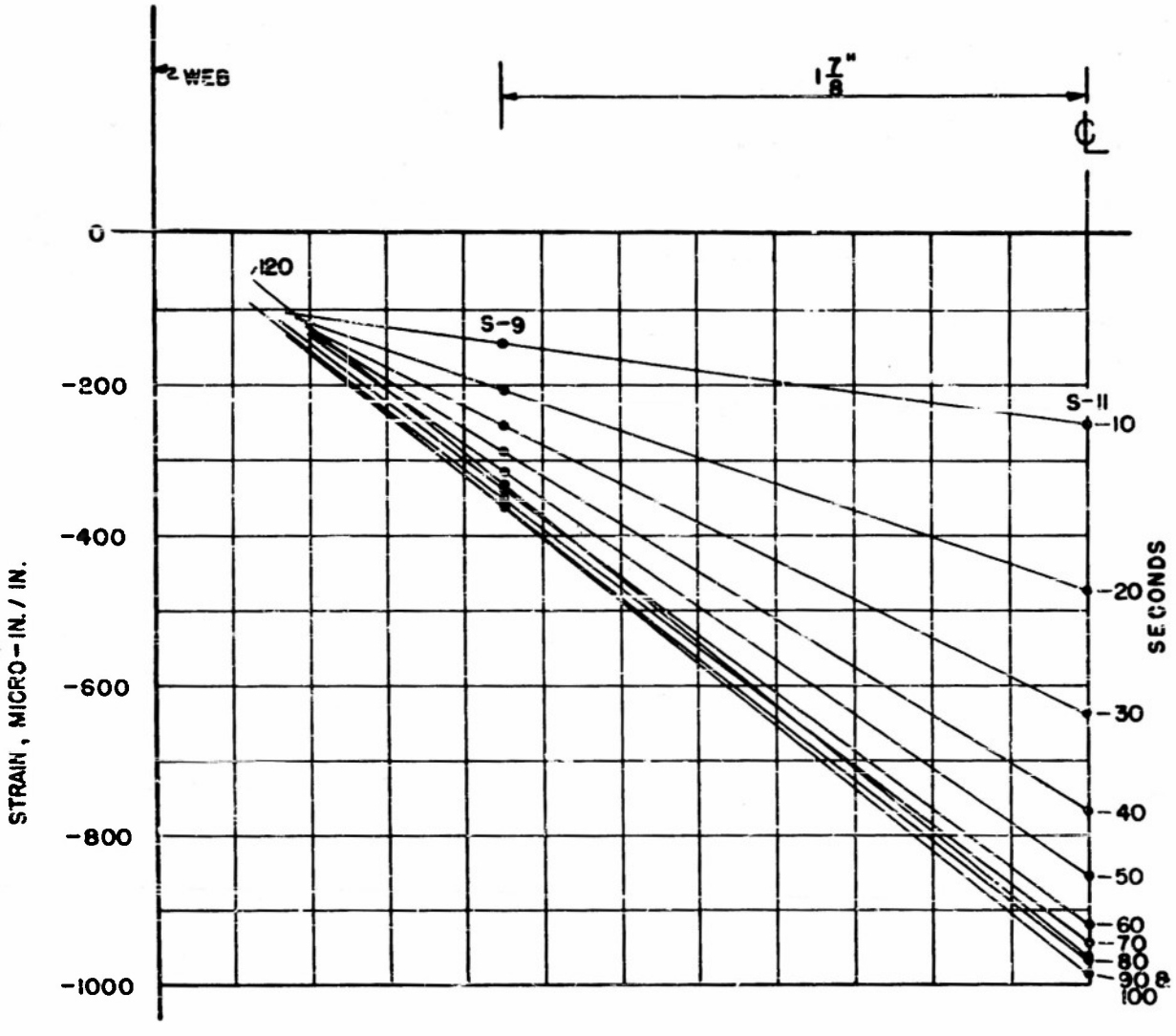

FIGURE 3.8 DISTRIBUTION OF STRAIN DUE TO STRESS IN BOTTOM SKIN AT VARIOUS TIMES

SECTION IV

ANALYSIS OF RESULTS

In principle, the calculation of the three-dimensional distribution of thermal stress is simple if the temperation variation in the structure has been determined. For practical reasons, it is desirable and, indeed, often necessary to idealize the problem to an extent that there are minor effects superimposed upon a major effect. These minor effects are then ignored.

The stress measurements in these experiments were taken at the mid-span section so as to minimize the effects of the root and the free end of the cantilever beam. The idealized analytical structure is an infinitely long beam which, of course, cannot be attained in the laboratory. Instead, St. Venant's Principle must be invoked.

The gages were oriented so as to measure stresses in the spanwise direction and, hence, chordwise stresses were ignored. In addition, the gages were placed on only one side of the skin. This procedure assumes that there is no stress gradient across the skin thickness. The assumptions which have been described here are those made for the elementary theory of the bending of beams.

The analysis of the experimental results will be considered from the following three viewpoints:

4.1 Elementary beam theory

4.2 Distortion of the cross section

4.3 Spanwise effects.

4.1 Elementary Beam Theory

Timoshenko and Goodier (Ref. 18) describe the physical reasoning involved in the deduction of a simple theory about thermal stresses. In this simplified theory as presented for application to the experimental results, it is necessary to assume: (a) that the temperature distribution is symmetrical about the Z-axis (see Figure 4.1) and (b) that the temperature distribution is not a function of the spanwise coordinate. Thus, the change in temperature can be written as

$$\Delta T = \Delta T(S)$$

where S is a peripheral coordinate.

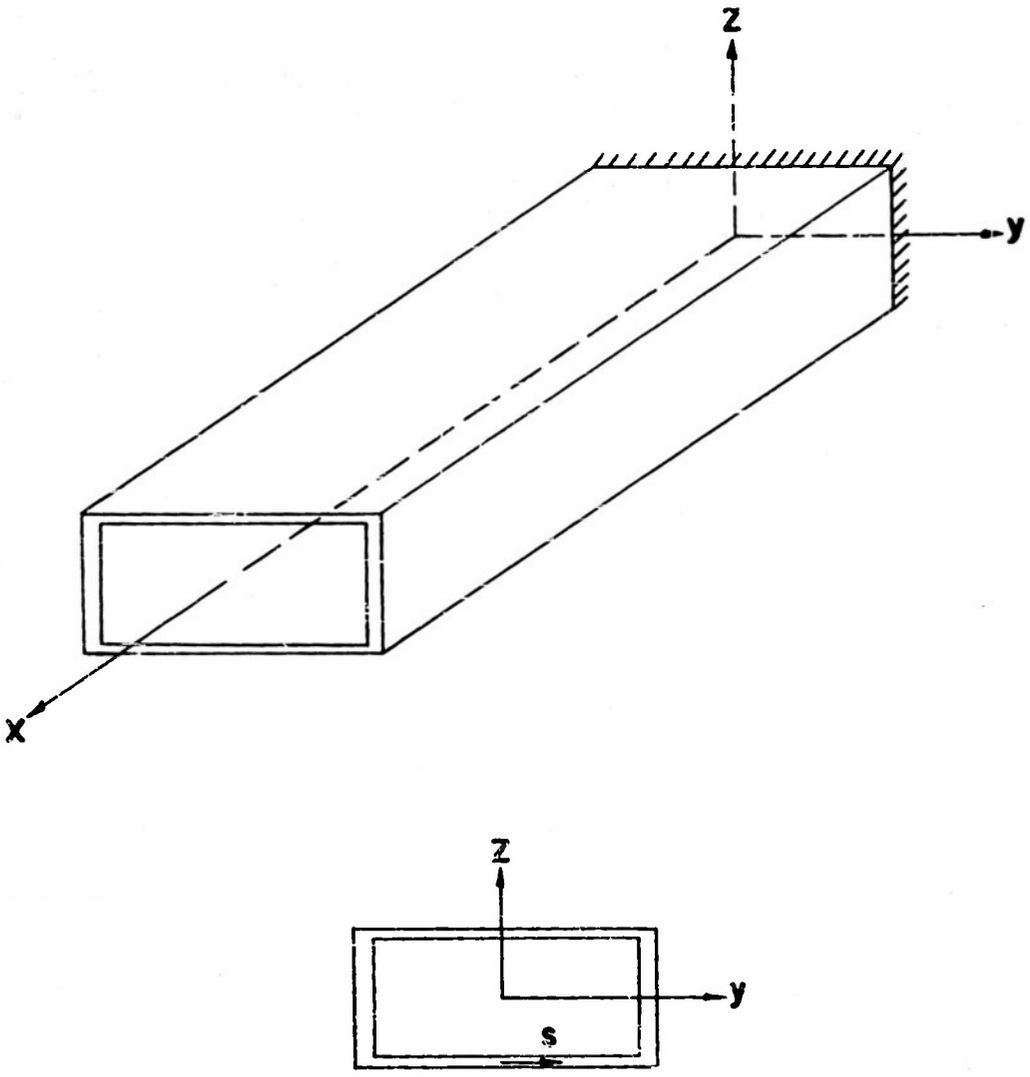

FIGURE 4.1 COORDINATES USED IN ANALYSIS

The behavior of the beam in adjusting its distortion and internal stresses to a certain temperature distribution is explained as follows:

(1) Each element of the beam is allowed to expand freely as the cross section attains some particular temperature distribution above the ambient value. At this stage, the beam is regarded essentially as an assemblage of independent elements which were initially fitted together in the shape of a beam.

(2) In order to fit the elements together again, stresses sufficient to compress the elements back to their original sizes and shapes are applied. As in the elementary beam theory, it is assumed that the important distortions and stresses are those in the spanwise direction. Hence, only the spanwise temperature distortions are considered, and the important compressive stresses which need to be applied are those in the spanwise direction. These stresses are denoted as follows:

$$\sigma_{x,1}(S) = -E(T)\bar{\alpha}\Delta T(S) \tag{4.1}$$

where

E is Young's modulus which is a function of the temperature,

$\bar{\alpha}$ is the coefficient of thermal expansion which is a function of the temperature,

ΔT is the temperature rise above the ambient value.

(3) The beam can now be re-assembled, but the force equilibrium of the beam has been disturbed by the application of the compressive stresses described above. To restore equilibrium, a fictitious axial load and bending moment, statically equivalent but opposite in character to the summation and moment of the compressive stresses across the cross section, must be applied to the free end of the beam. On the basis of St. Venant's Principle, the local effects of the force and moment are deemed negligible at cross sections not in the immediate vicinity of the points of application.

(4) The stress distribution at cross sections far removed from the root and the free end is obtained by the superposition of the effects described in (2) and (3) above as follows:

$$\sigma_x(S) = \sigma_{x,1} + \sigma_{x,2} + \sigma_{x,3} \tag{4.2}$$

where

$$\sigma_{x,2} = \frac{F}{A} \tag{4.3}$$

$$\sigma_{x,3} = -\frac{Mz}{I_y} \tag{4.4}$$

F is the statically equivalent axial load of opposite character

M is the statically equivalent bending moment of opposite character

A is the cross-sectional area

I_y is the moment of inertia of cross section about the y-axis.

The axial load, F , and bending moment, M , applied at the free end, are obtained from the following expressions:

$$F = -\int_A \sigma_{x,1}\, dA = \int_A E\bar{\alpha}\,\Delta T\, dA \tag{4.5}$$

$$M = -\left[-\int \sigma_{x,1}\, z\, dA\right] = -\int_A E\bar{\alpha}\,\Delta T\, z\, dA \tag{4.6}$$

For purposes of calculation, it is necessary to replace the integral over the cross section by a summation because the experimentally determined temperature distribution, $\Delta T(S)$, cannot be written easily in analytical form. The cross section of the experimental box beam was divided into forty-two elements (see Figure 4.2). Only twenty-one had to be considered because of the model symmetry and the assumed temperature symmetry about the Z-axis. The expressions for the three components of the total stress are

$$(\sigma_{x,1})_i = -E\bar{\alpha}\Delta T_i \tag{4.7}$$

$$(\sigma_{x,2})_i = \frac{1}{A}\sum_{i=1}^{21} 2\cdot E\bar{\alpha}\Delta T_i \tag{4.8}$$

$$(\sigma_{x,3})_i = -\frac{z_i}{I_y}\sum_{i=1}^{21} 2\cdot E\bar{\alpha}\Delta T_i z_i \tag{4.9}$$

where the subscript, i , denotes each element. The values for $\bar{\alpha}$ and E were corrected for temperature as shown in Figure 4.3.

The stresses as calculated from the above expressions are tabulated in Table A.4. It must be remembered that the temperatures used in these calculations were extrapolated and interpolated from eleven measured temperatures.

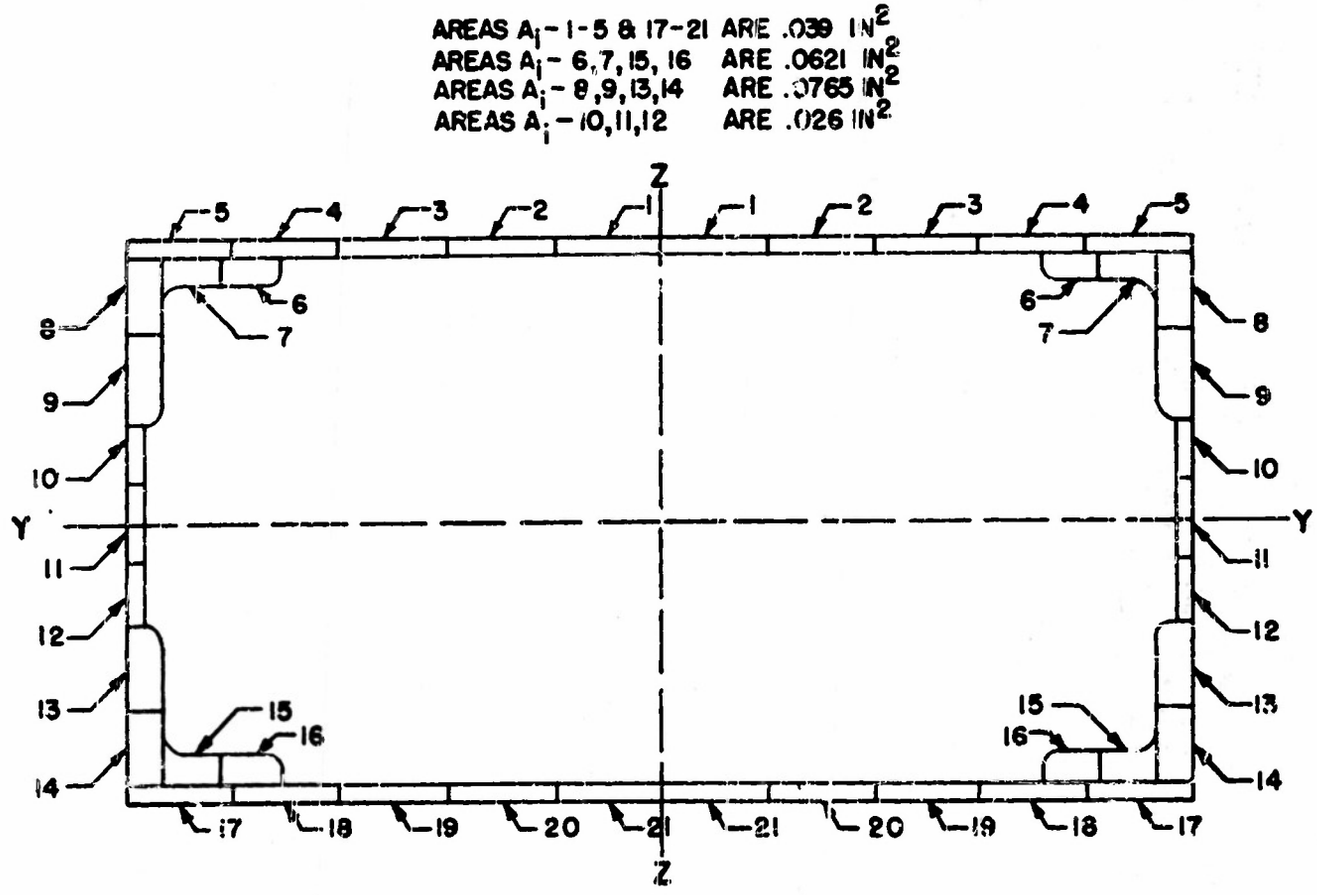

FIGURE 4.2 NUMBERING SYSTEM USED TO INDICATE THE INCREMENTAL AREAS, a_i ; IN THE ANALYTICAL METHOD

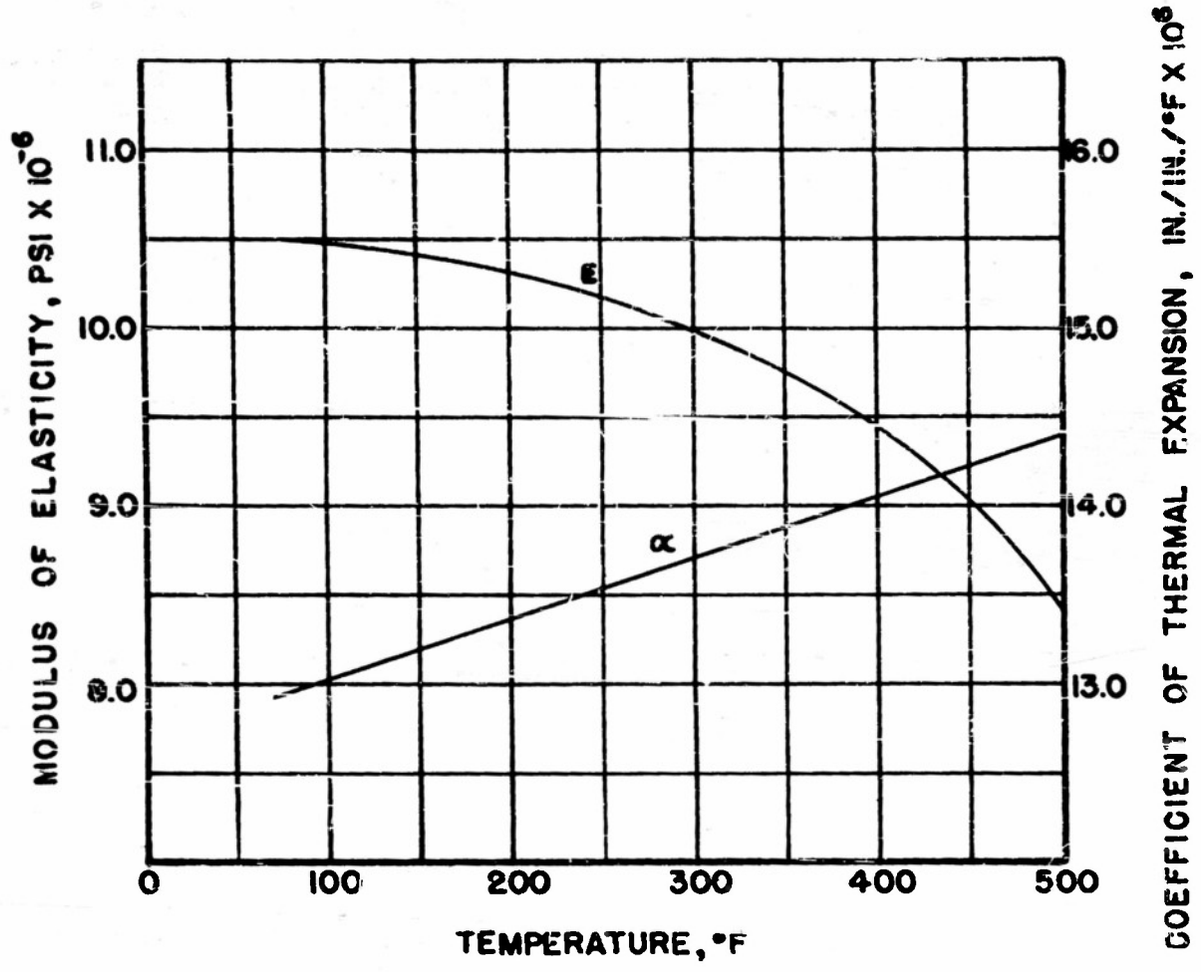

FIGURE 4.3 VARIATION OF MODULUS OF ELASTICITY AND COEFFICIENT OF THERMAL EXPANSION OF 24 S-T ALUMINUM ALLOY VS TEMPERATURE

These calculated stresses together with the experimental values are shown for heating times of 30, 60, 90 and 120 seconds in Figures 4.4, 4.5, 4.6 and 4.7 for Configuration 1 and in Figures 4.8, 4.9, 4.10 and 4.11 for Configuration 2. The agreement in the bottom skin is fair while the agreement in the web is poor.

4.2 The Distortion of the Mid-Span Cross Section

If the box beam is visualized as a collection of closed rigid frames (see Figure 4.12), then the existence of a temperature change can be seen to cause a distortion of the rigid frame. Since the rigid frame is an indeterminate structure, this distortion will induce both axial stresses and bending stresses. In this case, the terms, "axial stresses" and "bending stresses", are to be considered with reference to the behavior of the rigid frame.

The concept of an elastic center together with the superposition equations will be used in this analysis (see Ref. 14). These superposition equations are applied to the primary structure (see Fig. 4.13) which is statically determinate.

$$\begin{bmatrix} \delta_{aa} & \delta_{ab} & \delta_{ac} \\ \delta_{ba} & \delta_{bb} & \delta_{bc} \\ \delta_{ca} & \delta_{cb} & \delta_{cc} \end{bmatrix} \begin{bmatrix} X_a \\ X_b \\ X_c \end{bmatrix} + \begin{bmatrix} \delta_{aT} \\ \delta_{bT} \\ \delta_{cT} \end{bmatrix} = 0 \qquad (4.10)$$

where

X_a, X_b, X_c, are the redundant bending moment, axial load and shear force which act at the elastic center (see Figure 4.13)

δ_{mn} is the relative displacement of the points of application of redundant m due to a unit value of redundant n

δ_{mT} is the relative displacement of the points of application of redundant m due to the temperature distribution, $\Delta T(s)$.

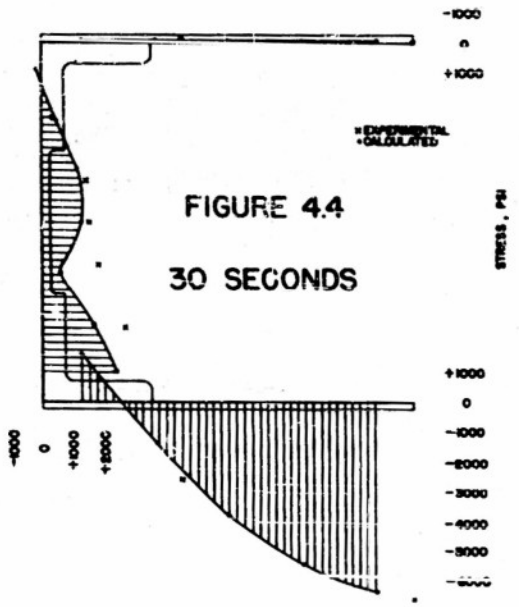

FIGURE 4.4

30 SECONDS

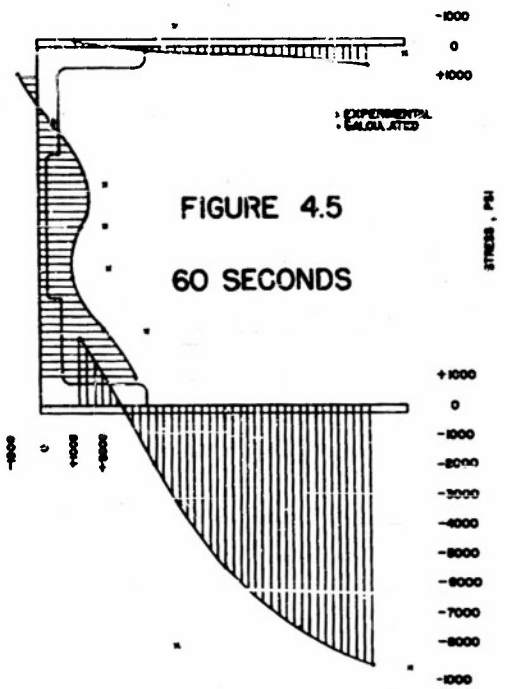

FIGURE 4.5

60 SECONDS

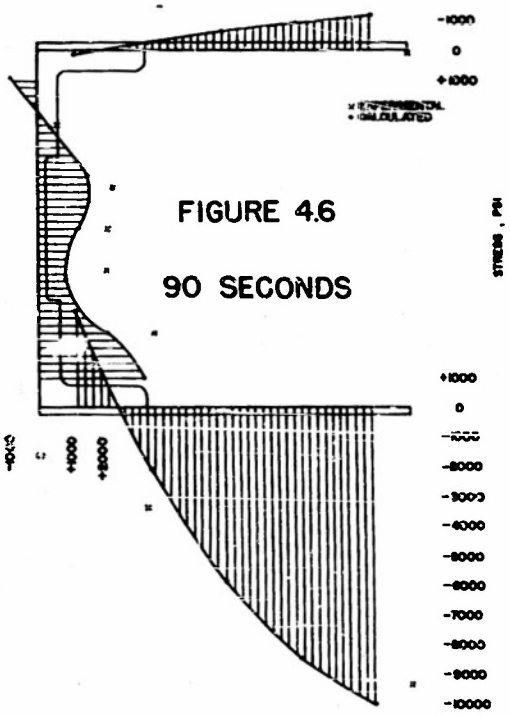

FIGURE 4.6

90 SECONDS

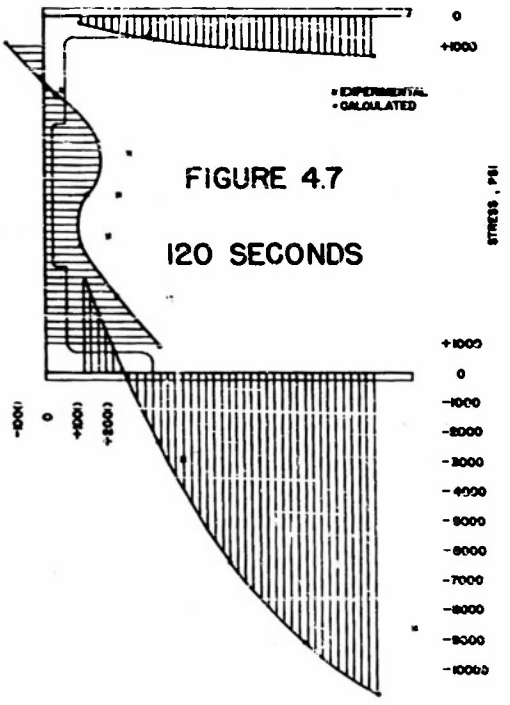

FIGURE 4.7

120 SECONDS

COMPARISON OF ANALYTICAL AND EXPERIMENTAL STRESSES - CONFIGURATION 1

(Note: Stresses are plotted normal to the center line. Compressive stresses are plotted on the outside of the cross section, tensile stresses on the inside.)

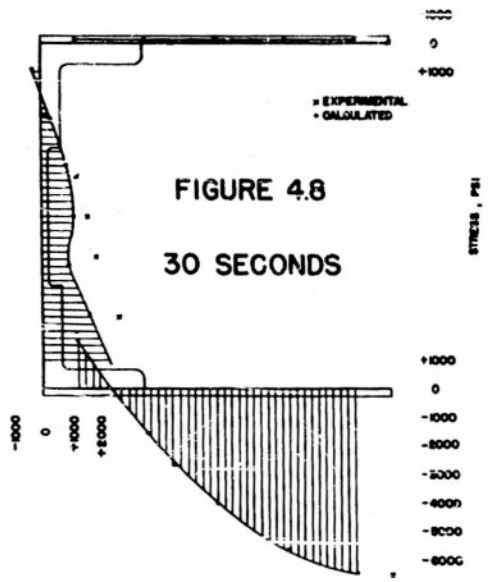

FIGURE 4.8

30 SECONDS

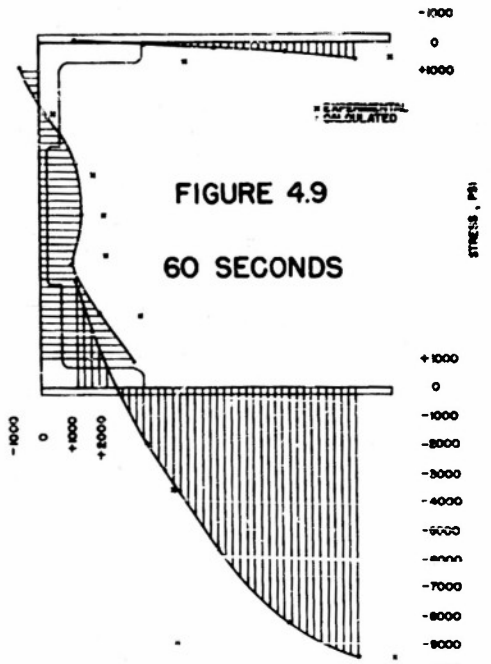

FIGURE 4.9

60 SECONDS

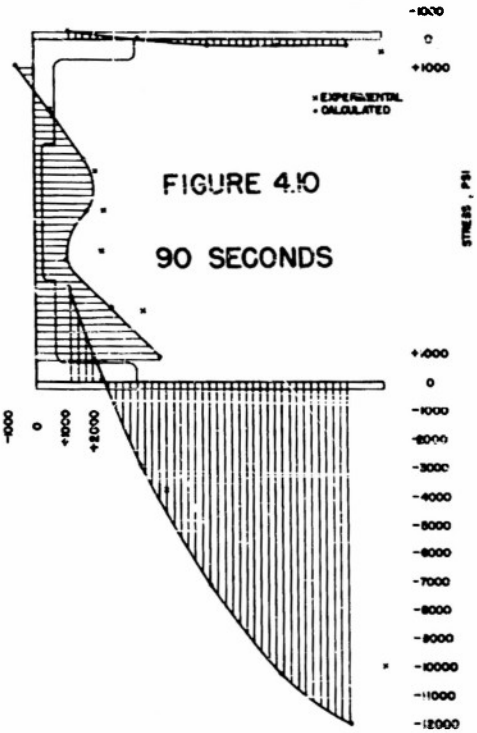

FIGURE 4.10

90 SECONDS

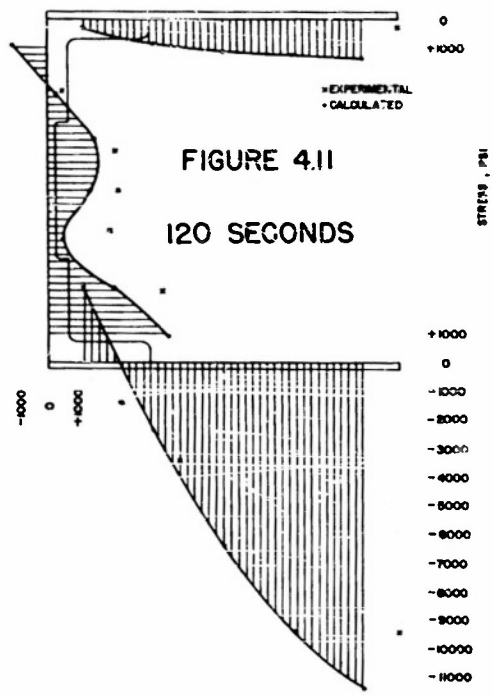

FIGURE 4.11

120 SECONDS

COMPARISON OF ANALYTICAL AND EXPERIMENTAL STRESSES - CONFIGURATION 2

(Note: Stresses are plotted normal to the center line. Compressive stresses are plotted on the outside of the cross section, tensile stresses on the inside.)

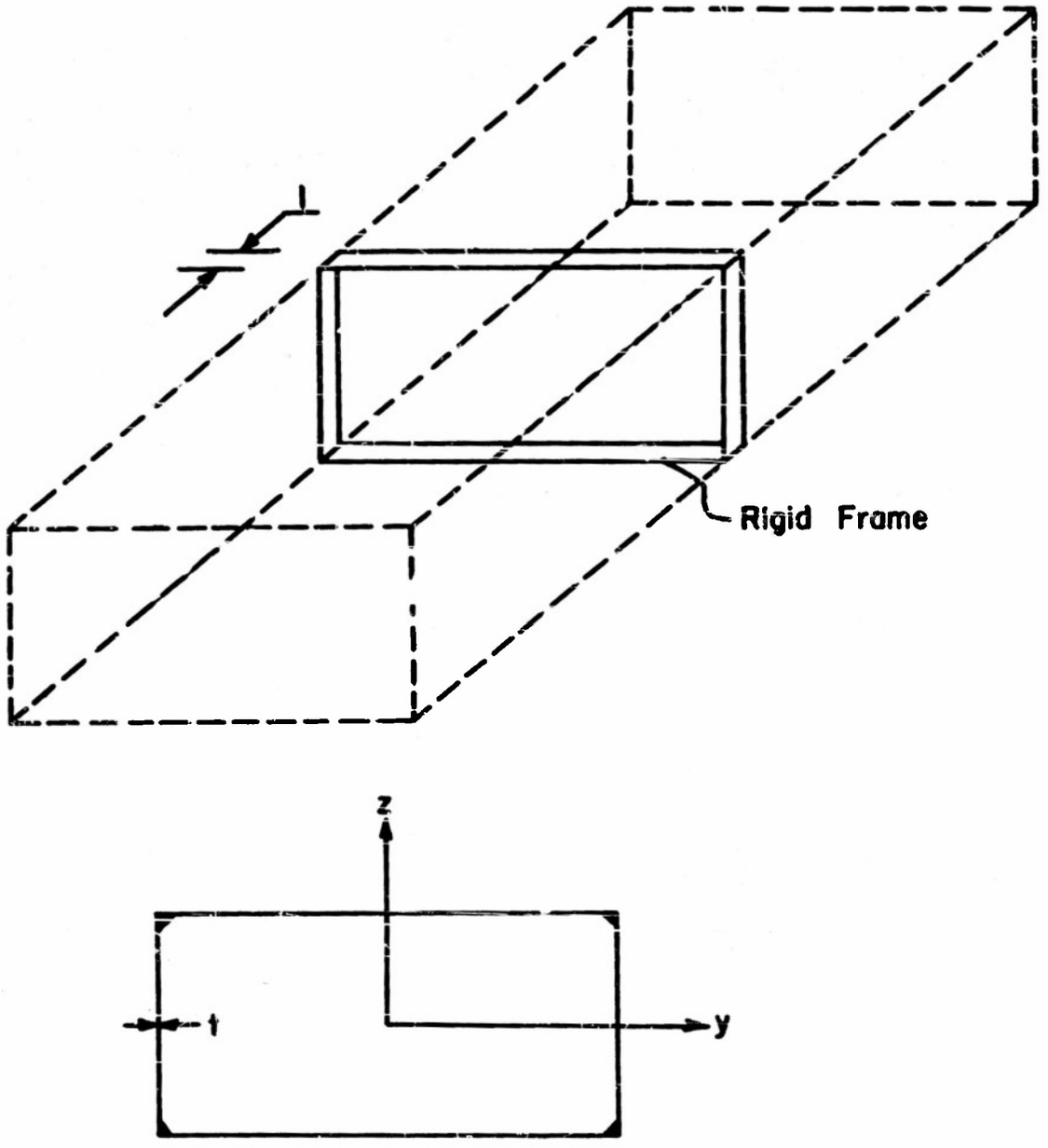

FIGURE 4.12 RIGID FRAME COMPONENTS OF THE MODEL

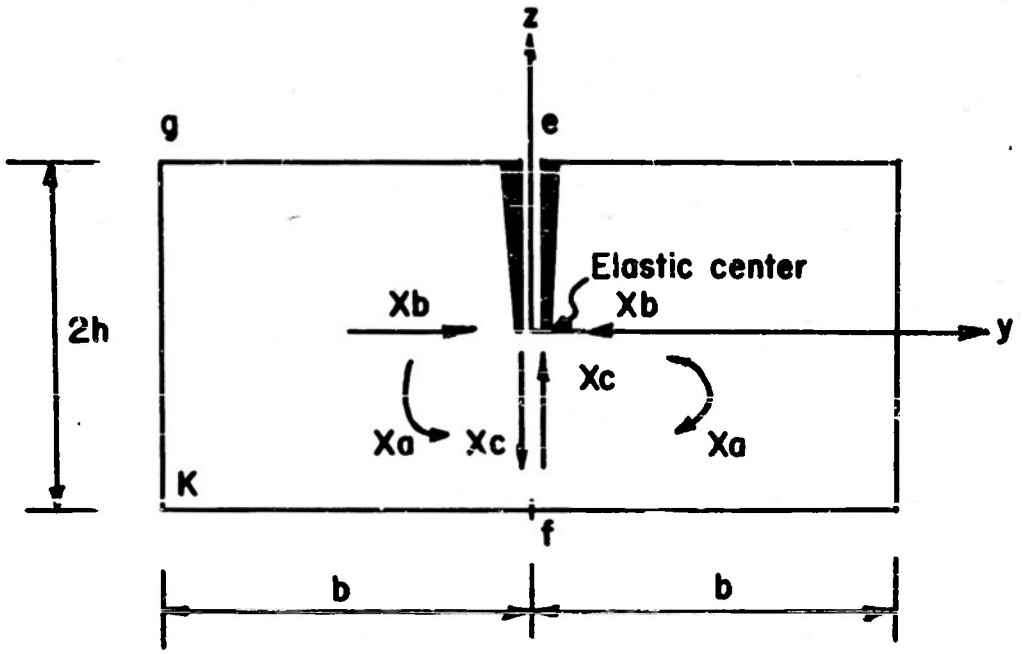

FIGURE 4.13 PRIMARY STRUCTURE

It will be assumed that the temperature is uniform across the thickness of the frame. The virtual work expressions for the influence coefficients, δ_{mn} and δ_{mT}, are as follows:

$$\delta_{ao} = \sum \left\{ \int M_a M_o \frac{ds}{EI} + \int F_a F_o \frac{ds}{EA} \right\}$$

$$\delta_{aa} = \sum \left\{ \int M_a^2 \frac{ds}{EI} + \int F_a^2 \frac{ds}{EA} \right\}$$

$$\delta_{ab} = \sum \left\{ \int M_a M_b \frac{ds}{EI} + \int F_a F_b \frac{ds}{EA} \right\}$$

$$\delta_{ac} = \sum \left\{ \int M_a M_c \frac{ds}{EI} + \int F_a F_c \frac{ds}{EA} \right\} \qquad (4.11)$$

$$\delta_{aT} = \sum \bar{\alpha} \int F_a \Delta T ds$$

$$\delta_{bT} = \sum \bar{\alpha} \int F_b \Delta T ds$$

$$\delta_{cT} = \sum \bar{\alpha} \int F_c \Delta T ds$$

where

E is Young's modulus

I is the moment of inertia $= \frac{(i)t^3}{12}$

A is the cross-sectional area $= (i)t$

M_m is the bending moment in the primary structure caused by a unit value of redundant m

F_m is the axial load in the primary structure caused by a unit value of redundant m

M_o is the bending moment in the primary structure caused by external loads

F_o is the axial load in the primary structure caused by external loads.

From the symmetry of the cross section and of the temperature distribution, the following results are obtained:

$$\delta_{aa} = 2\left\{2\int_f^K \frac{ds}{EI} + \int_g^K \frac{ds}{EA}\right\}$$

$$\delta_{ab} = 0$$

$$\delta_{ac} = 0$$

$$\delta_{bb} = \sum \oint z^2 \frac{ds}{EI} + 4\int_f^K \frac{ds}{EA}$$

$$\delta_{cc} = \sum \oint y^2 \frac{ds}{EI} + 2\int_f^a \frac{ds}{EA} \qquad (4.12)$$

$$\delta_{bc} = 0$$

$$\delta_{aT} = 0$$

$$\delta_{bT} = \alpha \sum \oint F_b \Delta T ds$$

$$\delta_{cT} = 0$$

Thus, it is seen that

$$X_a = 0$$
$$X_c = 0 \qquad (4.13)$$

The temperature distribution of Table A. 2 for a heating time of 120 seconds has been used to evaluate δ_{bT} numerically with the result that

$$E\,\delta_{bT} = \alpha \sum F_b \Delta S \cdot \Delta T = -529.6\alpha = -6880 \times 10^{-6} \qquad (4.14)$$

$$E\,\delta_{bb} = 5.93 \times 10^{-4} + 0.132 \times 10^{-4} = 6.06 \times 10^{-4}$$

The redundant axial load, X_b , has the value

$$X_b = -\frac{-6.880 \times 10^{-6}}{6.06 \times 10^{-4}} = 11.35 \text{ lbs.} \qquad (4.15)$$

Plots of the bending moment and axial load distribution are shown in Figure 4.14.

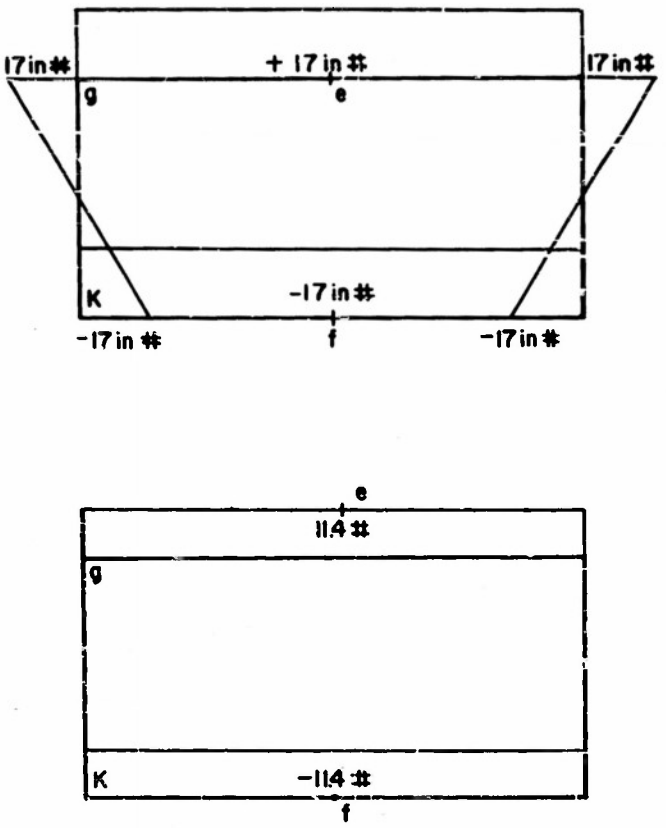

FIGURE 4.14 BENDING MOMENT DISTRIBUTION

At point e in Figure 4.14, the maximum stresses are

$$(\sigma_s)_e = -\frac{M\frac{t}{2}}{I} \pm \frac{F}{A} \qquad (4.16)$$

The outside fiber at point e has the stress

$$(\sigma_s)_e = -\frac{(17)(0.0325)}{(1)(12)(0.274)(10)^{-3}} + \frac{11.4}{(1)(0.065)} \qquad (4.17)$$

$$\cong 7 \text{ psi}$$

The inside fiber at point e has the stress

$$(\sigma_s)_e = -168 - 175 = -343 \text{ psi} \qquad (4.18)$$

Thus, the stresses which result from the distortion of the cross section are inconsequential.

4.3 Spanwise Effects

The principle of minimum potential energy can be used to obtain approximate solutions to the three-dimensional equations of elasticity. If there are no external or body forces acting upon the structure, the differential equations of equilibrium have the following form (Ref. 18):

$$\begin{aligned}
&(\lambda+G)\frac{\partial}{\partial x}\left(\frac{\partial u}{\partial x}+\frac{\partial v}{\partial y}+\frac{\partial w}{\partial z}\right)+G\nabla^2 u-\frac{E\bar{\alpha}}{1-2\nu}\frac{\partial T}{\partial x}=0\\
&(\lambda+G)\frac{\partial}{\partial y}\left(\frac{\partial u}{\partial x}+\frac{\partial v}{\partial y}+\frac{\partial w}{\partial z}\right)+G\nabla^2 v-\frac{E\bar{\alpha}}{1-2\nu}\frac{\partial T}{\partial y}=0\\
&(\lambda+G)\frac{\partial}{\partial z}\left(\frac{\partial u}{\partial x}+\frac{\partial v}{\partial y}+\frac{\partial w}{\partial z}\right)+G\nabla^2 w-\frac{E\bar{\alpha}}{1-2\nu}\frac{\partial T}{\partial z}=0
\end{aligned} \qquad (4.19)$$

where the constants are defined as

$$\begin{aligned}
\lambda &= \frac{\nu E}{(1+\nu)(1-2\nu)}\\
G &= \frac{E}{2(1+\nu)}
\end{aligned} \qquad (4.20)$$

ν = Poisson's ratio.

The stress-strain relations become

$$\epsilon_x = \frac{1}{E}\left[\sigma_x - \nu(\sigma_y + \sigma_z)\right] + \bar{\alpha}\Delta T$$
$$\epsilon_y = \frac{1}{E}\left[\sigma_y - \nu(\sigma_z + \sigma_x)\right] + \bar{\alpha}\Delta T$$
$$\epsilon_z = \frac{1}{E}\left[\sigma_z - \nu(\sigma_x + \sigma_y)\right] + \bar{\alpha}\Delta T$$
$$\gamma_{xy} = \frac{1}{G}\tau_{xy} \qquad (4.21)$$
$$\gamma_{yz} = \frac{1}{G}\tau_{yz}$$
$$\gamma_{xz} = \frac{1}{G}\tau_{xz}$$

When properly minimized, the potential energy expression which will yield the above equations of equilibrium and stress-strain relations has the form shown below:

$$\Pi = \frac{1}{2}\iiint \left\{\lambda(\epsilon_x + \epsilon_y + \epsilon_z)^2 + 2G(\epsilon_x^2 + \epsilon_y^2 + \epsilon_z^2)\right. \qquad (4.22)$$
$$\left. + G(\gamma_{xy}^2 + \gamma_{yz}^2 + \gamma_{xz}^2) - \frac{2\bar{\alpha}E\Delta T}{1-2\nu}(\epsilon_x + \epsilon_y + \epsilon_z)\right\} dx\, dy\, dz$$

It is readily shown that the vanishing of the variation of the above integral will lead to the three differential equations of equilibrium. Furthermore, if the strain energy density function is defined as

$$W = \frac{1}{2}\left\{\lambda(\epsilon_x + \epsilon_y + \epsilon_z)^2 + 2G(\epsilon_x^2 + \epsilon_y^2 + \epsilon_z^2) + G(\gamma_{xy}^2 + \gamma_{yz}^2 + \gamma_{xz}^2)\right. \qquad (4.23)$$
$$\left. - \frac{2\bar{\alpha}E\Delta T}{1-2\nu}(\epsilon_x + \epsilon_y + \epsilon_z)\right\}$$

it is also readily shown that

$$\sigma_x = \frac{\partial W}{\partial \epsilon_x} \qquad \tau_{xy} = \frac{\partial W}{\partial \gamma_{xy}}$$
$$\sigma_y = \frac{\partial W}{\partial \epsilon_y} \qquad \tau_{yz} = \frac{\partial W}{\partial \gamma_{yz}}$$
$$\sigma_z = \frac{\partial W}{\partial \epsilon_z} \qquad \tau_{xz} = \frac{\partial W}{\partial \gamma_{xz}} \qquad (4.24)$$

Thus, it is seen that the potential energy function satisfies all the pre-requisites necessary for the three-dimensional equations of thermoelasticity in which external and body forces are absent.

4.3.1 Application to the Box Beam

The principle of minimum potential energy as stated will be specialized to the problem of the box beam. It will be necessary to make the following assumptions:

(1) The cross-sectional shape is preserved by many closed diaphragms which are rigid in their own plane but completely flexible out of their plane, i.e., there is no resistance to warping. In addition, it is necessary to assume that these diaphragms are perfectly insulated from the rest of the structure.

(2) The wall (or shell) of the box beam is in a state of membrane stress, i.e., the stresses and hence the temperature is constant over the thickness of the shell.

These assumptions are the familiar ones used in the analysis of the effects of warping restraint on the stress distribution in shell beams (Refs. 11, 12 and 13).

The expression for the potential energy of strain is thus reduced to the following expression:

$$\Pi_S = \frac{1}{2}\int\oint t\left\{E'(\epsilon_x^2+\epsilon_s^2+2\nu\epsilon_x\epsilon_s)+G\gamma^2-2E''\bar{\alpha}\cdot\Delta T(\epsilon_x+\epsilon_s)\right\}ds\,dx \quad (4.25)$$

The pertinent stress-strain relations are

$$\begin{aligned}\sigma_x &= E'(\epsilon_x+\nu\epsilon_s)-E''\bar{\alpha}\Delta T\\ \sigma_s &= E'(\epsilon_s+\nu\epsilon_x)-E''\bar{\alpha}\Delta T\end{aligned} \quad (4.26)$$

where

$$\begin{aligned}E' &= \frac{E}{1-\nu^2}\\ E'' &= \frac{E}{1-\nu}\\ G &= \frac{E}{2(1+\nu)}\end{aligned} \quad (4.27)$$

γ is the shear strain

ϵ_x is the strain in a spanwise direction

ϵ_s is the strain in a peripheral direction

σ_x is the normal stress in a spanwise direction

σ_s is the normal stress in a peripheral direction

α is the coefficient of thermal expansion

ΔT is the change in temperature

t is the thickness.

Points on the cross section are located by a peripheral coordinate, s, and an angle, σ, which the tangent at point s makes with the y-axis (see Figure 4.16). Displacements in the spanwise (x), vertical (z) and peripheral (s) directions will be denoted by v, w and ξ, respectively. Rotational and horizontal displacements are neglected since both the cross section of the model and the temperature distribution are symmetrical about the z-axis. A vertical displacement of the cross section causes a peripheral displacement of the amount (see Figure 4.15)

$$\xi = w \sin \chi \tag{4.28}$$

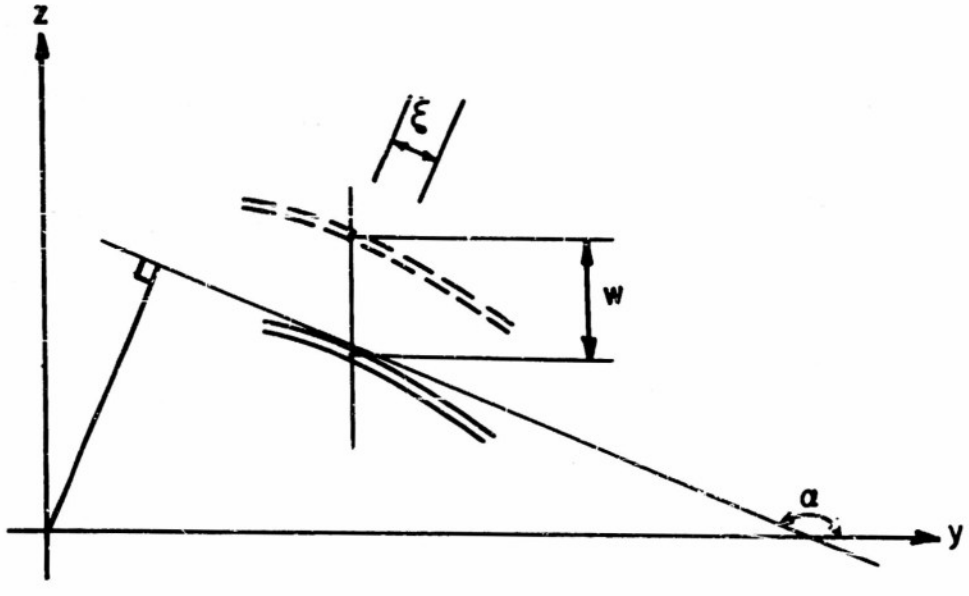

FIGURE 4.15 RELATION BETWEEN VERTICAL AND PERIPHERAL DISPLACEMENTS

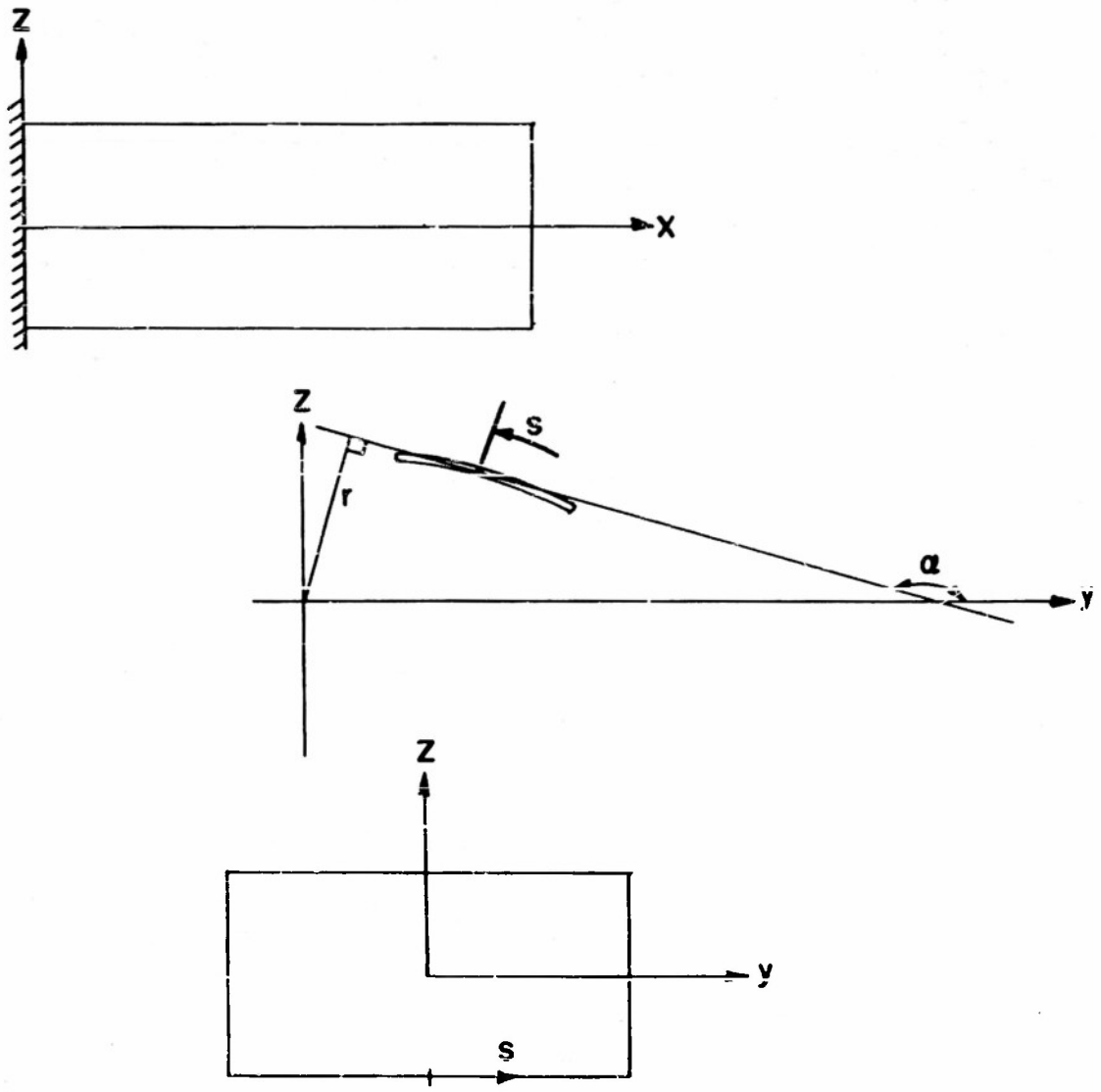

FIGURE 4.16 COORDINATE SYSTEM TO DESCRIBE WARPING OF CROSS SECTION

Thus, the potential energy expression becomes

$$\Pi_s = \frac{1}{2}\int\int t\left\{E' U_x^2 + G(U_s + w_x \sin\alpha)^2 - 2\bar{\alpha} E'' \cdot \Delta T \cdot U_x\right\} ds\, dx \qquad (4.29)$$

where

$$\epsilon_x = \frac{\partial U}{\partial x} = U_x$$

$$\gamma = \frac{\partial U}{\partial s} + \frac{\partial s}{\partial x} = U_s + w_x \sin\alpha \qquad (4.30)$$

The peripheral strain, ϵ_s , vanishes because the assumption of rigid diaphragms prevents the occurrence of such strains.

It has been found that the temperature distribution at any particular time can be adequately represented by an expression of the form,

$$\Delta T(S) = \bar{A} e^{-\frac{\pi}{S_0} S}\left(\cos\frac{\pi}{S_0} S + \sin\frac{\pi}{S_0} S\right) + \bar{B} \qquad (4.31)$$

where $\bar{A}$ and B are constants

S_0 = 1/2 total peripheral length = 9 inches.

Figures 4.17 and 4.18 are plots which show the agreement between the experimental temperature distribution and the distribution given by the above assumed function. This agreement suggests the following assumed function for the spanwise displacement:

$$U(x,S) = \phi_0(x) + \phi_1(x)\left[(2S-9)\sin\alpha - 3\cos\alpha\right] + \phi_2(x) e^{-\frac{\pi}{S_0} S}\cos\frac{\pi}{S_0} S + \phi_4(x) e^{-\frac{\pi}{S_0} S}\sin\frac{\pi}{S_0} S \qquad (4.32)$$

The first term is not a function of S and, hence, represents a rigid translational displacement in which all points of the cross section move the same amount. The coefficient of $\phi_1(x)$ represents a rigid planar displacement which corresponds to the application of a bending moment about the y -axis. The warping modes are represented by ϕ_2 and ϕ_4 .

With the substitution of these expressions for ΔT and U , the potential energy expression becomes

$$\pi_S = 2\cdot\tfrac{1}{2}\int_0^{\ell}\int_0^{s_0} t\Big\{E'\Big[\phi_{0x}+\phi_{1x}(2S\sin\alpha-9s\sin\alpha-3\cos\alpha) + \phi_{2x}e^{-as}\cos as+\phi_{4x}\,e^{-as}\sin as\Big]^2$$

$$+G\Big[\phi_1\tfrac{d}{ds}(2S\sin\alpha-9\sin\alpha-3\cos\alpha)-ae^{-as}(\cos as+\sin as)\phi_2 + ae^{-as}(\cos as-\sin as)\phi_4+w_x\sin\alpha\Big]^2 \qquad (4.33)$$

$$-2\Big[Ae^{-as}(\cos as+\sin as)+B\Big]\Big[\phi_{0x}+\phi_{1x}(2S\sin\alpha-9\sin\alpha-3\cos\alpha) + \phi_{2x}e^{-as}\cos as+\phi_{4x}e^{-as}\sin as\Big]\Big\}\,ds\,dx$$

where

ℓ is the span length

$$a=\frac{\pi}{9}$$

$$A=\bar{\alpha}\,E''\,\bar{A} \qquad (4.34)$$

$$B=\bar{\alpha}\,E''\,\bar{B}$$

It is convenient to make the following substitutions:

$$p_1(s)=e^{-as}\cos as$$

$$p_2(s)=e^{-as}\sin as$$

$$p_3(s)=e^{-as}(\cos as+\sin as)=p_1+p_2 \qquad (4.35)$$

$$p_4(s)=e^{-as}(\cos as-\sin as)=p_1-p_2$$

$$p_5(s)=(2S-9)\sin\alpha-3\cos\alpha$$

$$p_6(s)=\frac{d}{ds}(p_5)$$

$$p_7(s)=\sin\alpha$$

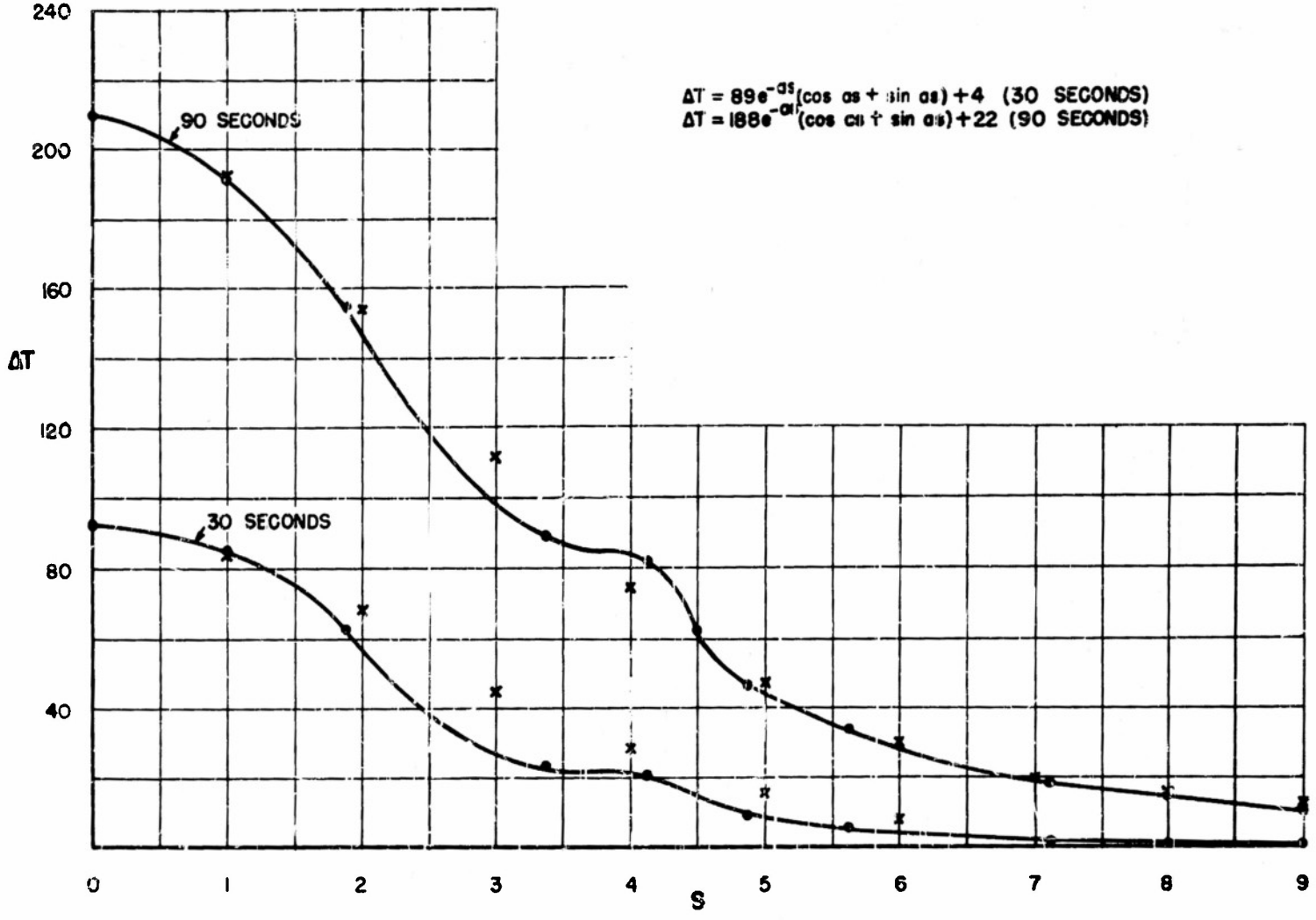

FIGURE 4. 17 COMPARISON OF ASSUMED $\Delta T(S)$ AND EXPERIMENTAL TEMPERATURES (30 and 90 SECONDS)

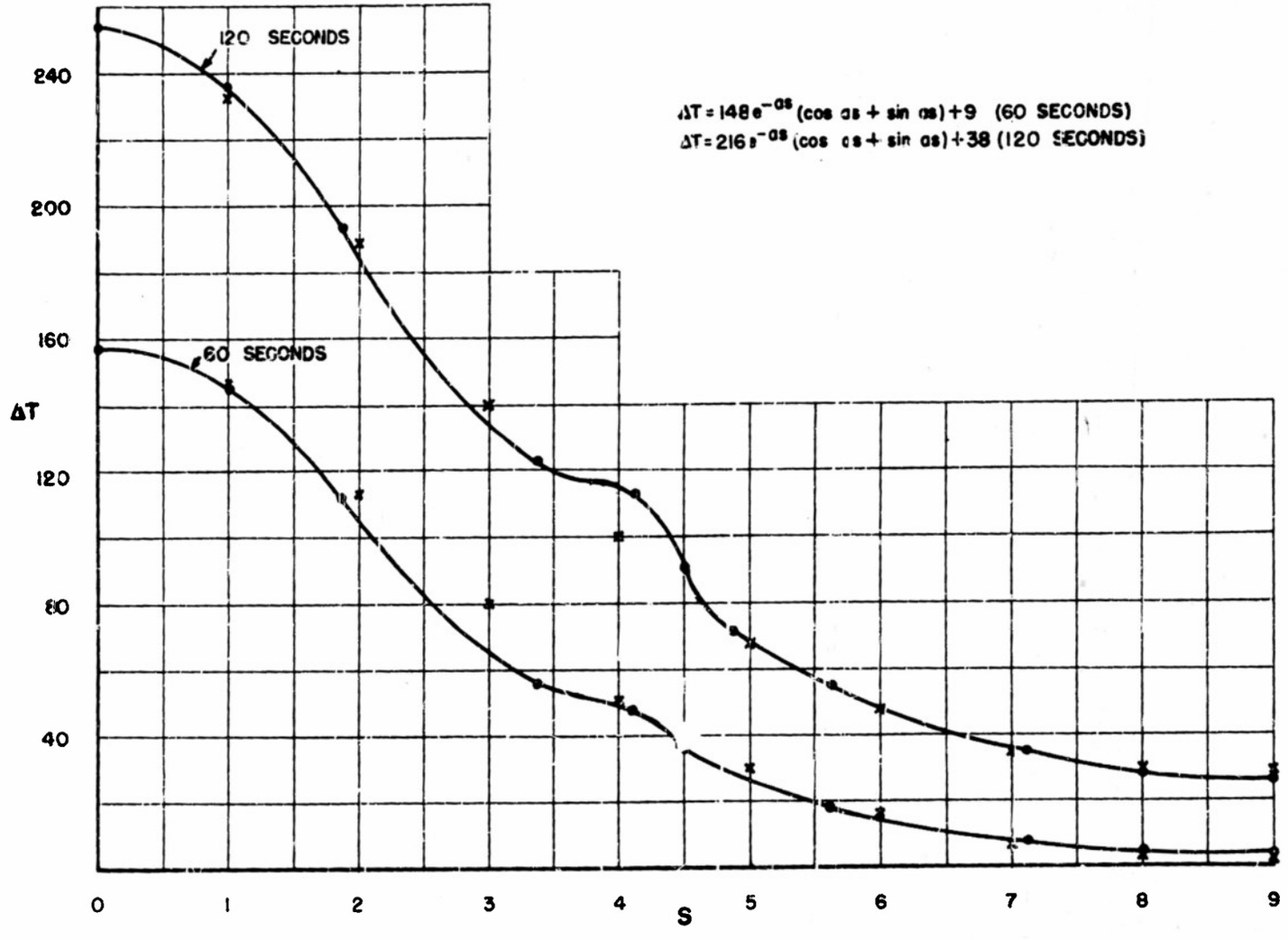

FIGURE 4.18 COMPARISON OF ASSUMED $\Delta T(S)$ AND EXPERIMENTAL TEMPERATURES (60 AND 120 SECONDS)

The stress–strain expression now becomes

$$\sigma_x = E'\left\{\phi_{ox} + \phi_{1x} p_5 + \phi_{2x} p_1 + \phi_{4x} p_2\right\} - \left\{A p_3 + B\right\} \tag{4.36}$$

The variation of the integral yields

$$\begin{aligned}\delta \Pi_3 = 2\int_0^{\ell}\int_0^{s_0} t \Big\{ & E'\left[\phi_{ox} + p_3 \phi_{1x} + p_1 \phi_{2x} + p_2 \phi_{4x}\right]\left[\delta\phi_{ox} + p_5\,\delta\phi_{1x} + p_1\,\delta\phi_{2x} + p_2\,\delta\phi_{4x}\right] \\ & + G\left[p_6 \phi_1 - a p_3 \phi_2 + a p_4 \phi_4 + p_7 w_x\right]\left[p_6\,\delta\phi_1 - a p_3\,\delta\phi_2 + a p_4\,\delta\phi_4 + p_7\,\delta w_x\right] \\ & - \left[A p_3 + B\right]\left[\delta\phi_{ox} + p_5\,\delta\phi_{1x} + p_1\,\delta\phi_{2x} + p_2\,\delta\phi_{4x}\right]\Big\}\, ds\, dx\end{aligned} \tag{4.37}$$

It is noted that the following integrals appear in the above expression:

$$\begin{aligned}
a_0 &= 2\int_0^{s_0} t\, ds = 2.1604 & a_{10} &= 2a\int_0^{s_0} t\, p_4 p_7\, ds = 0 \\
a_1 &= 2\int_0^{s_0} t\, p_1\, ds = 0.2670 & a_{11} &= 2\int_0^{s_0} t\, p_7^2\, ds = 0.7680 \\
a_2 &= 2\int_0^{s_0} t\, p_2\, ds = 0.3932 & a_{12} &= 2\int_0^{s_0} t\, p_3\, ds = 0 \\
a_3 &= 2\int_0^{s_0} t\, p_1^2\, ds = 0.1651 & a_{13} &= 2\int_0^{s_0} t\, p_5^2\, ds = 15.421 \\
a_4 &= 2\int_0^{s_0} t\, p_2^2\, ds = 0.09651 & a_{14} &= 2\int_0^{s_0} t\, p_5 p_1\, ds = -1.1134 \\
a_5 &= 2\int_0^{s_0} t\, p_1 p_2\, ds = 0.07455 & a_{15} &= 2\int_0^{s_0} t\, p_5 p_2\, ds = -0.5498 \\
a_6 &= 2a^2\int_0^{s_0} t\, p_3^2\, ds = 0.0500 & a_{16} &= 2\int_0^{s_0} t\, p_6^2\, ds = 3.0720 \\
a_7 &= 2a^2\int_0^{s_0} t\, p_3 p_4\, ds = 0.008356 & a_{17} &= 2a\int_0^{s_0} t\, p_2 p_3\, ds = 0 \\
a_8 &= 2a^2\int_0^{s_0} t\, p_4^2\, ds = 0.01371 & a_{18} &= 2a\int_0^{s_0} t\, p_6 p_4\, ds = 0 \\
a_9 &= 2a\int_0^{s_0} t\, p_3 p_7\, ds = 0 & a_{19} &= 2\int_0^{s_0} t\, p_6 p_7\, ds = 1.5360
\end{aligned} \tag{4.38}$$

These constants were evaluated on the basis of the idealization of the cross section shown in Figure 4.19.

The vanishing of the variation of the strain energy yields the following differential equations:

$$a_0 \phi_{0xx} + a_1 \phi_{2xx} + a_2 \phi_{4xx} = 0 \qquad \text{(a)}$$

$$-E'(a_{13} \phi_{1xx} + a_{14} \phi_{2xx} + a_{15} \phi_{4xx}) + G(a_{16} \phi_1 + a_{19} w_x) = 0 \qquad \text{(b)}$$

$$-E'(a_1 \phi_{0xx} + a_{14} \phi_{1xx} + a_3 \phi_{2xx} + a_5 \phi_{4xx}) + G(a_6 \phi_2 - a_7 \phi_4) = 0 \qquad \text{(c)} \quad (4.39)$$

$$-E'(a_2 \phi_{0xx} + a_{15} \phi_{1xx} + a_5 \phi_{2xx} - a_4 \phi_{4xx}) + G(-a_7 \phi_2 + a_8 \phi_4) = 0 \qquad \text{(d)}$$

$$a_{19} \phi_{1x} + a_{11} w_{xx} = 0 \qquad \text{(e)}$$

The natural boundary conditions at $x = \ell$ are

$$E'(a_0 \phi_{0x} + a_1 \phi_{2x} + a_2 \phi_{4x}) = A(a_1 + a_2) + B a_0 \qquad \text{(a)}$$

$$E'(a_{13} \phi_{1x} + a_{14} \phi_{2x} + a_{15} \phi_{4x}) = A(a_{14} + a_{15}) \qquad \text{(b)}$$

$$E'(a_1 \phi_{0x} + a_{14} \phi_{1x} + a_3 \phi_{2x} + a_5 \phi_{4x}) = A(a_3 + a_5) + B a_1 \qquad \text{(c)} \quad (4.40)$$

$$E'(a_2 \phi_{0x} + a_{15} \phi_{1x} + a_5 \phi_{2x} + a_4 \phi_{4x}) = A(a_5 + a_4) + B a_2 \qquad \text{(d)}$$

$$a_{19} \phi_1 + a_{11} w_x = 0 \qquad \text{(e)}$$

From differential equation (4.39e) and boundary condition (4.40e), the following is true everywhere

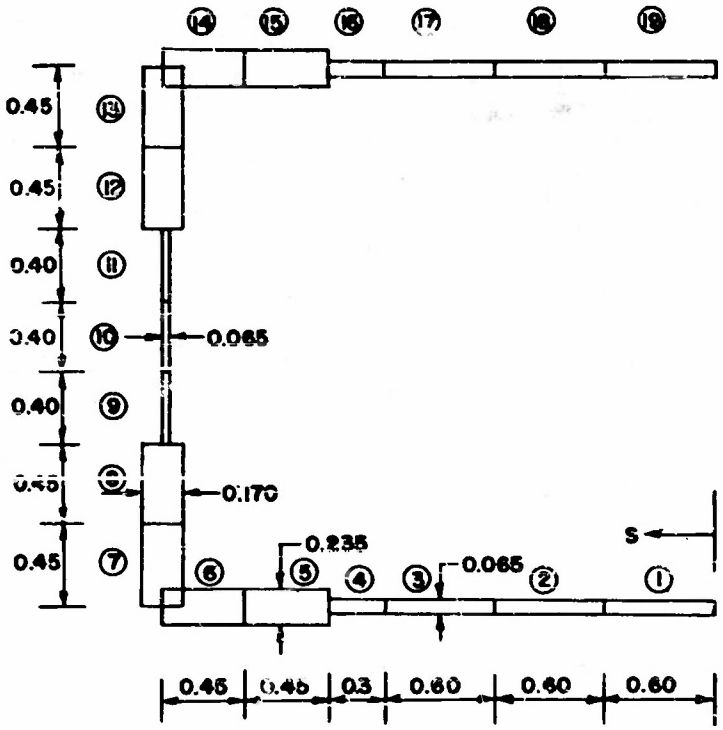

FIGURE 4.19 IDEALIZATION OF CROSS SECTION FOR CALCULATION OF a_1, $a_2, \ldots a_{19}$ PARAMETERS

$$w_x = -\frac{a_{19}}{a_{11}}\phi_1 \tag{4.41}$$

It can also be shown that

$$a_{16}\phi_1 + a_{19}w_x = \left(a_{16} - \frac{a_{19}^2}{a_{11}}\right)\phi_1 \tag{4.42}$$

and that

$$a_{16} - \frac{a_{19}^2}{a_{11}} = 0 \tag{4.43}$$

This result reduces equation (4.39b) to the following form:

$$-E'\left(a_{13}\phi_{1xx} + a_{14}\phi_{2xx} + a_{15}\phi_{4xx}\right) = 0 \tag{4.44}$$

Thus, equations (4.39a) and (4.39b) together with boundary conditions (4.40a) and (4.40b) insure the satisfaction of axial force and bending moment equilibrium at every cross section. These relations are

$$E'\left(a_0\phi_{0x} + a_1\phi_{2x} + a_2\phi_{4x}\right) - \left[A(a_1 + a_2) + Ba_0\right] = 0 \tag{4.45}$$

$$E'\left(a_{13}\phi_{1x} + a_{14}\phi_{2x} + a_{15}\phi_{4x}\right) - \left[A(a_{14} + a_{15})\right] = 0 \tag{4.46}$$

By eliminating ϕ_{0xx} and ϕ_{1xx} from the equations (4.45) and (4.46), the two differential equations for the warping modes, ϕ_2 and ϕ_4, are seen to be

$$-E'\left\{\left(a_3 - \frac{a_1^2}{a_0} - \frac{a_{14}^2}{a_{13}}\right)\phi_{2xx} + \left(a_5 - \frac{a_1 a_2}{a_0} - \frac{a_{14}a_{15}}{a_{13}}\right)\phi_{4xx}\right\} + G\left\{a_6\phi_2 - a_7\phi_4\right\} = 0 \tag{4.47}$$

$$-E'\left\{\left(a_5 - \frac{a_2 a_1}{a_0} - \frac{a_{14}a_{15}}{a_{13}}\right)\phi_{2xx} + \left(a_4 - \frac{a_2^2}{a_0} - \frac{a_{15}^2}{a_{13}}\right)\phi_{4xx}\right\} + G\left\{-a_7\phi_2 + a_8\phi_4\right\} = 0 \tag{4.48}$$

The solutions for ϕ_2 and ϕ_4 are of the form

$$\phi_2 = F_2^{(1)} \sinh r_1 x + F_2^{(2)} \sinh r_2 x$$
$$\phi_4 = F_4^{(1)} \sinh r_1 x + F_4^{(2)} \sinh r_2 x \qquad (4.49)$$

where

$$r_1 = 0.56836$$
$$r_2 = 1.63930 \qquad (4.50)$$

The hyperbolic sine terms must vanish in order to satisfy the boundary conditions at the root of the beam.

In order to illustrate the spanwise effects, the constants for the temperature change in equation (4.31) were taken to be (see Figure 4.18)

$$\bar{A} = 216$$
$$\bar{B} = 38$$

These constants approximate the experimental temperature distribution at the end of the heating period of 120 seconds. The remaining constants for ϕ_2 and ϕ_4 were obtained from boundary conditions (4.40c) and (4.40d). Thus,

$$[F] = \begin{bmatrix} 0.9585 \times 10^{-8} & 0.1335 \times 10^{-19} \\ -0.4782 \times 10^{-8} & 0.4761 \times 10^{-19} \end{bmatrix} \qquad (4.51)$$

By substituting equations (4.49) and (4.51) into equation (4.36) the normal stress expression becomes

$$\sigma_x = [A - E' \phi_{2x}] \left\{ \frac{a_{14}}{a_{13}} p_5 - p_1 + \frac{a_1}{a_0} \right\}$$
$$+ [A - E' \phi_{4x}] \left\{ \frac{a_{15}}{a_{13}} p_5 - p_2 + \frac{a_2}{a_0} \right\} \qquad (4.52)$$

It can be shown that if the span, ℓ, is infinitely long, the warping modes, ϕ_2 and

ϕ_4 will disappear. Thus,

$$\sigma_x = A\left\{\frac{a_{14}}{a_{13}} p_5 - p_1 + \frac{a_1}{a_0}\right\} + A\left\{\frac{a_{15}}{a_{13}} p_5 - p_2 + \frac{a_2}{a_0}\right\} \tag{4.53}$$

A good measure of the effect of the free end is seen to be the two expressions,

$$\frac{[A - E'\phi_{2x}]}{[A - E'\phi_{4x}]} \tag{4.54}$$

These are shown plotted in Figure 4.20. The effects of the free end are thus shown to be reduced to negligible proportions at a distance of about one-third of the total peripheral length of 18 inches from the free end.

Figures 4.21, 4.22, 4.23 and 4.24 are comparisons of the stress distributions corresponding to the above analysis and the experimental stresses at heating times of 30, 60, 90 and 120 seconds, respectively. The agreement is reasonably good for 30 and 60 seconds but rather poor at 90 and 120 seconds. The latter discrepancies may be due to the thermal buckling of the lower skin which would change the stress distribution.

4.4 The Deflection at the Free End

The deflection at the free end can be calculated accurately by elementary beam theory. From this theory, it can be shown that the tip deflection of a cantilever beam acted upon by a tip bending moment is given by

$$\delta = \frac{M l^2}{2EI} \tag{4.55}$$

The analyses of Section 4.1 yielded bending moments of -20,970 in.-lbs. and -20,360 in.-lbs. for Configurations 1 and 2, respectively, at the end of the heating period. Thus,

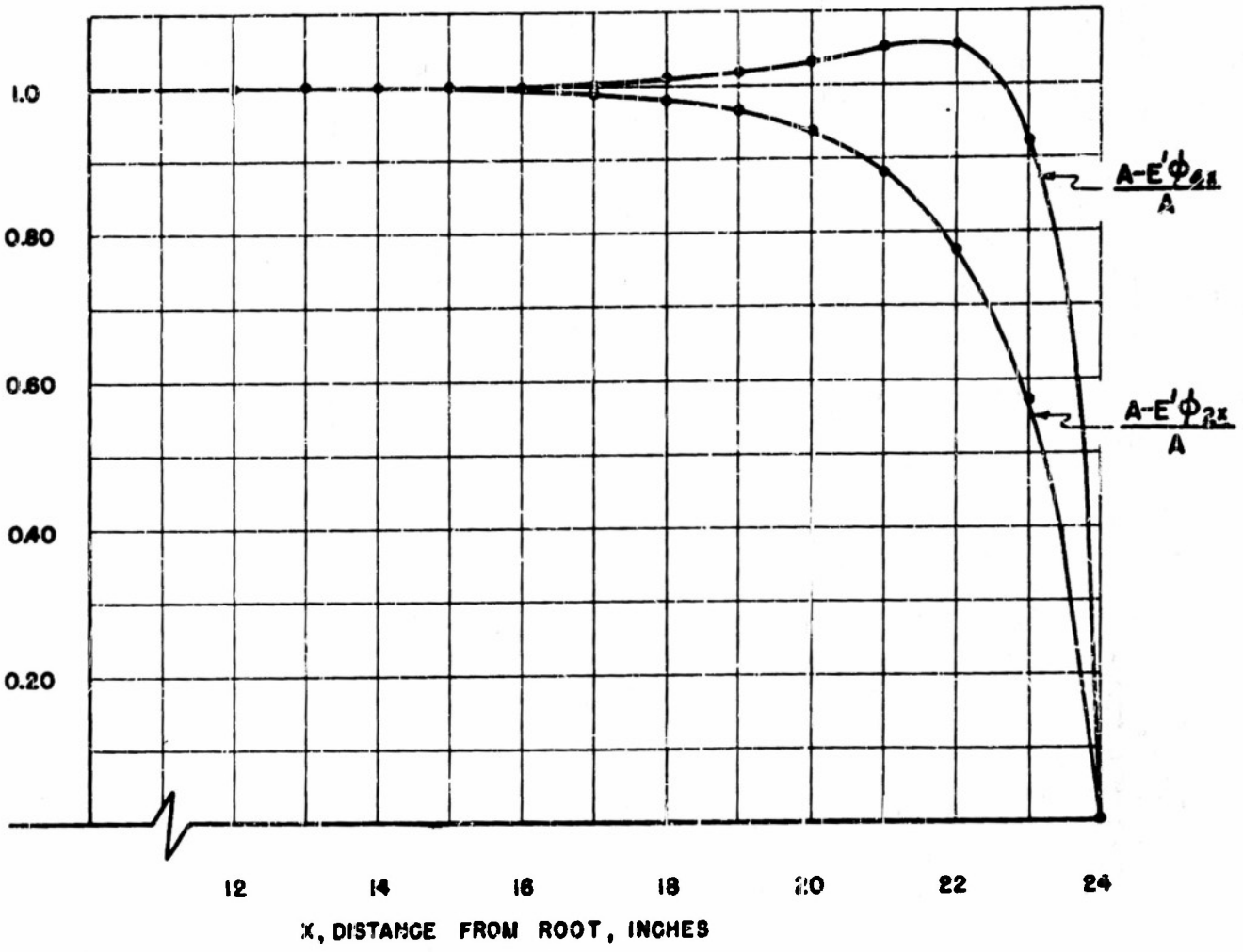

FIGURE 4.20 SPANWISE VARIATION OF PARAMETERS WHICH INDICATE INFLUENCE OF FREE END ON NORMAL STRESSES

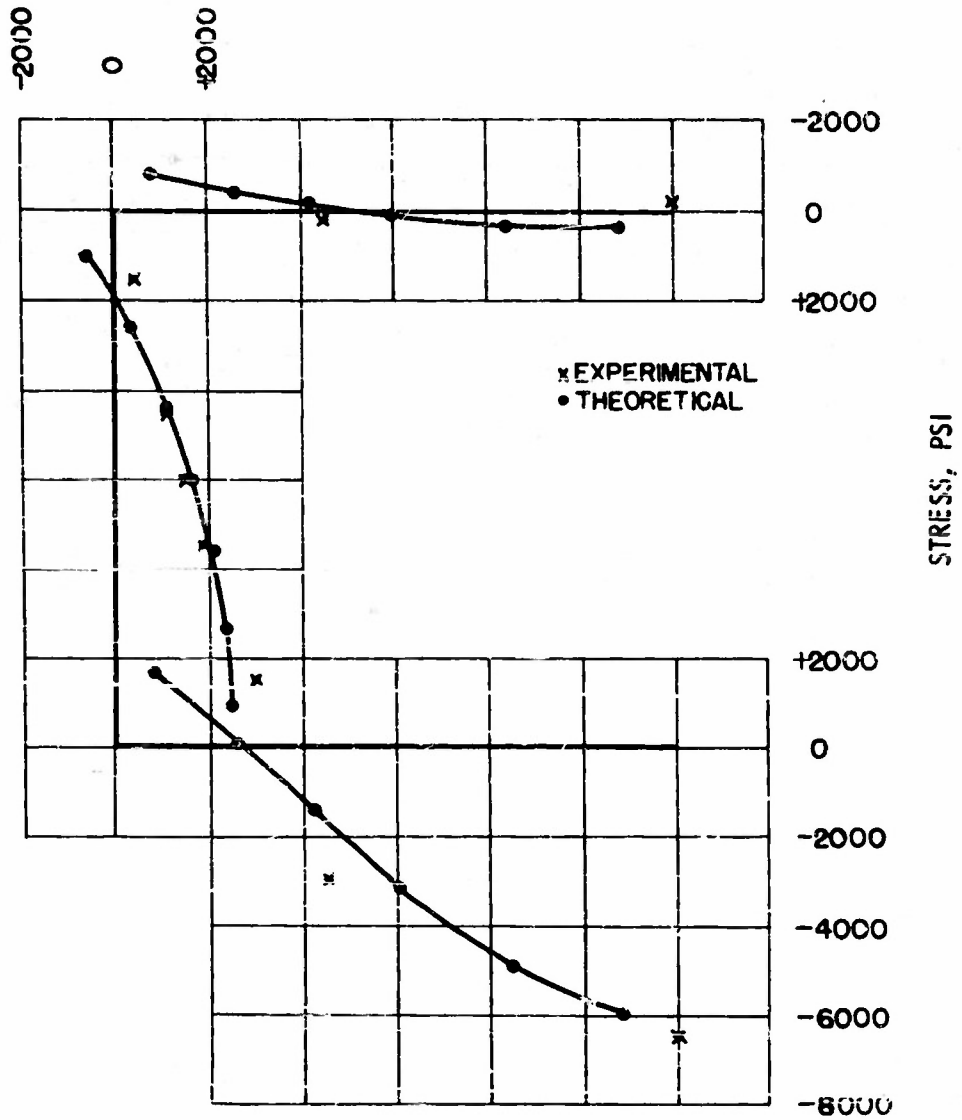

FIGURE 4.21. COMPARISON OF THEORETICAL AND EXPERIMENTAL STRESS FOR 30 SECONDS - CONFIGURATION 2

(Note: Stresses are plotted normal to the center line. Compressive stresses are plotted on the outside of the cross section, tensile stresses on the inside.)

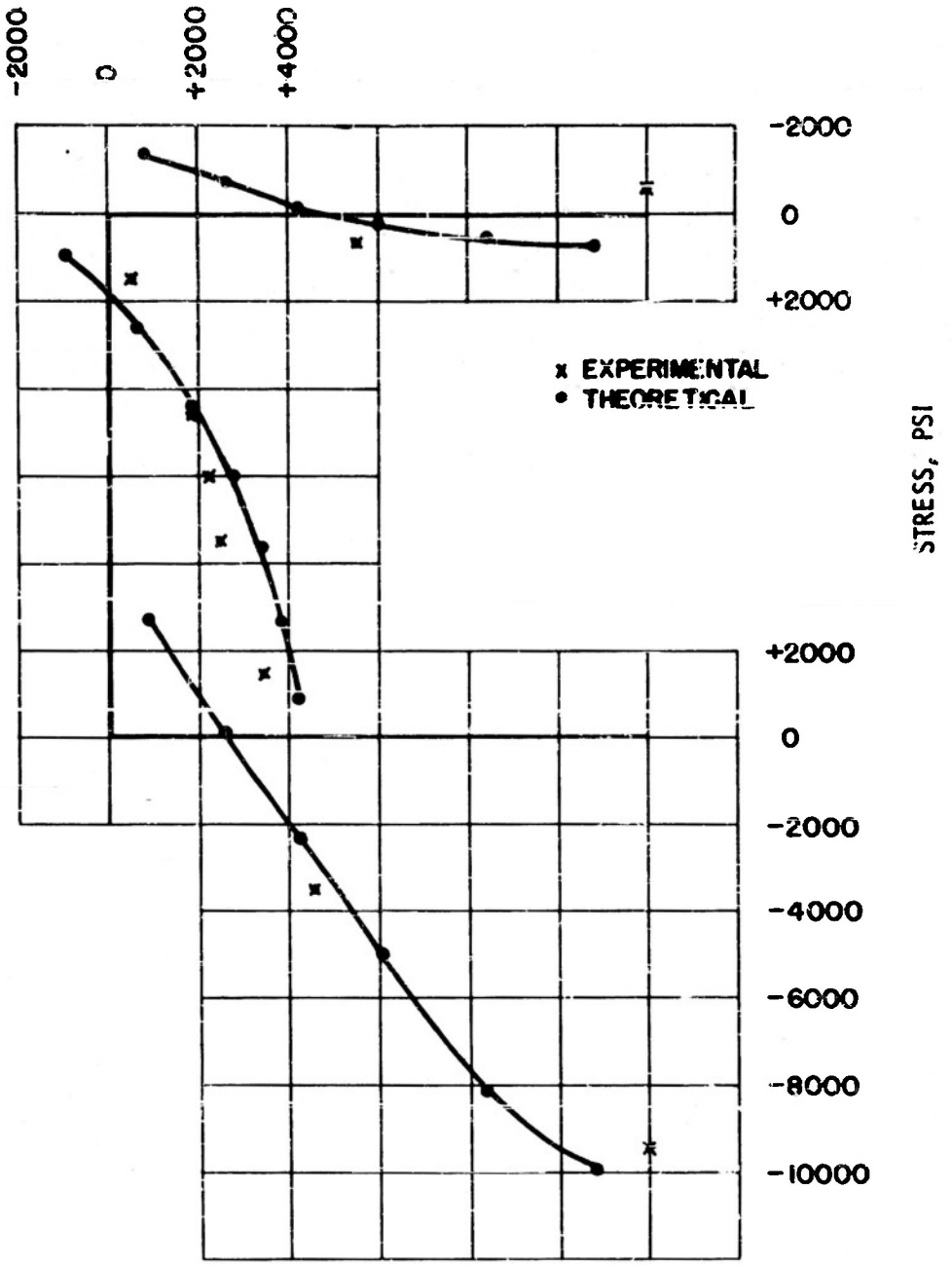

FIGURE 4.22 COMPARISON OF THEORETICAL AND EXPERIMENTAL STRESSES FOR 60 SECONDS - CONFIGURATION 2

(Note: Stresses are plotted normal to the center line. Compressive stresses are plotted on the outside of the cross section, tensile stresses on the inside.)

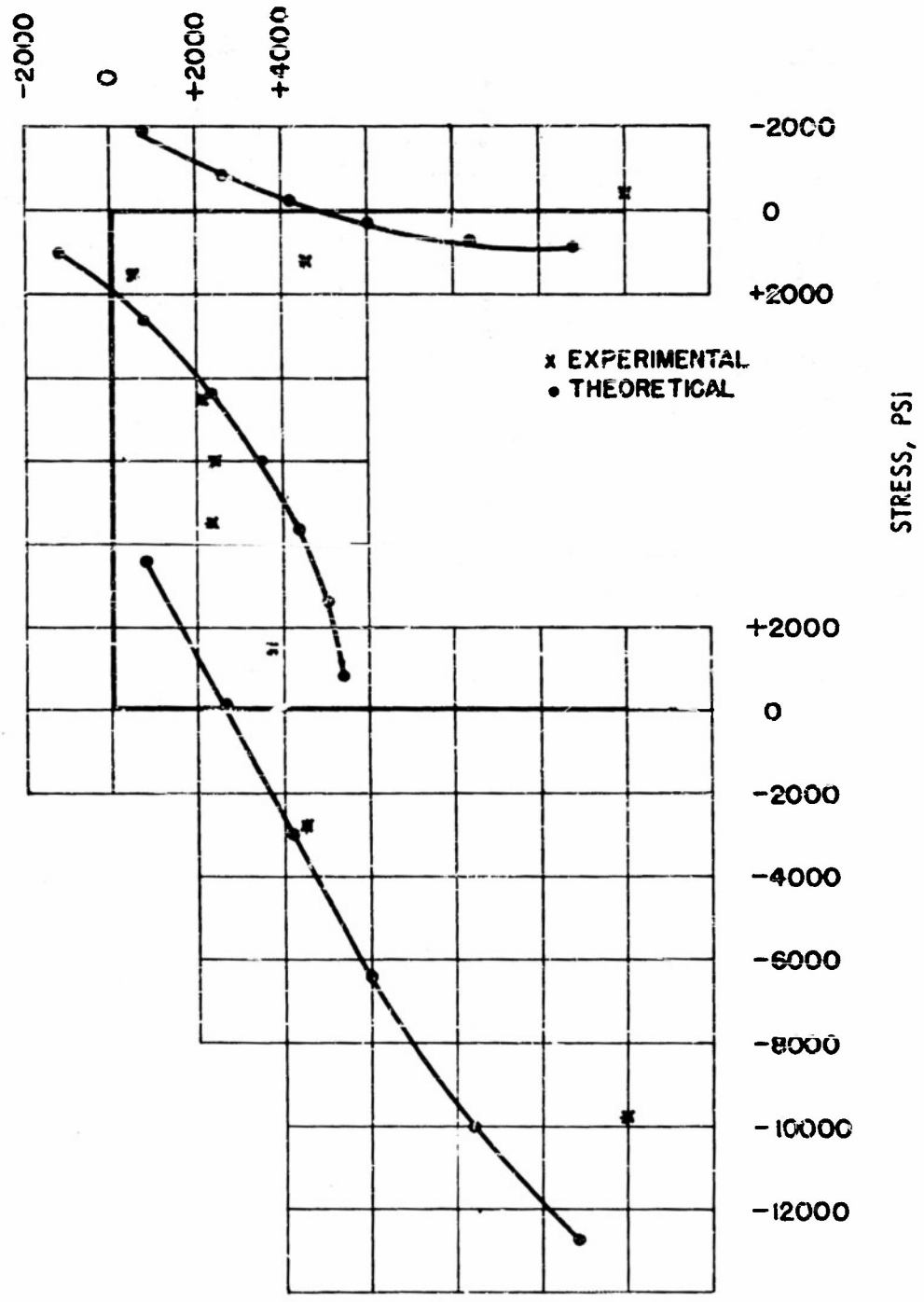

FIGURE 4.23 COMPARISON OF THEORETICAL AND EXPERIMENTAL STRESSES FOR 90 SECONDS - CONFIGURATION 2

(Note: Stresses are plotted normal to the center line. Compressive stresses are plotted on the outside of the cross section, tensile stresses on the inside.)

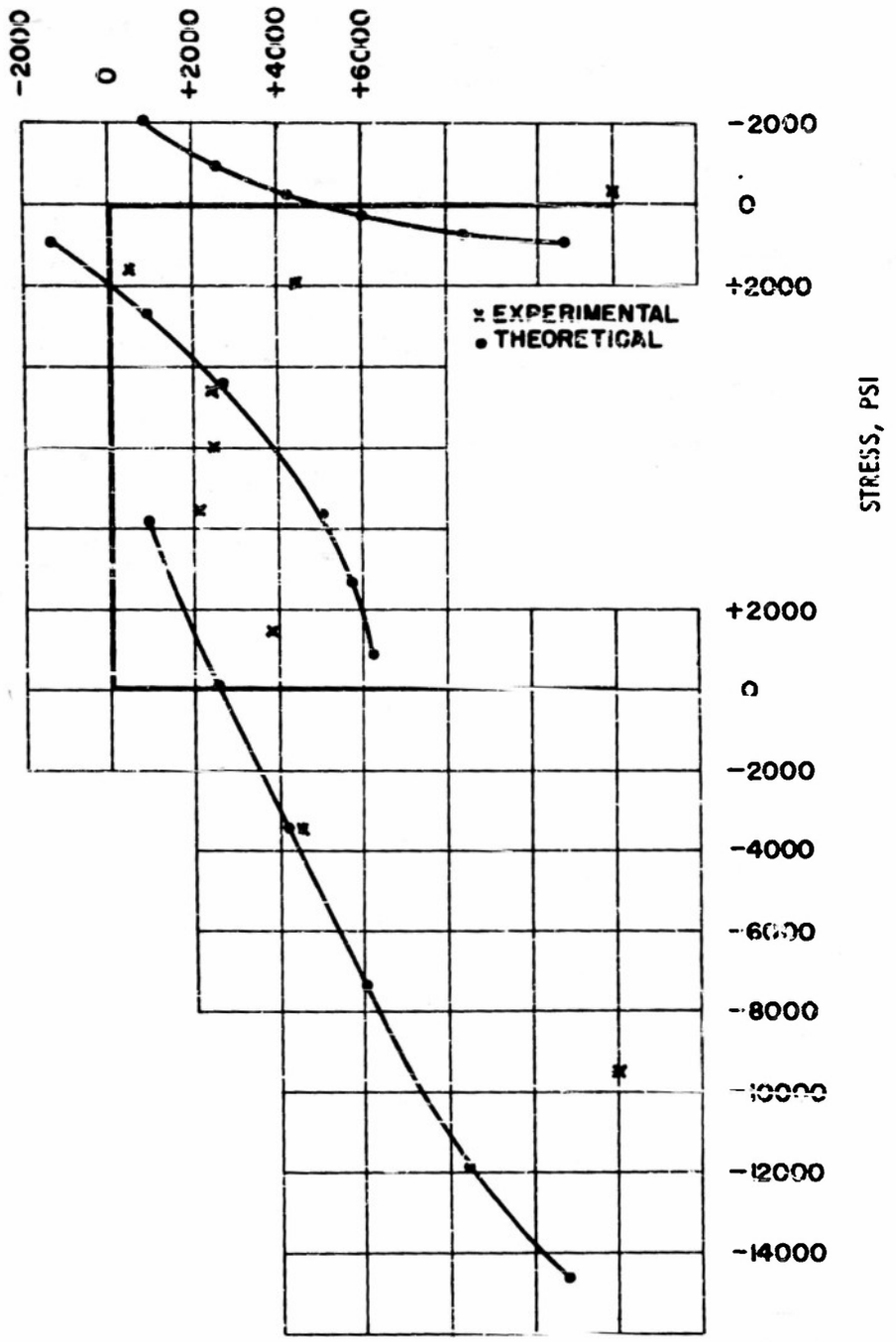

FIGURE 4.24 COMPARISON OF THEORETICAL AND EXPERIMENTAL STRESSES FOR 120 SECONDS - CONFIGURATION 2

(Note: Stresses are plotted normal to the center line. Compressive stresses are plotted on the outside of the cross section, tensile stresses on the inside.)

$$|\delta_1| = \frac{(20{,}970)(24)^2}{(2)(10.5)(10)^6(3.565)} = 0.161 \text{ inches}$$

$$|\delta_2| = \frac{(20{,}360)(24)^2}{(2)(10.5)(10)^6(3.565)} = 0.157 \text{ inches} \qquad (4.56)$$

These calculated values compare favorably with the observed displacements of 0.168 inches and 0.161 inches, respectively.

SECTION V

CONCLUSIONS AND RECOMMENDATIONS

(1) The primary mode of heat transfer in these experiments was conduction. Convection and radiation were relatively unimportant because of the precautions taken.

(2) The agreement between the experimental stress distribution and the stress distributions calculated by two different methods on the basis of temperatures measured at eleven points (see Sections 4.1 and 4.3) is fair for heating times of 30 and 60 seconds. But the agreement is poor for times of 90 and 120 seconds. This variation suggests that buckling of the lower skin may have occurred although there was no discernible evidence at the conclusion of the tests. It was not possible to observe the heated surface during the tests, and the buckling of the skin could account for the lower experimental stresses at these two longer heating times. Another reason for the differences at all times is that the conditions at the corner flanges could not be determined experimentally with sufficient detail as to temperatures and stresses. The relatively large flange areas play a dominant role in the satisfaction of force and moment equilibria over the cross section. Thus, an error in the determination of the flange temperature will be magnified in the calculations of the stresses over the entire cross section.

(3) The highest stresses were in the region of the highest temperatures. Thus, the largest stresses were in the bottom skin which received the direct thermal radiation and were compressive in nature. The smallest stresses occurred in the upper skin.

(4) As expected, the center portion of the vertical web was in tension in order to counterbalance the compressive stresses in the bottom skin.

(5) By contrast, the tension in the lower legs of the corner flanges on the bottom of the cross section was not expected. Measurements at the bottom of the corner flange could not be obtained because of the difficulty of squeezing a strain gage between bolt holes. The calculated stresses, however, indicate tension. Thus, the behavior of the beam is such that the tensile stresses in the flanges on the bottom help to balance out the bending moment induced by the large compressive stresses in the heated skin. This effect relieves the load which the upper skin would have had to carry if the entire bottom of the beam had been in compression and explains why such low stress levels were encountered in the unheated upper surface.

(6) The severest temperature gradient occurred in the bottom and, hence, was in the chordwise direction. It is suspected that the furnace radiates a flux which is not uniformly distributed over the cross section and which falls off rather significantly at the edges. This uneven distribution contributes to a chordwise temperature gradient. But even with a uniformly distributed thermal flux, the flow of heat into the relatively large

masses represented by the corner flanges and from them into the web would cause a rather large chordwise gradient.

(7) The distortion of the cross section due to the increase in temperature induces negligible stresses in the chordwise direction.

(8) The effect of the free end on the stress distribution is confined to a region within one-third of the total peripheral length from the tip. Since the experimental stresses were measured at mid-span which is equal to two-thirds of the peripheral length, they were unaffected by the finite span. Thus, the model was long enough to be considered an infinite beam.

(9) It is felt that the conditions at the corners should be investigated in greater detail despite the difficult experimental problems.

(10) The characteristics of the radiant furnace should also be determined. A calculation of the temperatures in the structure presumes a knowledge of the heat source, and the electrical power input to the heater is not sufficient data for such computations.

(11) The high compressive stress levels in the skin as compared to the low stress levels in the flanges suggest that thermal buckling will be a serious problem. These large skin stresses occur at fairly high temperatures so that thermoplastic rather than thermoelastic buckling will need to be investigated.

REFERENCES

1. Los Alamos Scientific Laboratory, U. S. Atomic Energy Commission. The Effects of Atomic Weapons. U. S. Government Printing Office, Washington, D. C., 1950.

2. Cobb, J. and Brouns, R. Studies of Thermal Effects in Aircraft Wings. S. M. Thesis, Department of Aeronautical Engineering, Massachusetts Institute of Technology, 1952.

3. Kaye, J. The Transient Temperature Distribution in a Wing Flying at Supersonic Speeds. Jour. Aero. Sci., Vol. 17 No. 12, December 1950, pp. 787-807.

4. Durham, F. P. The Effect of Flight and Configuration Variables on Thermal Stresses in Diamond-Shaped Supersonic Wings. Jour. Aero. Sci., Vol. 18 No. 11, November 1951, pp. 755-766.

5. Eisenhardt, G. H. and Rohsenow, W. M. The Thermal Stresses in a Wing at Supersonic Speeds. Report B, D.I.C. Project No. 6580, Massachusetts Institute of Technology, June 1949.

6. Heldenfels, R. R. The Effects of Non-Uniform Temperature Distributions on the Stress and Distortions of Stiffened-Shell Structures. NACA T.N. 2240, November 1950.

7. Heldenfels, R. R. A Numerical Method for the Stress Analysis of Stiffened-Shell Structures Under Non-Uniform Temperature Distributions. NACA T.N. 2241, November 1950.

8. Heldenfels, R. R. and Roberts, W. M. Experimental and Theoretical Determination of Thermal Stresses in A Flat Plate. NACA T.N. 2769, August 1952.

9. Gossard, M. L., Seide, P. and Roberts, W. M. Thermal Buckling of Plates. NACA T.N. 2771, August 1952.

10. Isakson, G. A Study of Thermal Stresses in Aircraft Structures Due to Aerodynamic Heating. Sc.D. Thesis, Department of Aeronautical Engineering, Massachusetts Institute of Technology, 1953.

11. von Kármán, T. and Chien, W. -Z. Torsion with Variable Twist. Jour. Aero. Sci., Vol. 13 No. 10, October 1946, pp. 503-510.

12. O'Brien, T. F. Some Effects of Warping Restraints on the Stresses and Deflections of Monocoque and Semi-Monocoque Wings Under Various Loadings. S. M. Thesis, Department of Aeronautical Engineering, Massachusetts Institute of Technology, 1951.

13. Benscoter, S. U. Secondary Stresses in Thin-Walled Beams with Closed Sections. NACA T.N. 2529, October 1951.

14. Fife, W. M. and Wilbur, J. B. Theory of Statically Indeterminate Structures. First Edition. McGraw-Hill Book Company, New York, 1937.

15. Structural Aluminum Handbook. Aluminum Company of America, Pittsburgh, Pa., 1940.

16. Lyman, T., ed. Metals Handbook. The American Society for Metals, Cleveland, Ohio, 1948.

17. Munitions Board Aircraft Committee. Strength of Metal Aircraft Elements, ANC-5. U. S. Government Printing Office, Washington, D. C., June 1951.

18. Timoshenko, S. and Goodier, J. Theory of Elasticity. Second Edition. McGraw-Hill Book Company, New York, 1952.

19. Niles, A. S. and Newell, J. S. Airplane Structures. Vols. I and II. First Edition. John Wiley and Sons, Inc., New York, 1929.

20. Day, E. D. Characteristics of Electric Strain Gages at Elevated Temperatures. Experimental Stress Analysis, Vol. 9 No. 1, Cambridge, Massachusetts, 1951, pp. 141-151.

21. Eshbach, O. W., ed. Handbook of Engineering Fundamentals. First Edition. John Wiley and Sons, Inc., New York, 1949.

22. Coulbert, C. D., MacInnes, W. F., Ishimato, T., Bussell, B. and Ambrosio, A. Temperature Response of Infinite Flat Plates and Slabs to Heat Inputs of Short Duration at One Surface. University of California at Los Angles, Engineering Aircraft Heat Transfer Research, Contract AF33(038)-14381, April 1951.

23. Hetenyi, M. I., ed. Handbook of Experimental Stress Analysis. First Edition. John Wiley and Sons, New York, 1950.

APPENDIX A

TABLES

TABLE A.1

PHYSICAL PROPERTIES OF 24 S-T AND 61 S-T ALUMINUM ALLOY

PROPERTY		24 S-T	61 S-T
Specific Gravity, gm/cm^3		2.77	2.70
Weight, lbs/in^3		0.100	0.098
Ultimate Tensile Stress, lbs/in^2, at	68°F	68000	45000
	212°F	61000	41000
	300°F	43000	32000
	400°F	26000	19000
	500°F	14000	7000
Yield Tensile Stress, lbs/in^2 at	68°F	48000	40000
	212°F	45000	37000
	300°F	37000	30000
	400°F	22000	16000
	500°F	10000	5000
Elongation in 2 in, %		19	12
Modulus of Elasticity, lbs/in^2		10.5×10^6	10.1×10^6
Approximate Melting Range, °F		935-1180	1080-1205
Plastic Flow Range, °F		600-900	600-900
Specific Heat, BTU/lb/°F		0.23	0.22
Coefficient of Thermal Conductivity, BTU/hr/ft^2/°F/ft, (0-212°F)		70.1	89.5
Average Coefficient of Thermal Expansion /°F,	68-212°F	12.9×10^{-6}	13.1×10^{-6}
	68-392°F	13.3×10^{-6}	13.5×10^{-6}
	68-572°F	13.7×10^{-6}	14.1×10^{-6}

Modulus of elasticity and coefficient of thermal expansion vs. temperature are shown in Figure 4.3 and were obtained from References 1 and 2.

The above physical properties have been compiled from References 1, 2, 3, 11, and 12.

TABLE A.2

EXPERIMENTAL TEMPERATURE VARIATION AT EACH GAGE LOCATION, °F

	GAGE NO. T-1		GAGE NO. T-2		GAGE NO. T-3	
	CONFIGURATION		CONFIGURATION		CONFIGURATION	
TIME SEC.	1	2	1	2	1	2
0	78	78	78	78	78	78
10	78	78	78	78	78	78
20	78	78	78	78	79	78
30	79	78	79	79	80	80
40	81	80	81	80	82	81
50	82	80	83	81	86	83
60	85	82	86	83	88	85
70	88	84	90	95	93	89
80	92	86	94	89	99	93
90	97	91	100	92	104	97
100	103	95	105	97	111	103
110	110	100	110	101	117	108
120	115	104	117	106	124	114

TABLE A. 2 (Continued)

EXPERIMENTAL TEMPERATURE VARIATION AT EACH GAGE LOCATION, °F

	GAGE NO. T-4 CONFIGURATION		GAGE NO. T-5 CONFIGURATION		GAGE NO. T-6 CONFIGURATION	
TIME SEC.	1	2	1	2	1	2
0	78	78	78	78	78	78
10	79	79	81	80	83	81
20	81	81	84	84	88	86
30	84	84	89	88	95	92
40	88	87	95	93	103	99
50	93	91	102	99	112	106
60	99	96	109	105	121	114
70	105	100	116	111	130	122
80	112	106	124	118	140	131
90	119	112	133	125	150	140
100	127	119	142	133	161	148
110	135	125	151	141	170	157
120	144	133	160	149	180	167

TABLE A.2 (Continued)

EXPERIMENTAL TEMPERATURE VARIATION AT EACH GAGE LOCATION, °F

	GAGE NO. T-7 CONFIGURATION		GAGE NO. T-8 CONFIGURATION		GAGE NO. T-9 CONFIGURATION	
TIME SEC.	1	2	1	2	1	2
0	78	78	78	78	78	78
10	84	82	86	83	108	103
20	93	90	97	91	129	123
30	103	99	108	101	148	141
40	113	109	120	112	166	159
50	123	118	132	122	183	174
60	135	127	145	134	199	190
70	146	140	157	145	124	205
80	157	150	170	156	229	218
90	168	160	182	167	243	233
100	179	170	195	179	259	247
110	189	181	206	189	272	259
120	199	191	218	201	285	272

TABLE A. 2 (Continued)

EXPERIMENTAL TEMPERATURE VARIATION AT EACH GAGE LOCATION, °F

TIME SEC.	GAGE NO. T-10 CONFIGURATION 1	GAGE NO. T-10 CONFIGURATION 2	GAGE NO. T-11 CONFIGURATION 1	GAGE NO. T-11 CONFIGURATION 2
0	78	78	78	78
10	116	110	120	111
20	145	140	149	143
30	169	163	177	171
40	191	185	202	194
50	210	203	222	216
60	229	223	242	235
70	246	240	260	254
80	262	255	279	271
90	277	269	294	288
100	294	287	312	303
110	307	300	326	318
120	322	314	341	332

TABLE A.3

EXPERIMENTAL STRAIN AND STRESS

STRAIN GAGE NUMBER S - 1

TIME	CONFIGURATION 1			CONFIGURATION 2		
SEC.	$\epsilon \cdot 10^{6}$	$E \cdot 10^{-6}$	(psi)	$\epsilon \cdot 10^{6}$	$E \cdot 10^{-6}$	(psi)
10	- 2	10.5	- 21	- 4	10.5	- 42
20	8	10.5	84	1	10.5	11
30	15	10.5	160	15	10.5	120
40	26	10.5	270	25	10.5	260
50	33	10.5	350	31	10.5	330
60	27	10.5	280	51	10.5	540
70	19	10.5	200	64	10.5	670
80	18	10.49	190	53	10.5	560
90	8	10.49	80	44	10.48	460
100	- 5	10.48	- 50	41	10.47	430
110	-15	10.47	-160	29	10.46	300
120	-15	10.46	-160	29	10.46	300

TABLE A. 3 (Continued)

EXPERIMENTAL STRAIN AND STRESS

STRAIN GAGE NUMBER S - 3

TIME	CONFIGURATION 1			CONFIGURATION 2		
SEC.	$e \cdot 10^{6}$	$E \cdot 10^{-6}$	(psi)	$e \cdot 10^{6}$	$E \cdot 10^{-6}$	(psi)
10	- 7	10.5	- 74	- 8	10.5	- 84
20	- 7	10.5	- 74	- 8	10.5	- 84
30	- 10	10.5	- 105	- 20	10.5	- 210
40	- 27	10.5	- 280	- 37	10.5	- 390
50	- 33	10.5	- 350	- 54	10.5	- 570
60	- 64	10.5	- 670	- 65	10.5	- 680
70	-122	10.49	-1280	-105	10.5	-1100
80	-130	10.49	-1360	-114	10.49	-1200
90	-150	10.48	-1540	-120	10.48	-1260
100	-168	10.47	-1760	-155	10.47	-1620
110	-182	10.46	-1900	-176	10.46	-1840
120	-203	10.45	-2120	-187	10.46	-1960

TABLE A. 3 (Continued)

EXPERIMENTAL STRAIN AND STRESS

STRAIN GAGE NUMBER S - 4

TIME	CONFIGURATION 1			CONFIGURATION 2		
SEC.	$e \cdot 10^{6}$	$E \cdot 10^{-6}$	(psi)	$e \cdot 10^{6}$	$E \cdot 10^{-6}$	(psi)
10	23	10.5	245	14	10.5	140
20	33	10.5	350	24	10.5	250
30	40	10.5	420	31	10.5	330
40	47	10.49	490	39	10.49	410
50	52	10.49	540	43	10.49	450
60	53	10.48	560	46	10.48	480
70	57	10.47	590	49	10.47	520
80	58	10.46	610	51	10.46	540
90	60	10.46	630	51	10.46	540
100	60	10.45	630	50	10.45	520
110	57	10.44	590	49	10.45	510
120	57	10.43	590	47	10.45	490

TABLE A. 3 (Continued)

EXPERIMENTAL STRAIN AND STRESS

STRAIN GAGE NUMBER S - 5

TIME	CONFIGURATION 1			CONFIGURATION 2		
SEC.	$e \cdot 10^6$	$E \cdot 10^{-6}$	(psi)	$e \cdot 10^6$	$E \cdot 10^{-6}$	(psi)
10	57	10.5	600	46	10.5	490
20	104	10.5	1090	86	10.5	910
30	140	10.49	1470	115	10.5	1210
40	164	10.48	1720	141	10.49	1480
50	186	10.48	1950	160	10.48	1680
60	206	10.47	2160	174	10.47	1820
70	218	10.46	2280	189	10.47	1980
80	227	10.45	2370	200	10.47	2100
90	234	10.44	2440	204	10.45	2130
100	257	10.43	2680	211	10.45	2210
110	265	10.42	2760	214	10.43	2230
120	268	10.40	2790	221	10.42	2310

TABLE A.3 (Continued)

EXPERIMENTAL STRAIN AND STRESS

STRAIN GAGE NUMBER S - 6

TIME	CONFIGURATION 1			CONFIGURATION 2		
SEC.	$e \cdot 10^{6}$	$E \cdot 10^{-6}$	(psi)	$e \cdot 10^{6}$	$E \cdot 10^{-6}$	(psi)
10	73	10.5	760	75	10.5	790
20	115	10.49	1210	120	10.5	1260
30	151	10.48	1590	154	10.49	1610
40	176	10.47	1850	181	10.48	1900
50	193	10.46	2010	199	10.47	2080
60	206	10.45	2160	210	10.46	2200
70	214	10.45	2230	216	10.45	2260
80	218	10.43	2270	223	10.45	2330
90	218	10.42	2270	229	10.43	2390
100	230	10.40	2390	231	10.42	2410
110	238	10.38	2470	229	10.40	2380
120	235	10.36	2430	231	10.38	2400

TABLE A.3 (Continued)

EXPERIMENTAL STRAIN AND STRESS

STRAIN GAGE NUMBER S - 7

TIME	CONFIGURATION 1			CONFIGURATION 2		
SEC.	$\epsilon \cdot 10^6$	$E \cdot 10^{-6}$	(psi)	$\epsilon \cdot 10^6$	$E \cdot 10^{-6}$	(psi)
10	118	10.5	1230	108	10.5	1130
20	155	10.49	1630	150	10.5	1580
30	175	10.47	1830	182	10.48	1900
40	205	10.46	2140	199	10.47	2080
50	216	10.45	2260	214	10.46	2240
60	218	10.44	2270	215	10.45	2250
70	218	10.43	2270	216	10.43	2260
80	219	10.42	2280	224	10.42	2330
90	214	10.40	2220	223	10.40	2310
100	210	10.37	2180	211	10.38	2190
110	209	10.35	2160	208	10.36	2150
120	205	10.32	2120	204	10.34	2110

TABLE A.3 (Continued)

EXPERIMENTAL STRAIN AND STRESS

STRAIN GAGE NUMBER S - 8

TIME	CONFIGURATION 1			CONFIGURATION 2		
SEC.	$e \cdot 10^{6}$	$E \cdot 10^{-6}$	(psi)	$e \cdot 10^{6}$	$E \cdot 10^{-6}$	(psi)
10	135	10.5	1420	145	10.5	1520
20	209	10.48	2190	211	10.49	2220
30	258	10.47	2700	258	10.48	2700
40	291	10.46	3050	291	10.47	3050
50	318	10.45	3320	314	10.46	3280
60	334	10.43	3480	328	10.45	3420
70	345	10.41	3590	336	10.43	3510
80	354	10.38	3670	348	10.41	3620
90	361	10.36	3740	358	10.40	3720
100	380	10.34	3930	366	10.37	3810
110	390	10.32	4020	373	10.35	3860
120	396	10.30	4110	380	10.32	3920

TABLE A. 3 (Continued)

EXPERIMENTAL STRAIN AND STRESS

STRAIN GAGE NUMBER S - 9

TIME	CONFIGURATION 1			CONFIGURATION 2		
SEC.	$e \cdot 10^6$	$E \cdot 10^{-6}$	(psi)	$e \cdot 10^6$	$E \cdot 10^{-6}$	(psi)
10	-135	10.47	-1410	-150	10.47	-1570
20	-205	10.45	-2140	-210	10.45	-2190
30	-250	10.42	-2600	-255	10.43	-2660
40	-279	10.40	-2900	-293	10.40	-3040
50	-305	10.36	-3160	-321	10.37	-3330
60	-318	10.33	-3280	-345	10.34	-3570
70	-326	10.28	-3350	-358	10.30	-3680
80	-330	10.24	-3380	-366	10.27	-3760
90	-331	10.20	-3380	-368	10.23	-3760
100	-318	10.16	-3230	-364	10.18	-3700
110	-307	10.10	-3100	-353	10.15	-3580
120	-288	10.05	-2900	-339	10.10	-3420

TABLE A.3 (Continued)

EXPERIMENTAL STRAIN AND STRESS

STRAIN GAGE NUMBER S - 11

TIME	CONFIGURATION 1			CONFIGURATION 2		
SEC.	$e \cdot 10^{6}$	$E \cdot 10^{-6}$	(psi)	$e \cdot 10^{6}$	$E \cdot 10^{-6}$	(psi)
10	-269	10.46	-2810	-254	10.47	-2660
20	-491	10.42	-5120	-476	10.43	-4970
30	-639	10.37	-6620	-639	10.38	-6630
40	-756	10.32	-7800	-768	10.34	-7940
50	-836	10.26	-8580	-855	10.28	-8690
60	-886	10.20	-9040	-921	10.23	-9420
70	-919	10.15	-9330	-946	10.17	-9520
80	-933	10.08	-9400	-969	10.11	-9790
90	-931	10.02	-9330	-983	10.04	-9860
100	-933	9.93	-9270	-983	9.98	-9810
110	-907	9.87	-8950	-978	9.90	-9680
120	-878	9.80	-8610	-961	9.84	-9460

TABLE A.4

TABULATION OF ANALYTICAL STRESSES FOR 30 SECONDS OF HEATING TIME FOR CONFIGURATION 1

CALCULATION OF ANALYTICAL STRESSES

AREA NO.	T_1	T .	c_{x_1}	N_i	A_i	F	c_{x_2}	E	FZ	x_3	x
1	79	1	- 140	2	0.039	11	3540	1.533	17	-3496.5	- 96.500
2	79	1	- 140	2	0.039	11	3540	1.533	17	-3496.5	- 96.500
3	79	1	- 140	2	0.039	11	3540	1.533	17	-3496.5	- 96.500
4	79	1	- 140	2	0.039	11	3540	1.533	17	-3496.5	- 96.500
5	79	1	- 140	2	0.039	11	3540	1.533	17	-3496.5	- 96.500
6	84	6	- 810	2	0.0621	100	3540	1.415	142	-3227.3	- 497.30
7	84	6	- 810	2	0.0621	100	3540	1.415	142	-3227.3	- 497.30
8	84	6	- 810	2	0.0765	120	3540	1.275	150	-2908.0	- 178.00
9	87	9	- 1220	2	0.0765	190	3540	0.825	150	-1881.7	+ 438.30
10	89	11	- 1490	2	0.026	80	3540	0.40	30	- 912.32	+1137.7
11	95	17	- 2300	2	0.026	120	3540	0	0	0	1240.0
12	103	25	- 3900	2	0.026	180	3540	-0.40	- 70	+ 912.32	552.32
13	106	28	- 3790	2	0.0765	580	3540	-0.825	- 480	1831.7	1631.7
14	108	30	- 4070	2	0.0765	620	3540	-1.275	- 790	2908.0	2378.0
15	108	30	- 4070	2	0.0621	505	3540	-1.415	- 715	3227.3	2697.3
16	108	30	- 4070	2	0.0621	505	3540	-1.415	- 715	3227.3	2697.3
17	118	40	- 5420	2	0.039	420	3540	-1.533	- 650	3496.5	1616.5
18	140	62	- 8400	2	0.039	655	3540	-1.533	-1010	3496.5	-1363.5
19	158	80	- 10840	2	0.039	850	3540	-1.533	-1300	3496.5	-3803.5
20	170	92	- 12470	2	0.039	970	3540	-1.533	-1490	3496.5	-5433.5
21	177	99	- 13420	2	0.039	1050	3540	-1.533	-1610	3496.5	-6383.5
					SUM	11000					

TABLE A.4 (Continued)

TABULATION OF ANALYTICAL STRESSES FOR 60 SECONDS OF HEATING TIME FOR CONFIGURATION 1

CALCULATION OF ANALYTICAL STRESSES

AREA NO.	T_1	T	c_{x_1}	N_1	A_1	F	c_{x_2}	Z	Fz	x_3	x
1	83	5	- 680	2	0.039	50	7210	1.533	80	-6011.7	318.30
2	84	6	- 810	2	0.039	60	7210	1.533	100	-6011.7	382.30
3	85	7	- 950	2	0.039	70	7210	1.533	110	-6011.7	248.30
4	86	8	- 1080	2	0.039	80	7210	1.533	130	-6011.7	118.30
5	87	9	- 1220	2	0.039	95	7210	1.533	150	-6011.7	- 21.700
6	99	21	- 2850	2	0.0621	350	7210	1.415	500	-5548.9	-1188.9
7	99	21	- 2850	2	0.0621	350	7210	1.415	500	-5548.9	-1188.9
8	99	21	- 2650	2	0.0765	440	7210	1.275	560	-4999.9	- 639.90
9	104	26	- 3520	2	0.0765	540	7210	0.825	450	-3235.2	+ 454.80
10	109	31	- 4200	2	0.026	220	7210	0.40	90	-1568.6	1441.4
11	121	43	- 5830	2	0.026	300	7210	0	0	0	1380.0
12	135	57	- 7720	2	0.026	400	7210	-0.40	-160	+1568.6	1068.6
13	140	62	- 8400	2	0.0765	1290	7210	-0.825	-1060	3235.2	2045.2
14	145	67	- 9080	2	0.0765	1390	7210	-1.275	-1770	4999.9	3129.9
15	145	67	- 9080	2	0.0621	1130	7210	-1.415	-1600	5548.9	3678.9
16	145	67	- 9080	2	0.0621	1130	7210	-1.415	-1600	5548.9	3678.9
17	159	81	-10980	2	0.039	856	7210	-1.533	-1310	6011.7	2241.7
18	190	112	-15180	2	0.039	1180	7210	-1.533	-1810	6011.7	-1959.3
19	216	130	-18700	2	0.039	1460	7210	-1.533	-2240	6011.7	-5478.3
20	231	153	-20730	2	0.039	1620	7210	-1.533	-2480	6011.7	-7508.3
21	240	162	-21950	2	0.039	1710	7210	-1.533	-2620	6011.7	-8728.3
					SUM	14740					

TABLE A. 4 (Continued)

TABULATION OF ANALYTICAL STRESSES FOR 90 SECONDS OF HEATING TIME FOR CONFIGURATION 1

CALCULATION OF ANALYTICAL STRESSES

AREA NO.	T_I	T	c_{x_1}	N_I	A_I	F	c_{x_2}	z	Fz	c_{x_3}	c_x
1	94	16	- 2170	2	0.0390	170	11090	1.533	260	-7723.1	1196.9
2	96	18	- 2440	2	0.0390	190	11090	1.533	290	-7723.1	926.90
3	99	21	- 2850	2	0.0390	220	11090	1.533	340	-7723.1	516.90
4	101	23	- 3120	2	0.0390	240	11090	1.533	370	-7723.1	246.90
5	104	26	- 3520	2	0.0390	275	11090	1.533	420	-7723.1	- 153.10
6	119	41	- 5560	2	0.0621	690	11090	1.415	980	-7128.6	-1598.6
7	119	41	- 5560	2	0.0621	690	11090	1.415	980	-7128.6	-1598.6
8	119	41	- 5560	2	0.0765	850	11090	1.275	1080	-6423.3	- 893.30
9	126	48	- 6500	2	0.0765	990	11090	0.825	820	-4156.3	+ 433.70
10	133	55	- 7450	2	0.026	390	11090	0.40	160	-2015.2	1624.80
11	150	72	- 9760	2	0.026	510	11090	0	0	0	1330.0
12	168	90	-12200	2	0.026	630	11090	-0.40	- 250	+2015.2	905.20
13	174	96	-13010	2	0.0765	1990	11090	-0.825	-1640	+4156.3	2236.3
14	182	104	-14090	2	0.0765	2160	11090	-1.275	-2750	+6423.3	3423.3
15	182	104	-14090	2	0.0621	1750	11090	-1.415	-2480	+7128.6	4128.6
16	182	104	-14090	2	0.0621	1750	11090	-1.415	-2480	+7128.6	4128.6
17	196	118	-15590	2	0.039	1250	11090	-1.533	-1920	+7723.1	3223.1
18	232	154	-20870	2	0.039	1630	11090	-1.533	-2500	+7723.1	-2056.9
19	260	182	-24660	2	0.039	1920	11090	-1.533	-2940	+7723.1	-5846.9
20	279	201	-27240	2	0.039	2120	11090	-1.533	-3250	+7723.1	-8426.9
21	291	213	-28860	2	0.039	2250	11090	-1.533	-3450	+7723.1	-10047.
					SUM	22670					

TABLE A.4 (Continued)

TABULATION OF ANALYTICAL STRESSES FOR 120 SECONDS OF HEATING TIME FOR CONFIGURATION 1

CALCULATION OF ANALYTICAL STRESSES

AREA NO.	T_i	T	c_{x_1}	N_i	A_i	F	c_{x_2}	z	Fz	x_3	N
1	114	36	- 4830	2	0.039	380	15220	1.533	580	-9017.4	1322.6
2	115	37	- 5010	2	0.039	390	15220	1.533	600	-9017.4	1192.6
3	116	38	- 5150	2	0.039	400	15220	1.533	620	-9017.4	1052.6
4	111	40	- 5470	2	0.039	420	15220	1.533	650	-9017.4	702.60
5	122	44	- 5960	2	0.039	465	15220	1.533	710	-9017.4	242.60
6	144	66	- 8940	2	0.0621	1110	15220	1.415	1570	-8323.3	-2043.3
7	144	66	- 8940	2	0.0621	1110	15220	1.415	1570	-8323.3	-2043.3
8	144	66	- 8940	2	0.0765	1370	15220	1.275	1750	-7499.8	-1219.8
9	152	74	-10000	2	0.0765	1530	15220	0.825	1260	-4852.8	+ 337.20
10	160	82	-11110	2	0.026	580	15220	0.40	230	-2352.9	1757.1
11	180	102	-13820	2	0.026	720	15220	0	0	0	1400.0
12	199	121	-16400	2	0.026	850	15220	-0.40	- 340	+2352.9	1172.9
13	209	131	-17750	2	0.0765	2720	15220	-0.825	-2240	4852.8	2322.8
14	218	140	-18970	2	0.0765	2900	15220	-1.275	-3700	7499.8	3749.8
15	218	140	-18970	2	0.0621	2360	15220	-1.415	-3340	8323.3	4573.3
16	218	140	-18970	2	0.0621	2360	15220	-1.415	-3340	8323.3	4573.3
17	234	156	-21140	2	0.039	1650	15220	-1.533	-2530	9017.4	3097.4
18	274	196	-26560	2	0.039	2070	15220	-1.533	-3170	9017.4	-2322.6
19	304	226	-30620	2	0.039	2390	15220	-1.533	-3660	9017.4	-6382.6
20	324	246	-33330	2	0.039	2600	15220	-1.533	-3990	9017.4	-9092.6
21	337	259	-35090	2	0.039	2740	15220	-1.533	-4200	9017.4	-10853.
					SUM	31120					

TABLE A.4 (Continued)

TABULATION OF ANALYTICAL STRESSES FOR 30 SECONDS OF HEATING TIME FOR CONFIGURATION 2

CALCULATION OF ANALYTICAL STRESSES

AREA NO.	T_1	T	c_{x_1}	N_1	A_1	F	c_{x_2}	z	F_2	x3	x
1	79	1	- 140	2	0.039	10	3020	1.533	15	-3003.6	- 123.60
2	79	1	- 140	2	0.039	10	3020	1.533	15	-3003.6	- 123.60
3	79	1	- 140	2	0.039	10	3020	1.533	15	-3003.6	- 123.60
4	79	1	- 140	2	0.039	10	3020	1.533	15	-3003.6	- 123.60
5	79	1	- 140	2	0.039	10	3020	1.533	15	-3003.6	- 123.60
6	84	6	- 810	2	0.0621	100	3020	1.415	140	-2772.4	- 562.40
7	84	6	- 810	2	0.0621	100	3020	1.415	140	-2772.4	- 562.40
8	84	6	- 810	2	0.0765	120	3020	1.275	150	-2498.1	- 288.10
9	86	8	- 1080	2	0.0765	170	3020	0.825	140	-1616.4	+ 323.60
10	88	10	- 1360	2	0.026	70	3020	0.40	30	- 783.72	876.28
11	92	14	- 1900	2	0.026	100	3020	0	0	0	1120.0
12	99	21	- 2850	2	0.026	150	3020	-0.40	- 60	783.72	953.72
13	100	22	- 2980	2	0.0765	460	3020	-0.825	-380	1616.4	1656.4
14	101	23	- 3120	2	0.0765	480	3020	-1.275	-610	2498.1	2398.1
15	101	23	- 3120	2	0.0621	390	3020	-1.415	-550	2772.4	2672.4
16	101	23	- 3120	2	0.0621	390	3020	-1.415	-550	2772.4	2672.4
17	110	32	- 4340	2	0.039	340	3020	-1.533	-520	3003.6	1683.6
18	134	56	- 7590	2	0.039	590	3020	-1.533	-900	3003.6	-1566.4
19	152	74	-10030	2	0.039	780	3020	-1.533	-1200	3003.6	-4006.4
20	164	86	-11650	2	0.039	910	3020	-1.533	-1400	3003.6	-5626.4
21	170	92	-12470	2	0.039	970	3020	-1.533	-1490	3003.6	-6446.4
					SUM	6170					

TABLE A.4 (Continued)

TABULATION OF ANALYTICAL STRESSES FOR 60 SECONDS OF HEATING TIME FOR CONFIGURATION 2

CALCULATION OF ANALYTICAL STRESSES

AREA NO.	T_i	T	c_{x_1}	N_i	A_i	F	c_{x_2}	z	Fz	x_3	x
1	80	2	- 270	2	0.039	20	6290	1.533	30	-5413.9	606.10
2	82	4	- 540	2	0.039	40	6290	1.533	60	-5413.9	336.10
3	83	5	- 680	2	0.039	50	6290	1.533	80	-5413.9	196.10
4	84	6	- 810	2	0.039	60	6290	1.533	100	-5413.9	66.100
5	85	7	- 950	2	0.039	70	6290	1.533	110	-5413.9	- 73.900
6	96	18	- 2440	2	0.0621	300	6290	1.415	420	-4997.2	-1147.2
7	96	18	- 2440	2	0.0621	300	6290	1.415	420	-4997.2	-1147.2
8	96	18	- 2440	2	0.0765	370	6290	1.275	470	-4502.8	- 652.80
9	101	23	- 3120	2	0.0765	480	6290	0.825	400	-2913.6	+ 256.40
10	105	27	- 3660	2	0.026	190	6290	0.40	80	-1412.6	1217.4
11	114	36	- 4880	2	0.026	250	6290	0	0	0	1410.0
12	127	49	- 6640	2	0.026	350	6290	-0.40	-140	+1412.6	1062.6
13	131	53	- 7180	2	0.0765	1100	6290	-0.825	-910	2913.6	2023.6
14	134	56	- 7590	2	0.0765	1160	6290	-1.275	-1400	4502.8	3202.8
15	134	56	- 7590	2	0.0621	940	6290	-1.415	-1330	4997.2	3697.2
16	134	56	- 7590	2	0.0621	940	6290	-1.415	-1330	4997.2	3697.2
17	137	59	- 7990	2	0.039	620	6290	-1.533	- 950	5413.9	3713.9
18	179	101	-13690	2	0.039	1070	6290	-1.533	-1640	5413.9	-1986.1
19	206	128	-17340	2	0.039	1350	6290	-1.533	-2070	5413.9	-5636.1
20	225	147	-19920	2	0.039	1550	6290	-1.533	-2380	5413.9	-8216.1
21	234	156	-21140	2	0.039	16500	6290	-1.533	-2530	5413.9	-9436.1
					SUM	12870					

TABLE A. 4 (Continued)

TABULATION OF ANALYTICAL STRESSES FOR 90 SECONDS OF HEATING TIME FOR CONFIGURATION 2

CALCULATION OF ANALYTICAL STRESSES

AREA NO.	T_1	T	c_{x_1}	N_1	A_1	F	c_{x_2}	z	Fz	x_3	x
1	91	13	- 1760	2	0.039	140	9020	1.533	210	-7048.0	212.00
2	91	13	- 1760	2	0.039	140	9020	1.533	210	-7048.0	212.00
3	91	13	- 1760	2	0.039	140	9020	1.533	210	-7048.0	212.00
4	93	15	- 2030	2	0.039	160	9020	1.533	240	-7048.0	- 58.000
5	95	17	- 2300	2	0.039	180	9020	1.533	270	-7048.0	- 328.00
6	106	28	- 3790	2	0.0621	470	9020	1.415	670	-6505.5	-1275.5
7	106	28	- 3790	2	0.0621	470	9020	1.415	670	-6505.5	-1275.5
8	106	28	- 3790	2	0.0765	580	9020	1.275	740	-5861.8	- 631.80
9	112	34	- 4610	2	0.0765	710	9020	0.825	590	-3792.9	+ 617.10
10	118	40	- 5420	2	0.026	280	9020	0.40	110	-1839.0	1761.0
11	131	53	- 7180	2	0.026	370	9020	0	0	0	1840.0
12	150	72	- 9760	2	0.026	510	9020	-0.40	- 200	+1839.0	1099.0
13	153	75	-10160	2	0.0765	1550	9020	-0.825	-1280	3792.9	2652.9
14	156	78	-10570	2	0.0765	1620	9020	-1.275	-2070	5861.8	4311.8
15	156	78	-10570	2	0.0621	1310	9020	-1.415	-1850	6505.5	4955.5
16	156	78	-10570	2	0.0621	1310	9020	-1.415	-1850	6505.5	4955.5
17	172	94	-12740	2	0.039	940	9020	-1.533	-1520	7048.0	3328.0
18	218	140	-18970	2	0.039	1480	9020	-1.533	-2270	7048.0	2902.0
19	249	171	-23170	2	0.039	1810	9020	-1.533	-2770	7048.0	-7102.0
20	272	194	-26290	2	0.039	2050	9020	-1.533	-3140	7048.0	-10222.
21	285	207	-28050	2	0.039	2190	9020	-1.533	-3360	7048.0	-11982.
					SUM	18450					

TABLE A. 4 (Continued)

TABULATION OF ANALYTICAL STRESSES FOR 120 SECONDS OF HEATING TIME FOR CONFIGURATION 2

CALCULATION OF ANALYTICAL STRESSES

AREA NO.	T_i	Y	c_{x_1}	N_i	A_i	F	c_{x_2}	z	FZ	x_3	x
1	103	25	- 3390	2	0.039	260	13520	1.533	400	-8753.0	1377.0
2	104	26	- 3520	2	0.039	275	13520	1.533	420	-8753.0	1247.0
3	105	27	- 3660	2	0.039	285	13520	1.533	440	-8753.0	1107.0
4	107	29	- 3930	2	0.039	310	13520	1.533	470	-8753.0	837.00
5	111	33	- 4470	2	0.039	350	13520	1.533	535	-8753.0	297.00
6	133	55	- 7450	2	0.0621	930	13520	1.415	1320	-8079.2	- 2009.2
7	133	55	- 7450	2	0.0621	930	13520	1.415	1320	-8079.2	- 2009.2
8	133	55	- 7450	2	0.0765	1140	13520	1.275	1450	-7279.9	- 1209.9
9	141	63	- 8540	2	0.0765	1310	13520	0.825	1080	-4710.5	+ 269.50
10	149	71	- 9620	2	0.026	500	13520	0.40	200	-2283.9	1616.1
11	167	89	-12060	2	0.026	630	13520	0	0	0	1460.0
12	191	113	-15310	2	0.026	800	13520	-0.40	- 320	+2283.9	493.90
13	196	118	-15990	2	0.0765	2450	13520	-0.825	-2020	4710.5	2240.5
14	201	123	-16670	2	0.0765	2550	13520	-1.275	-3250	7279.9	4129.9
15	201	123	-16670	2	0.0621	2070	13520	-1.415	-2930	8079.2	4929.2
16	201	123	-16670	2	0.0621	2070	13520	-1.415	-2930	8079.2	4929.2
17	223	145	-19650	2	0.039	1530	13520	-1.533	-2350	8753.0	2623.0
18	260	182	-24660	2	0.039	1920	13520	-1.533	-2940	8753.0	- 2387.0
19	290	212	-28730	2	0.039	2240	13520	-1.533	-3430	8753.0	- 6457.0
20	312	234	-31710	2	0.039	2470	13520	-1.533	-3790	8753.0	- 9437.0
21	327	249	-33740	2	0.039	2630	13520	-1.533	-4030	-8753.0	-11467.
					SUM	27650					

DISTRIBUTION LIST

Technical Reports

Contract N5 ori-07833 Project NR 064-259

Chief of Naval Research
Department of the Navy
Washington 25, D.C.
Attn: Code 438 (2)

Director,
Office of Naval Research
Branch Office
150 Causeway St.
Boston 14, Mass. (2)

Chief of Bureau of Aeronautics
Navy Department
Washington 25, D.C.
Attn: TD-41, Technical Library (1)
: SE-42, C. W. Hurley (2)

Chief of Bureau of Ordnance
Navy Department
Washington 25, D.C.
Attn: Ad-3, Technical Library (1)
: Re9a (1)

Chief of Bureau of Ships
Navy Department
Washington 25, D.C.
Attn: Director of Research (1)
: Code 442 (1)

Chief of Bureau of Yards and Docks
Navy Department
Washington 25, D.C.
Attn: Research Division (2)

Librarian
U. S. Naval Postgraduate School
Monterey, California (1)

Naval Air Experimental Station
Naval Air Material Center
Naval Base
Philadelphia 12, Pa.
Attn: Head, Aeronautical Materials Laboratory (1)

Naval Ordnance Laboratory
Naval Gun Factory
Washington 25, D.C.
Attn: Dr. D. E. Mariowe (1)

Superintendent
Naval Gun Factory
Washington 25, D.C. (1)

Naval Ordnance Test Station
Inyokern, California
Attn: Scientific Officer (1)

Director
David Taylor Model Basin
Washington 7, D.C.
Attn: Structural Mechanics Division (2)

Director
Naval Engineering Experiment Station
Annapolis, Maryland (1)

Director
Materials Laboratory
New York Naval Shipyard
Brooklyn 1, New York (1)

Chief of Staff
Department of the Army
The Pentagon
Washington 25, D.C.
Attn: Director of Research and Development (1)

Office of Chief of Ordnance
Research and Development Service
Department of the Army
The Pentagon
Washington 25, D.C.
Attn: ORDTB (1)

Commanding Officer
Watertown Arsenal
Watertown, Massachusetts
Attn: Laboratory Division (1)

Commanding Officer
Frankford Arsenal
Philadelphia, Pa.
Attn: Laboratory Division (1)

Commanding Officer
Squier Signal Laboratory
Fort Monmouth, New Jersey
Attn: Components and Materials Branch (1)

Commanding General
Air Material Command
Wright-Patterson Air Force Base
Dayton, Ohio
Attn: E. H. Schwartz - MCREXA -6 (3)

Director
National Bureau of Standards
Washington, D.C.
Attn: Dr. W. H. Romberg (1)

U. S. Coast Guard
1300 E Street, NW
Washington, D.C.
Attn: Chief, Testing and Development Division (1)

Forest Products Laboratory
Madison, Wisconsin
Attn: L. J. Markwardt (1)

National Advisory Committee for Aeronautics
1724 F Street, NW
Washington, D.C.
Attn: Materials Research Coordination Group (2)

National Advisory Committee for Aeronautics
Langley Field, Virginia
Attn: Mr. E. Lundquist (1)
: Dr. Bernard Budiansky (1)

National Advisory Committee for Aeronautics
Cleveland Municipal Airport
Cleveland, Ohio
Attn: J. H. Collins, Jr. (1)

U. S. Maritime Commission
Technical Bureau
Washington, D.C.
Attn: Mr. Wanless (1)

Research and Development Board
Pentagon Building
Washington, D.C.
Attn: Library 3D641 (1)

Dr. S. P. Timoshenko
School of Engineering
Stanford University
Stanford, California (1)

Dr. D. C. Drucker
Graduate Division of Applied Mathematics
Brown University
Providence, Rhode Island (1)

Dr. J. E. Dorn
University of California
Berkeley, California (1)

Dr. T. J. Dolan
University of Illinois
Urbana, Illinois (1)

Professor R. L. Bisplinghoff
Massachusetts Institute of Technology
Cambridge 39, Massachusetts (15)

Dr. N. J. Hoff
Department of Aeronautical Engineering and Applied Mechanics
Polytechnic Institute of Brooklyn
99 Livingston Street
Brooklyn, New York (2)

Dr. N. M. Newmark
Department of Civil Engineering
University of Illinois
Urbana, Illinois (1)

Dr. J. N. Goodier
School of Engineering
Stanford University
Stanford, California (1)

Professor F. K. Teichmann
Department of Aeronautical Engineering
New York University
University Heights, Bronx
New York City, New York (1)

Professor Jesse Ormondroyd
University of Michigan
Ann Arbor, Michigan (1)

Dr. W. H. Hoppmann
Department of Applied Mechanics
Johns Hopkins University
Baltimore, Maryland (1)

Professor W. K. Krefeld
College of Engineering
Columbia University
New York, New York (1)

Professor R. M. Haines
University of Santa Clara
Santa Clara, California (1)

Commanding Officer
Office of Naval Research
Branch Office
346 Broadway
New York 13, New York (1)

Commanding Officer
Office of Naval Research
Branch Office
844 N. Rush Street
Chicago 11, Illinois (1)

Commanding Officer
Office of Naval Research
Branch Office
1000 Geary Street
San Francisco 9, California (1)

Commanding Officer
Office of Naval Research
Branch Office
1030 Green Street
Pasadena, California (1)

Contract Administrator, SE Area
Office of Naval Research
Department of Navy
Washington 25, D.C.
Attn: Mr. R. F. Lynch (1)

Director, Naval Research Laboratory
Washington 20, D.C.
Attn: Technical Information Officer (9)
: Technical Library (1)
: Mechanics Division (2)

Dr. A. C. Eringen
Purdue University
Lafayette, Indiana (1)

Dr. M. Hetenyi
Northwestern University
Evanston, Illinois (1)

Officer in Charge
Office of Naval Research
Branch Office
Navy #100
Fleet Post Office
New York, New York (5)

Dr. C. B. Smith
College of Arts and Sciences
Department of Mathematics
Walker Hall
University of Florida
Gainesville, Florida (1)

Professor R. D. Mindlin
Department of Civil Engineering
Columbia University
Broadway at 117th Street
New York 27, New York (1)

Professor H. Bleich
Department of Civil Engineering
Columbia University
Broadway at 117th Street
New York 27, New York (1)

Mr. Martin Goland
4049 Pennsylvania Avenue
Midwest Research Institute
Kansas City 2, Missouri (1)

Professor George H. Lee
Department of Mechanics
Rensselaer Polytechnic Institute
Troy, New York (1)

Commander
U. S. Naval Proving Grounds
Dahlgren, Virginia (1)

Naval Ordnance Laboratory
White Oak, Maryland
NFD 1, Silver Spring, Maryland
Attn: Dr. C. A. Truesdell (1)

Director of Research and Development
Headquarters, U. S. Air Force
AFDED-RE-3
Washington 25, D. C. (1)

Professor W. Flugge
School of Engineering
Stanford University
Stanford, California (1)

Professor A. S. Veletsos
Department of Civil Engineering
University of Illinois
Urbana, Illinois (1)